UNIVERSITI TEKNOLOGI MARA

SYNTHESIS OF 3D NITROGEN-DOPED REDUCED GRAPHENE OXIDE ADSORBENT FOR PHENOLIC PURIFICATION FROM MICROWAVE-EXTRACTED PALM KERNEL CAKE

ELLISA NATASYA BINTI ROSLI

MSc

July 2026

UNIVERSITI TEKNOLOGI MARA

SYNTHESIS OF 3D NITROGEN-DOPED REDUCED GRAPHENE OXIDE ADSORBENT FOR PHENOLIC PURIFICATION FROM MICROWAVE-EXTRACTED PALM KERNEL CAKE

ELLISA NATASYA BINTI ROSLI

Thesis submitted in fulfilment
of the requirements for the degree of
Master of Science
(Chemical Engineering)

Faculty of Chemical Engineering

July 2026

CONFIRMATION BY PANEL OF EXAMINERS

I certify that a Panel of Examiners has met on 19 December 2025 to conduct the final examination of Ellisa Natasya Rosli on her Masters of Science thesis entitled "Synthesis of 3D Nitrogen-Doped Reduced Graphene Oxide Adsorbent for Phenolic Purification from Microwave-Assisted Extraction Palm Kernel Cake" in accordance with Universiti Teknologi MARA Act 1976 (Akta 173). The Panel of Examiner recommends that the student be awarded the relevant degree. The Panel of Examiners was as follows:

Norin Zamiah Kassim Shaari, PhD
Associate Professor
Faculty of Chemical Engineering
Universiti Teknologi MARA
(Chairman)

Ana Najwa Mustapa, PhD
Associate Professor
Faculty of Chemical Engineering
Universiti Teknologi MARA
(Internal Examiner)

Chua Bee Lin, PhD
Associate Professor
Faculty of Engineering and Technology
Sunway Universiti
(External Examiner)

PROFESSOR DR HJH ZURAEDA IBRAHIM
Dean
Institute of Postgraduates Studies
Universiti Teknologi MARA

Date: 23 July 2026

AUTHOR'S DECLARATION

I declare that the work in this thesis was carried out in accordance with the regulations of Universiti Teknologi MARA. It is original and is the results of my own work, unless otherwise indicated or acknowledged as referenced work. This thesis has not been submitted to any other academic institution or non-academic institution for any degree or qualification.

I, hereby, acknowledge that I have been supplied with the Academic Rules and Regulations for Post Graduate, Universiti Teknologi MARA, regulating the conduct of my study and research.

Name of Student	:	Ellisa Natasya Rosli
Student ID. No.	:	2023290186
Programme	:	Master of Science (Chemical Engineering) – CEEH750
Faculty	:	Chemical Engineering
Thesis Title	:	Synthesis of 3D Nitrogen-Doped Reduced Graphene Oxide Adsorbent for Phenolic Purification from Microwave-Extracted Palm Kernel Cake
Signature of Student	:	
Date	:	23 July 2026

ABSTRACT

This study successfully demonstrated the development and application of three-dimensional nitrogen-doped reduced graphene oxide (3D-N/rGO) as a selective adsorbent for the purification of phenolic compounds extracted from palm kernel cake (PKC). Although PKC is abundant and rich in bioactive phenolics, it remains underutilized due to the limitations of conventional purification approaches that lack selectivity and efficiency when treating complex matrices. By integrating microwave-assisted extraction (MAE) with an adsorption-based purification strategy, this research addressed the need for an improved recovery system capable of enhancing phenolic enrichment while maintaining process feasibility. The synthesized 3D-N/rGO, prepared via a hydrothermal method using varying urea loadings of 0.5–10 wt.% as a nitrogen dopant and glucose as a cross-linking agent, exhibited successful structural modification confirmed through XPS, HRTEM, FTIR, BET, and TGA analyses. Characterization results indicated the formation of a stable three-dimensional porous network, partial reduction of graphene oxide, and successful incorporation of pyridinic and graphitic nitrogen species, which enhanced surface functionality and active site availability. Among the different urea loadings investigated, the 10 wt.% 3D-N/rGO demonstrated the highest adsorption capacity, indicating that enhanced surface chemistry played a more significant role than surface area alone in improving adsorption performance. Nitrogen incorporation introduced pyridinic and graphitic nitrogen species that enhanced electronic properties and promoted π–π interactions and hydrogen bonding with aromatic phenolic molecules, thereby improving adsorption selectivity despite a relatively moderate surface area. Experimental evaluation in batch and fixed-bed systems showed that adsorption performance was significantly influenced by temperature, initial phenolic concentration, and adsorbent mass with optimal conditions identified at 50 °C, 50 mg/L, and 0.50 g adsorbent dosage, achieving a maximum adsorption capacity of 87.73 mg/g. Isotherm modelling indicated that the Langmuir model provided the best fit ($R^2 = 0.9962$), suggesting monolayer adsorption on homogeneous active sites, while kinetic analysis followed the pseudo-second-order model ($R^2 = 0.9920$), implying chemisorption involvement. Thermodynamic parameters further confirmed that the adsorption process was spontaneous ($\Delta G° < 0$), endothermic ($\Delta H° = +18.49$ kJ/mol), and entropy-driven ($\Delta S° = +0.072$ kJ/mol·K), with increased randomness at the solid–liquid interface. Overall, this work demonstrates that combining nitrogen doping with three-dimensional graphene structuring enhances adsorption selectivity and recovery efficiency for high-value phenolic compounds from agro-industrial waste. The proposed 3D-N/rGO system provides a promising platform for sustainable phenolic purification and supports the valorization of PKC into value-added bioactive products.

ACKNOWLEDGEMENT

All praises and gratitude are due to Allah SWT for granting me the strength, patience, and perseverance to complete this thesis successfully.

I would like to express my deepest appreciation to my supervisor, Dr. Norhusna Mohd Nor, for her invaluable guidance, constant encouragement, and dedicated support throughout the course of this research. Her insightful feedback and continuous motivation have been instrumental in shaping the direction of this thesis.

My sincere thanks also go to my co-supervisors, Dr. Ir. Mohd Azahar Mohd Ariff and Ir. Mohamed Syazwan Osman, for their constructive advice, technical input, and unwavering support throughout this journey. Their expertise and mentorship have contributed significantly to the development and completion of my research.

I am also thankful to all the academic and technical staff of the Faculty of Chemical Engineering, Universiti Teknologi MARA (UiTM) Cawangan Pulau Pinang, for providing the resources, facilities, and assistance that greatly supported my experimental work, particularly during the synthesis and characterization of 3D nitrogen-doped reduced graphene oxide and the fixed-bed adsorption studies.

Special thanks to my labmates, friends, and postgraduate peers for their companionship, motivation, and moral support throughout the highs and lows of this research journey. Your kindness and shared laughter helped make this experience more bearable and memorable.

A special thank you goes to my beloved parents and my entire family for their unconditional love, prayers, and encouragement. I would especially like to thank my mother, who has been my pillar of strength and accompanying me every single day and night while I was writing this thesis, for staying by my side through the stress, and for always offering comfort, warmth, and love when I needed it most.

Last but not least, I gratefully acknowledge the financial support provided by the Geran Penyelidikan Pascasiswazah, Universiti Teknologi MARA (600-RMC/FRGS 5/3 (158/2022), which enabled the successful execution of this research project.

To everyone who has been part of this journey directly or indirectly, thank you from the bottom of my heart.

TABLE OF CONTENTS

		Page
CONFIRMATION BY PANEL OF EXAMINERS		**ii**
AUTHOR'S DECLARATION		**iii**
ABSTRACT		**iv**
ACKNOWLEDGEMENT		**v**
TABLE OF CONTENTS		**vi**
LIST OF TABLES		**x**
LIST OF FIGURES		**xii**
LIST OF PLATES		**xiv**
LIST OF SYMBOLS		**xv**
LIST OF ABBREVIATIONS		**xvi**
LIST OF NOMENCLATURE		**xvii**
CHAPTER 1 INTRODUCTION		**1**
1.1	Research Background	1
	1.1.1 Phenolic Compound from Oil Palm Waste	3
	1.1.2 Microwave-Assisted Extraction for Phenolic Compound	5
	1.1.3 Graphene Oxide in Phenolic Compound Purification	5
1.2	Problem Statement	6
1.3	Research Objectives	8
1.4	Scope of Work	9
1.5	Significance of Study	10
CHAPTER 2 LITERATURE REVIEW		**12**
2.1	Introduction	12
2.2	Palm Kernel Cake (PKC) in Palm Oil Industry	12
2.3	Phenolic Compounds in PKC	15
	2.3.1 Phytochemical Compounds	16
	2.3.2 Phenolic Compounds	20
	2.3.3 Application of Phenolic Compounds	23
2.4	Extraction of Phenolic Compounds	24

2.4.1 Conventional Extraction Techniques 25
2.4.2 Microwave-Assisted Extraction 26
2.4.3 Challenges in Phenolic Compound Recovery 28
2.5 Graphene Oxide 30
2.5.1 GO-Based Adsorbents 31
2.6 Surface Modification of GO 32
2.6.1 Hydrophobic Interaction Chromatography (HIC) 34
2.6.2 Nitrogen doping in rGO 37
2.6.3 Three-Dimensional (3D) Graphene Structures 39
2.7 Purification Technologies 40
2.7.1 Purification using Adsorption-Desorption Process 43
2.7.2 Adsorbents in Phenolic Purification 46
2.8 Effect of Adsorption Parameters 48
2.9 Adsorption Isotherms Models 53
2.9.1 Langmuir Isotherm Model 55
2.9.2 Freundlich Isotherm Model 55
2.9.3 Temkin Isotherm Model 56
2.9.4 Dubinin-Radushkevich 56
2.9.5 Redlich-Peterson 57
2.10 Adsorption Thermodynamics 58
2.10.1 Van't Hoff Equation 60
2.11 Adsorption Kinetics 61
2.11.1 Pseudo-First Order 63
2.11.2 Pseudo-Second Order 63

CHAPTER 3 RESEARCH METHODOLOGY 64
3.1 Overview of Research Methodology 64
3.2 Materials and Chemicals 65
3.3 Equipment and Apparatus 66
3.4 Experiment Process Flowchart 67
3.5 Preparation of Palm Kernel Cake (PKC) 68
3.6 Microwave-Assisted Extraction (MAE) of Phenolic-rich Compounds From PKC 68

3.7 Preparation of 3-Dimensional Nitrogen-Doped Reduced Graphene Oxide (3D-N/rGO) Adsorbent 70
3.7.1 Synthesis of Graphene Oxide using Modified Hummer's Method 71
3.7.2 Synthesis of 3D-N/rGO Adsorbent 72
3.8 Purification of Phenolic Extract using 3D-N/rGO 73
3.8.1 Purification via Batch Adsorption 73
3.8.2 Purification via Fixed Bed Adsorption 74
3.9 Phenolic Compounds Identification 76
3.9.1 Total Phenolic Content (TPC) 76
3.9.2 Liquid Chromatography Mass Spectrophotometer (LC-MS) 76
3.9.3 Macro and Micronutrient 77
3.10 Characterization of 3D-N/rGO Adsorbent 78
3.10.1 Thermal Gravimetric Analysis (TGA) 78
3.10.2 N_2 Adsorption-Desorption 78
3.10.3 High Resolution Transmission Electron Microscope (HRTEM) 79
3.10.4 Fourier Transform Infrared Spectroscopy (FTIR) 79
3.10.5 X-Ray Photoelectron Spectroscopy (XPS) 80
3.11 Mechanistic Insight Exploration 80
3.11.1 Isotherm Analysis 80
3.11.2 Kinetic Analysis 81
3.11.3 Thermodynamics 81

CHAPTER 4 RESULTS AND DISCUSSION 83
4.1 Introduction 83
4.2 Batch Adsorption–Desorption Purification of Phenolic Compounds Using 3D-N/rGO with Varying Urea Ratios 83
4.2.1 Liquid Chromatography-Mass Spectrometry (LC-MS) Analysis 88
4.2.2 Macro and Micronutrient 91
4.3 Characterization of Hydrophobic Nanostructure 3D-N/rGO Adsorbent 93
4.3.1 Physical Stability and Surface Characteristics 93
4.3.2 Functional Groups and Surface Chemistry 102
4.4 Continuous Fixed-Bed Purification of Phenolic Compounds Using 3D-N/rGO Adsorbent 106
4.4.1 Effect of Adsorption Temperature 106

4.4.2 Effect of Phenolic Concentration 110
4.4.3 Effect of Mass of Adsorbent 113
4.5 Adsorption Mechanism Insight 115
4.5.1 Adsorption Kinetics 115
4.5.2 Adsorption Thermodynamic 123
4.5.3 Adsorption Isotherm 125
4.5.4 Proposed Adsorption Mechanism 129

CHAPTER 5 CONCLUSION **131**
5.1 Conclusions 131
5.2 Recommendations 132

REFERENCES **134**

APPENDICES **155**

AUTHOR'S PROFILE **166**

LIST OF TABLES

Tables	Title	Page
Table 2.1	Waste Generated from Palm Oil Production (Abdullah & Sulaiman, 2013b)	14
Table 2.2	Comparison Percentage Yield of Phenolics from Various Biomass Sources	16
Table 2.3	Main Sources of Difference Phenolic Compounds	17
Table 2.4	Free Methanol Soluble and Bound Phenolic Of PKC	18
Table 2.5	Physical and Chemical Properties of Phenolic Compound	22
Table 2.6	Application of Phenolic Compound in Various Industries	24
Table 2.7	Different Type of Extraction Method and Percentage Yield of Total Phenolic Content	25
Table 2.8	Different Type of Biomass and Percentage Yield of Phenolic Content	28
Table 2.9	Advantages and Disadvantages of Different Extraction Method	29
Table 2.10	Yield of Phenolic Extraction from Different Extraction Method	30
Table 2.11	GO-Based Adsorbents for Organic Compound Removal	32
Table 2.12	Different GO-Based Adsorbent Used to Remove Phenol from Aqueous Solution	38
Table 2.13	Different Adsorbent Used to Remove Phenol from Aqueous Solution	40
Table 2.14	Advantages and Disadvantages of Different Purification Method and ts Efficiency (Suliman et al., 2023)	41
Table 2.15	Previous Study of Phenolic Adsorption Using Various Adsorbents	47
Table 2.16	Adsorption Parameters Influencing Phenolic Compound Recovery from Different Sources	49
Table 2.17	Isotherm Studies on The Adsorption of Phenolic Compounds Using Various Adsorbents	54

Table 2.18	Thermodynamic Parameters for Adsorption of Phenolic Compounds Using Various Adsorbents	59
Table 2.19	Kinetic Parameters for Adsorption of Phenolic Compounds Using Various Adsorbents	62
Table 3.1	The Chemicals Used for Research Study	65
Table 3.2	The Apparatus Used for Research Study	66
Table 3.3	Summary of Mechanistic Insight Study	81
Table 4.1	Identified Compounds in The Extract Before and After Purification Using 3D-N/rGO Adsorbent Based on LC-MS Analysis	88
Table 4.2	The Macro and Micro-Nutrients Composition of Phenolic Compound Before and After Purification Using 3D/N/rGO Adsorbent	92
Table 4.3	Proximate Analysis of GO and 3D-N/rGO at Different Urea Loading	95
Table 4.4	Summary of BET Analysis	97
Table 4.5	Effect of Temperature on Adsorption Capacity of 3D-N/rGO Adsorbents	107
Table 4.6	Effect of Concentration on Adsorption Capacity of 3D-N/rGO Adsorbents	111
Table 4.7	Effect of Mass adsorbent on Adsorption Capacity of 3D-N/rGO Adsorbents	114
Table 4.8	Pseudo-First-Order and Pseudo-Second-Order Parameters at Different Temperature	117
Table 4.9	Pseudo-First-Order and Pseudo-Second-Order Parameters at Different Concentration	119
Table 4.10	Pseudo-First-Order and Pseudo-Second-Order Parameters at Different Mass of Adsorbent	122
Table 4.11	Thermodynamic Properties of 3D-N/rGO Adsorbent	124
Table 4.12	Summary of Isotherm Model	128

LIST OF FIGURES

Figures	Title	Page
Figure 2.1	*Elais Guineensis* (African oil palm tree) (Bakewell-Stone, 2023)	13
Figure 2.2	Waste generation process in palm oil mill (R. P. Singh et al., 2010)	14
Figure 2.3	Palm Kernel Cake (PKC)	15
Figure 2.4	Structure of Phenolic Compound (Al Mamari, n.d.)	21
Figure 2.5	Groups of Phenolic Compounds	21
Figure 2.6	Microwave-Assisted Extraction (MAE) (Aparamarta et al., 2022)	27
Figure 2.7	Binding of Phenolics to Hydrophobic Adsorbents	34
Figure 2.8	Phenolic Compounds Immobilization on 3D-Graphene Oxide	35
Figure 2.9	The Synthetic Processes and Chemical Structures of Reduced Graphene Oxide, Graphene, and Reduced Graphene Oxide (Bellier et al., 2022)	36
Figure 2.10	Schematic Diagram of Adsorption - Desorption Process (*The General Mechanism of the Adsorption Process. | Download Scientific Diagram*, n.d.)	44
Figure 2.11	Effect of Temperature (Yeddou & Bensmaili, 2007)	50
Figure 2.12	Effect of Concentration (Babu & Gupta, 2005)	51
Figure 2.13	Breakthrough Curve at Varying Adsorbent Masses (Karunarathne & Amarasinghe, 2013)	52
Figure 3.1	Experimental Flowchart for Overall Research Objectives	67
Figure 3.2	Schematic Diagram of MAE	70
Figure 3.3	Schematic Diagram of Continuous Fixed-Bed Column	75
Figure 4.1	Effect of Urea Loading on TPC Before and After Purification	84
Figure 4.2	Effect of Urea Loading on The Adsorption and Desorption of Phenolic Compounds	86
Figure 4.3	LC-MS Chromatograph Results (a) Before Purification and (b) After Purification	90

Figure 4.4	TGA Curves of GO and 3D-N/rGO at Different Urea Loading	94
Figure 4.5	BET Analysis of 3D-N/rGO With Different Urea Loading	97
Figure 4.6	HRTEM Images; (a-b) GO at Different Magnification and (c-d) 3D-N/rGO at Different Magnification.	100
Figure 4.7	FTIR of GO and 3D-N/rGO at Different Urea Loading	102
Figure 4.8	XPS Survey Spectrum of GO and 3D/rGO Before and After Purification; (a) Survey Scan, (b-d) C 1s Spectra, (e-g) N 1s Spectra and (h-j) O 1s Spectra	104
Figure 4.9	Breakthrough Curve at Different Temperatures	107
Figure 4.10	Breakthrough Curve at Different Concentration	110
Figure 4.11	Breakthrough Curve at Different Mass of Adsorbent	113
Figure 4.12	Kinetic Study at Different Temperature; a) Pseudo-First-Order and b) Pseudo-Second-Order	116
Figure 4.13	Kinetic Study at Different Concentration; a) Pseudo-First-Order and b) Pseudo-Second-Order	119
Figure 4.14	Kinetic Study at Different Mass of Adsorbent; a) Pseudo-First-Order and b) Pseudo-Second-Order	121
Figure 4.15	Van't Hoff Equation	123
Figure 4.16	Isotherm Model; a) Langmuir, b) Freundlich, c) Temkin, d) Dubinin-Radushkevic, and e) Redlich-Peterson	128

LIST OF PLATES

Plates	Title	Page
Plate 3.1	Oven Used to Dry PKC	68
Plate 3.2	PKC After Drying	68
Plate 3.3	Synthesis GO Using Modified Hummer Method (Pandey et al., 2022)	72

LIST OF SYMBOLS

Symbols

Co	Initial concentration of phenolic compound (mg/L)
Ce	Varies concentration of phenolic compound (mg/L)
Ct	Concentration of phenolic compound at time t (mg/L)
ΔG^o	Gibbs free energy change (kJ/mol)
ΔH^o	Enthalpy change (kJ/mol)
ΔS^o	Entropy change (kJ/mol.K)
k_1	Pseudo-first-order rate constant (min^{-1})
k_2	Pseudo-second-order rate constant (g/mg.min)
K_F	Freundlich adsorption constant
m	Mass of adsorbent (g)
n	Freundlich intensity parameter
qe	Total adsorption capacity (mg/g)
qt	Adsorption capacity at time t (mg/g)
Q_m	Maximum adsorption capacity (mg/g)
R^2	Correlation coefficient
t	Time (min)
T	Temperature (K)
V	Volume of solution (L)

LIST OF ABBREVIATIONS

Abbreviations

3D-N/rGO	Three-Dimensional Nitrogen Doped Reduced Graphene Oxide
GO	Graphene Oxide
MAE	Microwave-Assisted Extraction
PKC	Palm Kernel Cake
rGO	Reduced Graphene Oxide
TPC	Total Phenolic Content

LIST OF NOMENCLATURE

Nomenclatures

Co	Initial Concentration of Phenolic Compound (mg/L)
Ce	Varies Concentration of Phenolic Compound (mg/L)
Ct	Concentration of Phenolic Compound at Time t (mg/L)
ΔG^o	Gibbs Free Energy Change (kJ/mol)
ΔH^o	Enthalpy Change (kJ/mol)
ΔS^o	Entropy Change (kJ/mol.K)
k_1	Pseudo-First-Order Rate Constant (min^{-1})
k_2	Pseudo-Second-Order Rate Constant (g/mg.min)
K_F	Freundlich Adsorption Constant
m	Mass of Adsorbent (g)
n	Freundlich Intensity Parameter
qe	Total Adsorption Capacity (mg/g)
qt	Adsorption Capacity at Time t (mg/g)
Q_m	Maximum Adsorption Capacity (mg/g)
R^2	Correlation Coefficient
t	Time (min)
T	Temperature (K)
V	Volume of solution (L)

CHAPTER 1
INTRODUCTION

1.1 Research Background

Phenolic compounds are a category of naturally occurring organic molecules distinguished by the presence of one or more hydroxyl groups bonded to an aromatic ring (Lattanzio, 2013). These molecular features are particularly important for their extraction and adsorption behaviour, as the hydroxyl groups impart moderate polarity and hydrogen-bonding capability, while the aromatic rings enable π–π interactions with conjugated carbon-based surfaces. In palm kernel cake (PKC), phenolic compounds are commonly embedded within a complex lignocellulosic matrix, and their polarity allows effective extraction using polar organic solvents such as ethanol (Jing et al., 2025). During purification, the presence of aromatic rings and oxygen-containing functional groups enhances the affinity of phenolic compounds towards hydrophobic and π-electron-rich adsorbent surfaces (Jing et al., 2025). This makes graphene-based materials, particularly nitrogen-doped reduced graphene oxide (3D-N/rGO), highly suitable adsorbents due to their large conjugated π systems, tunable surface polarity, and functional groups capable of hydrogen bonding.

Phenolic compound also derive from diverse precursors, such as simple phenols, phenolic acids, flavonoids, tannins, lignans, and stilbenes, each with distinct structural characteristics and biological functions (Lattanzio, 2013). These secondary metabolites, extensively found in plants, are crucial for structural integrity, pigmentation, and defense systems. Their chemical structure renders them extremely reactive, facilitating interactions with free radicals, chelation of metal ions, and scavenging of reactive oxygen species, so enhancing their potent antioxidant activities (Albuquerque et al., 2021). The characteristics of phenolic compounds have facilitated their use across several sectors such as health and nutrition, pharmaceuticals, cosmetic, food and agriculture (Albuquerque et al., 2021). In health and nutrition, they mitigate oxidative damage associated with chronic illnesses, including cardiovascular ailments, cancer, and neurological disorders (W. Sun & Shahrajabian, 2023). In medications, they demonstrate antibacterial, anti-inflammatory, and anticancer activities, whilst in cosmetics, they are used for anti-aging and skin-protective advantages (W. Sun &

Shahrajabian, 2023). In the food sector, phenolic chemicals serve as natural preservatives, extending shelf life by inhibiting oxidation and microbiological proliferation (Panzella et al., 2020). Furthermore, in agriculture, they are essential for regulating plant development and enhancing insect resistance, hence promoting sustainable agricultural techniques (Albuquerque et al., 2021). The diversity and extensive uses of phenolic compounds highlight the need for further study into their extraction and purification from natural sources.

Impurities in phenolic extracts from natural sources arise from the complex composition of raw materials, which include phytochemicals, inorganic substances, and structural components (Shi et al., 2022a). Proteins can co-extract with phenolics and form complexes that affect their bioactivity, stability, and antioxidant properties. Carbohydrates, particularly polysaccharides like starch and cellulose, can alter the solubility and bioavailability of phenolics, potentially reducing their effectiveness in applications such as food preservation or medicine (Petcharat et al., 2024). Lipids, common in plant tissues, may influence phenolic solubility in aqueous environments, reducing their biological activity. Non-phenolic organic compounds like flavonoids, terpenes, and saponins share solubility properties with phenolics and can complicate the extract's chemical profile, interfering with phenolic bioactivity through synergistic or antagonistic interactions (Cegledi, 2023). Inorganic impurities, such as minerals (calcium, magnesium, potassium) and trace metals (iron, copper, zinc), can bind to phenolics, altering their behavior and potentially reducing stability or catalyzing degradation reactions that decrease antioxidant capacity (Padma et al., 2019). Additionally, plant matrices contain structural components like lignins, cellulose, hemicellulose, and tannins, which can co-extract with phenolics. Lignins, with their polymeric structure, form complexes that reduce bioactivity, while cellulose and hemicellulose may trap phenolics, hindering extraction. Tannins can bind to phenolics, altering their solubility and stability (Padma et al., 2019). These impurities affect the purity, bioactivity, and functionality of phenolic compounds, complicating their use in applications.

Purification of phenolic compounds is necessary to ensure their effectiveness, quality, and suitability for various applications. Phenolic extracts from natural sources often contain impurities such as proteins, carbohydrates, lipids, minerals, and other non-phenolic compounds, which can interfere with the desired properties of phenolics (Sik et al., 2022). These impurities may reduce the stability, bioavailability, and bioactivity

of phenolic compounds, thereby limiting their potential antioxidant, anti-inflammatory, and antimicrobial effects (Shi et al., 2022a). Purification eliminates substances that may interfere with analytical assays, ensuring accurate evaluation of phenolic content and activity. Ultimately, purification enhances the functional quality, stability, and performance of phenolic compounds, allowing them to meet the specific requirements of their intended applications (Shi et al., 2022a). Various methods have been used to eliminate phenolic compounds from diverse feed sources. The techniques include adsorption, solvent extraction, distillation, Fenton's process, membrane filtration, enzymatic treatment, electrochemical oxidation, and cloud point extraction (Suliman et al., 2023).

Among them, adsorption method is a commonly used technique for purifying phytochemical compound from plants since it is high sorption capacity, design simplicity and has large surface area for reaction to occur (Suliman et al., 2023). The procedure involves the attachment of certain substances to a solid surface, referred to as the adsorbent, while impurities are left behind. This method exploits the diverse affinities of various chemicals for the adsorbent material, enabling selective separation. Column chromatography is a frequently used adsorption technique for purifying phytochemicals. The procedure involves filling a column with a dense adsorbent substance, such as activated carbon, silica gel, zeolites, graphene-based materials (graphene oxide and nitrogen-doped reduced graphene oxide and biochar (Doughari, 2012; Liu et al., 2020). Subsequently, the unrefined solution containing the combination of plant-derived chemicals is administered onto the upper part of the column. As the solvent passes through the column, various chemicals interact with the adsorbent to different extents, resulting in their separation. Elution using a solvent gradient or stepwise elution enables the isolation of pure fractions that contain targeted phytochemicals (Doughari, 2012).

1.1.1 Phenolic Compound from Oil Palm Waste

West African oil palm *Elaeis guineensis* is the most important species in the Palmae family (Teoh Cheng, 2002). In recent decades, oil palm production has become Malaysia's most important agriculture-based enterprise (N. Saifuddin et al., 2014). It is an approximately 115.86 million tons of oil palm Fresh Fruit Bunches (FFB) are processed annually in Malaysia (Awoh et al., 2023). This caused Malaysia to overtake

Indonesia as the world's second-largest palm oil producer (N. M. Saifuddin et al., 2018). 200 kg of crude palm oil and 50 kg of crude palm kernel oil come from 1000 kg of oil palm. Thus, palm oil production produces byproducts and solid trash such palm kernel cake (PKC), palm kernel shell (PKS), empty fruit bunch (EFB), and mesocarp fibre (MF), which weigh up to 750 kg (Tungchaisin et al., 2022). Solid waste disposal from the palm oil sector may pose environmental risks as byproducts rise. To address this issue, Malaysia has implemented regulations and policies aimed at reducing solid waste disposal in landfills, encouraging the adoption of sustainable waste management practices (Shakil & …, 2023). These include promoting the utilization of oil palm biomass for value-added applications like bioenergy, animal feed, and adsorbent materials (Nor et al., 2022). Such measures align with the country's commitment to environmental sustainability while maximizing the economic potential of oil palm by-products. In this research study, PKC was selected as the main precursor in this study due to its abundance, low cost, and high potential for value-added applications (Jalani & Zainal, 2024). PKC is a by-product of the palm oil industry, which generates millions of tons annually in Malaysia. Its widespread availability and low market price make it an economically viable precursor for developing advanced materials (Jalani & Zainal, 2024). Furthermore, PKC is rich in carbon content and contains natural organic compounds, making it a suitable candidate for conversion into high-performance adsorbents, such as nitrogen-doped reduced graphene oxide (N-rGO) (life & 2019, 2018).

PKC is a solid byproduct of palm kernel oil extraction (Saw et al., 2012). Since herbivores species use PKC as a feed supplement, its high protein and fibre content makes it an intriguing protein source (Tungchaisin et al., 2022). PKC contains 6.98% essential amino acids as arginine, leucine, valine, phenylalanine, and threonine (Tungchaisin et al., 2022). In PKC, crude protein (CP) ranges from 10.0 to 19.8% and crude fibre (CF) from 13 to 20% (Sharmila et al., 2014). PKC contains hemicellulose, cellulose, lignin, proteins, amino acids, oligosaccharides, phenolics, and phytosterols, according to chemical tests. This chemical has methyl, hydroxyl, and carboxyl functional groups that may enhance biology and therapy. PKC also includes organic acids, water-soluble vitamins, and phenolic antioxidants as flavonoids, polyphenols, and phenolic acids (Oskoueian et al., 2015). The most frequent phytochemicals in palm-based goods are phenolic compounds, terpenes, and sterol (Albuquerque et al., 2021). Among the compounds, the most intriguing phytochemical group is phenolic

compounds that are mainly consists of phenolic acids, flavonoids, tannins, and lignans components. Phenolic molecules, which are often produced as secondary metabolites, may be present in either an unbound or attached form. Their exceptional antioxidant activity stems from their ability to function as chelators of divalent cations, allowing them to eliminate free radicals and disrupt radical chain reactions. The antioxidant characteristic of phenolic compound is mostly due to their redox properties as reducing agents, hydrogen donors, and singlet oxygen quenchers (Gallo et al., 2010).

1.1.2 Microwave-Assisted Extraction for Phenolic Compound

Modern phenolic compound extraction methods comprise of conventional and non-conventional approaches (Osorio-Tobón, 2020). Conventional approach to recovering phenolics compound from solid materials include maceration, Soxhlet extraction, and hot reflux extraction (Osorio-Tobón, 2020). Whereas for non-conventional methods include ultrasound-assisted extraction (UAE), microwave-assisted extraction (MAE), ultrasound-microwave-assisted extraction (UMAE), supercritical fluid extraction (SFE), subcritical water extraction (SCWE), and high hydrostatic pressure processing. These methods minimize the dangerous pollutant emissions by reducing the utilization of organic solvent and are easy to apply (Khoddami et al., 2013). MAE is a new phenolic compound extraction method that take less extraction time, uses small volume of solvents, and simple to perform with a good production of total phenolic content (TPC) and antioxidant activity (AOA) (Gallo et al., 2010). Martino (2006) found that 50% aqueous ethanol with MAE extracted Melilotus officinalis blooming top phytocomponents best (Gallo et al., 2010).

1.1.3 Graphene Oxide in Phenolic Compound Purification

To remove impurities from phenolic compounds three-dimensional nitrogen doped graphene oxide (3D-N/rGO) will be proposed to be used as a hydrophobic adsorbent. The special structure and characteristics of reduced graphene oxide (rGO) make it an essential adsorbent. rGO has a great ability to attract and hold on onto a variety of substances due to its extremely porous and conductive surface (Malik et al., 2021). Strong interactions with molecules are possible due to its structure, especially with those that include aromatic rings. To customise rGO's adsorption characteristics

for certain substances, its surface may be readily altered. The benefit offered by graphene oxide's three-dimensional structure is it has large surface area increases its ability to adsorb substances (Liu et al., 2020).

The hydrophobic characteristic of 3D-N/rGO is further enhanced by nitrogen doped to offer unique advantages that enhance their properties and functionalities (Liu et al., 2020). This leads to an improvement in their responsiveness since the presence of a nitrogen atom on the material's surface generates active sites, facilitating particular interactions with the desired molecules during the adsorption process (Kumar et al., 2024). This modification also resulted in an enhanced adsorption capability for diverse compounds, making the material more flexible in collecting and holding molecules of interest.

1.2 Problem Statement

Palm kernel cake (PKC), a by-product of the palm oil industry, is an underutilised biomass despite its significant potential as a source of phenolic compounds. Phenolic compounds are bioactive molecules known for their strong antioxidant, antimicrobial, and anti-inflammatory properties, making them valuable for applications in the food, pharmaceutical, and cosmetic industries (Albuquerque et al., 2021). For these applications, particularly in pharmaceutical and cosmetic formulations, high phenolic purity and minimal contamination are essential to ensure product safety, stability, and bioactivity (Shakoor et al., 2023). This imposes stricter purification requirements compared to bulk food applications and necessitates the use of selective purification strategies.

Accordingly, an efficient extraction technique is required to recover phenolics from PKC followed by an advanced adsorption-based purification approach employing high-affinity adsorbents capable of selectively separating phenolic compounds from co-extracted impurities such as proteins, carbohydrates, and lignin (Padma et al., 2019). In this study, microwave-assisted extraction (MAE) is employed solely as an efficient technique for extracting phenolic compounds from PKC. However, the extract obtained through MAE still contains co-extracted impurities such as proteins, carbohydrates, and lignin. These impurities interfere with the isolation, purity, and functional quality of phenolic compounds, thereby limiting their application potential. Consequently, purification is a critical step to enhance phenolic quality, bioactivity, and applicability,

while simultaneously contributing to the valorisation of PKC as an agricultural by-product and supporting sustainable resource management. Therefore, extraction alone is insufficient highlighting the need for an effective purification step.

Adsorption-based purification has attracted increasing attention as a promising approach due to its operational simplicity, cost-effectiveness, and scalability. Nevertheless, the efficiency of adsorption processes is highly dependent on the physicochemical properties of the adsorbent and the operating conditions. Conventional adsorbents often exhibit limited adsorption capacity and selectivity when applied to complex biomass-derived extracts such as PKC. Although graphene-based materials have demonstrated potential for phenolic adsorption (Liu et al., 2020), studies specifically focusing on the purification of phenolic compounds from PKC using advanced graphene-based adsorbents remain limited. In particular, the influence of nitrogen doping and three-dimensional structural modification on adsorption performance has not been sufficiently explored for PKC derived phenolics.

The use of 3D nitrogen-doped reduced graphene oxide (3D-N/rGO) as an adsorbent offers unique advantages for phenolic compound purification due to its exceptional physicochemical properties (Liu et al., 2020). The three-dimensional porous structure of 3D-N/rGO provides a high surface area and improved accessibility for adsorption, while nitrogen doping enhances the material's chemical reactivity and binding affinity for phenolic molecules. These properties allow for superior adsorption performance compared to conventional adsorbents. Furthermore, the development of 3D-N/rGO aligns with sustainable practices, as it can be synthesized from renewable biomass such as PKC offering a cost-effective and eco-friendly solution for phenolic compound recovery (Kumar et al., 2024).

Adsorption is subsequently applied as the purification method to selectively separate and recover phenolic compounds from the crude PKC extract. The adsorption process parameters such as adsorption temperature, phenolic concentration, and adsorbent mass were selected because they directly govern adsorption kinetics, thermodynamic behaviour, and adsorption capacity, which are fundamental to understanding adsorbent performance and process feasibility (Ayoob et al., 2024). These parameters are also critical from an industrial perspective as they influence energy requirements, driving force for mass transfer, and adsorbent utilisation efficiency.

In addition, a deeper understanding of adsorption mechanisms through kinetic, isotherm, and thermodynamic analyses is essential to elucidate the interaction behaviour between phenolic compounds and adsorbent surfaces. Isotherm models, such as Langmuir and Freundlich, provide insights into the adsorption behavior, including whether it occurs as a monolayer or multilayer on the adsorbent surface, helping to maximize adsorbent efficiency (Zaini et al., 2023). Thermodynamic parameters, including Gibbs free energy (ΔG°), enthalpy (ΔH°), and entropy (ΔS°) reveal whether the process is spontaneous, endothermic, or exothermic, and determine its feasibility under varying conditions (Y. Li et al., 2012). Kinetic studies, such as pseudo-first-order and pseudo-second-order models, evaluate the rate of adsorption and the controlling mechanisms, such as diffusion or chemical interactions, which are critical for predicting adsorption performance and scaling up the process for industrial applications (Zaini et al., 2023)

Therefore, there is a clear need to investigate the purification of phenolic compounds from PKC with emphasis on the development of an effective adsorbent and systematic evaluation of adsorption behaviour. In this study, phenolic compounds extracted from PKC are purified using three-dimensional nitrogen-doped reduced graphene oxide (3D-N/rGO) (Liu et al., 2020) (Kumar et al., 2024), and the adsorption performance is examined through controlled parameter studies and mechanistic analysis to support efficient phenolic recovery and assess the potential scalability of the purification process.

1.3 Research Objectives

The main objective of this research work is to develop three-dimensional nitrogen-doped reduced graphene oxide (3D-N/rGO) adsorbent to enhance phenolic purification from microwave-assisted extraction of palm kernel cake (PKC). The measurable objectives are:

a) To synthesize and characterize 3D-N/rGO adsorbent with varying urea loadings for enhanced adsorption capacity of phenolic compounds extracted from PKC via microwave-assisted extraction.
b) To study the effect of adsorption process parameters on the purification of phenolic compounds using 3D-N/rGO adsorbent via fixed bed adsorption

column.

c) To elucidate the adsorption mechanism of phenolic compounds onto the 3D-N/rGO adsorbent through isotherms, thermodynamics, and kinetics analyses.

1.4 Scope of Work

This research was structured in several phases aligned with the objectives of the study. The first phase was the preparation of 3D-N/rGO to develop a high-performance adsorbent. The second phase involved the extraction of phenolic compounds from PKC using microwave-assisted extraction (MAE). In the third phase, the synthesized 3D-N/rGO was applied for purification of the extracted phenolics through batch and fixed-bed adsorption–desorption processes. The final phase evaluated the adsorption performance and investigated the adsorption mechanism through isotherm, kinetic, and thermodynamic studies.

The material synthesis and preparation involved producing 3D-N/rGO via a one-pot hydrothermal method using graphene oxide synthesized by the modified Hummer's method. Urea was used as a doping agent for nitrogen doping at varying loadings (0.5, 2, 5, 8, and 10 wt. %), while glucose was employed as a cross-linking agent to construct the 3D porous network. The synthesis was carried out under continuous microwave heating (850 W, 30 minutes) in a nitrogen atmosphere. The resulting materials were characterized using Fourier Transform Infrared Spectroscopy (FTIR), Brunauer–Emmett–Teller (BET) surface area analysis, Thermogravimetric Analysis (TGA), High-Resolution Transmission Electron Microscopy (HRTEM), and X-ray Photoelectron Spectroscopy (XPS) to assess structural features, surface chemistry, thermal stability, and doping efficiency.

The microwave-assisted extraction (MAE) was used to recover phenolic compounds from PKC under constant conditions of 300 W power, 25 minutes extraction time, and a solid-to-liquid ratio of 1:30 (Rosli, Mohd Ariff, et al., 2025). These parameters were maintained constant as they were adopted from previous work in which the MAE conditions had been optimised and validated for efficient phenolic extraction from PKC (Rosli, Mohd Ariff, et al., 2025). The phenolic-rich extract obtained was subsequently purified using the synthesized 3D-N/rGO adsorbent. The purification efficiency was evaluated using both batch and continuous adsorption–desorption

systems. For the batch adsorption tests, 1 g of the adsorbent was mixed with the phenolic solution in 100 mL conical flasks, sealed with parafilm, and agitated at 300 rpm for 60 minutes at 30 °C. Optimum adsorption conditions were then selected for further analysis via Liquid Chromatography–Mass Spectrometry (LC–MS).

The continuous adsorption–desorption studies were conducted in a fixed-bed column setup where the phenolic-rich solution was passed through a column packed with 10% 3D-N/rGO adsorbent. The 10% 3D-N/rGO packing ratio was selected from objective 1 findings. A fixed volume of 250 mL phenolic solution was maintained for all experiments, with the flow rate set at 4.17 mL/min. The effluent was collected at regular 5-minute intervals for a total duration of 60 minutes to construct breakthrough and desorption profiles, allowing evaluation of adsorption capacity. Adsorption performance evaluation involved optimizing key parameters including phenolic concentration (50–150 mg/L), adsorption temperature (30–70 °C), and adsorbent dosage (0.50–1.50 g). The total phenolic content (TPC) in both adsorption and desorption samples was measured using the Folin–Ciocalteu method to determine recovery efficiency.

Lastly, the adsorption mechanism was studied by fitting the experimental data to isotherm models (Langmuir, Freundlich, Temkin, Dubinin–Radushkevich, and Redlich–Peterson), kinetic models (pseudo-first-order and pseudo-second-order), and thermodynamic analysis using the Van't Hoff equation. These models provided insights into adsorption behaviour, surface interactions, energy changes, and the feasibility of phenolic recovery using the developed 3D-N/rGO adsorbent.

1.5 Significance of Study

This study introduces a novel synthesis approach for three-dimensional nitrogen-doped reduced graphene oxide (3D-N/rGO) with tailored nitrogen content, achieved through controlled urea loading. The work advances the understanding of how material structure and surface chemistry influence adsorption performance and selectivity in the purification of phenolic compounds. In addition, it contributes comprehensive datasets on adsorption isotherms, kinetics, and thermodynamics, providing valuable mechanistic insights into the interaction between phenolic compounds and graphene-based adsorbents.

From an industrial perspective, the research supports the palm oil sector by developing an efficient and selective purification method for phenolic compounds derived from palm kernel cake (PKC), an abundant yet underutilized byproduct. The integration of microwave-assisted extraction with advanced adsorbent technology demonstrates a rapid, energy-efficient process for recovering high-value bioactive compounds. This approach is scalable and adaptable for incorporation into existing biomass valorisation systems, ultimately enhancing both resource efficiency and product quality.

The study also promotes the valorisation of PKC, reducing agro-industrial waste disposal issues and supporting the principles of a circular economy. It encourages the sustainable production of phenolic antioxidants for applications in the food, pharmaceutical, and cosmetic industries. Furthermore, the approach aligns with Malaysia's bioeconomy agenda by transforming low-value biomass into commercially viable products, potentially creating new income streams and economic opportunities for rural and local communities.

Importantly, this research addresses a critical gap in the study of 3D nitrogen-doped rGO for phenolic purification from PKC extracts. Conventional adsorbents often face challenges such as low selectivity, poor reusability, and slow adsorption rates. By demonstrating the superior performance of 3D-N/rGO in phenolic recovery, this study overcomes these limitations, offering a more efficient, reusable, and high-selectivity adsorbent that holds promise for broader applications in sustainable bioresource utilisation.

CHAPTER 2
LITERATURE REVIEW

2.1 Introduction

This chapter reviews the key concepts and literature relevant to this study. The importance of phenolic compounds lies in their potent antioxidant, anti-inflammatory, and therapeutic properties, making them valuable for food, nutraceutical, and pharmaceutical applications. Recovering these compounds from agro-industrial waste offers environmental and economic benefits by reducing waste and creating high-value products. Palm kernel cake (PKC), a by-product of the palm oil industry, is rich in phenolics but remains underutilized due to its complex composition and interfering substances. While purification is crucial to improve extract quality, conventional methods often suffer from high solvent use, long processing times, and low selectivity. Three-dimensional nitrogen-doped reduced graphene oxide (3D-N/rGO), with its high surface area, tunable surface chemistry, and abundant active sites, presents a promising alternative for efficient adsorption-based purification.

2.2 Palm Kernel Cake (PKC) in Palm Oil Industry

The palm oil industry is one of the world's most important agricultural sectors, with *Elaeis guineensis* (African oil palm) cultivated extensively in tropical regions as depicted in Figure 2.1. Originally native to West Africa, oil palm is now grown commercially in Southeast Asia, Latin America, and parts of Africa. Global demand for palm oil continues to rise, driven largely by economic growth in major importing countries such as China and India. Malaysia alongside Indonesia is a dominant producer contributing significantly to global supply and export earnings. Over the past four decades, Malaysia's palm oil industry has expanded rapidly, positioning the country as the second-largest producer and exporter worldwide, generating billions in revenue and providing employment to millions (Bazargan et al., 2015).



Figure 2.1 *Elais Guineensis* (African oil palm tree) (Bakewell-Stone, 2023)

The processing of palm oil generates substantial quantities of both solid and liquid wastes as shown Figure 2.2 and Table 2.1. Solid wastes include empty fruit bunches (EFB), palm pressed fibre (PPF), palm kernel shell (PKS), and palm kernel cake (PKC), while liquid waste is primarily palm oil mill effluent (POME) (R. P. Singh et al., 2010). On average, processing one metric tonne of oil palm fruit produces approximately 0.07 tonnes of PKS, 0.103 tonnes of fibre, and 0.012 tonnes of kernels (Razuan et al., 2011). If improperly managed, these waste streams contribute to environmental issues such as greenhouse gas (GHG) emissions from biomass decomposition, water and soil pollution from POME discharge, and landfill burden from solid waste accumulation.

In recent years, research has focused on valorising these byproducts to mitigate environmental impacts while generating additional revenue. Potential valorisation routes include conversion to biofuels, production of activated carbon, synthesis of high-value chemicals, and extraction of bioactive compounds. This aligns with a growing trend towards sustainable resource utilisation, replacing the traditional disposal-oriented approach with circular economy practices (Abdullah & Sulaiman, 2013a). Among these waste streams, PKC has emerged as a particularly promising feedstock for value-added applications.

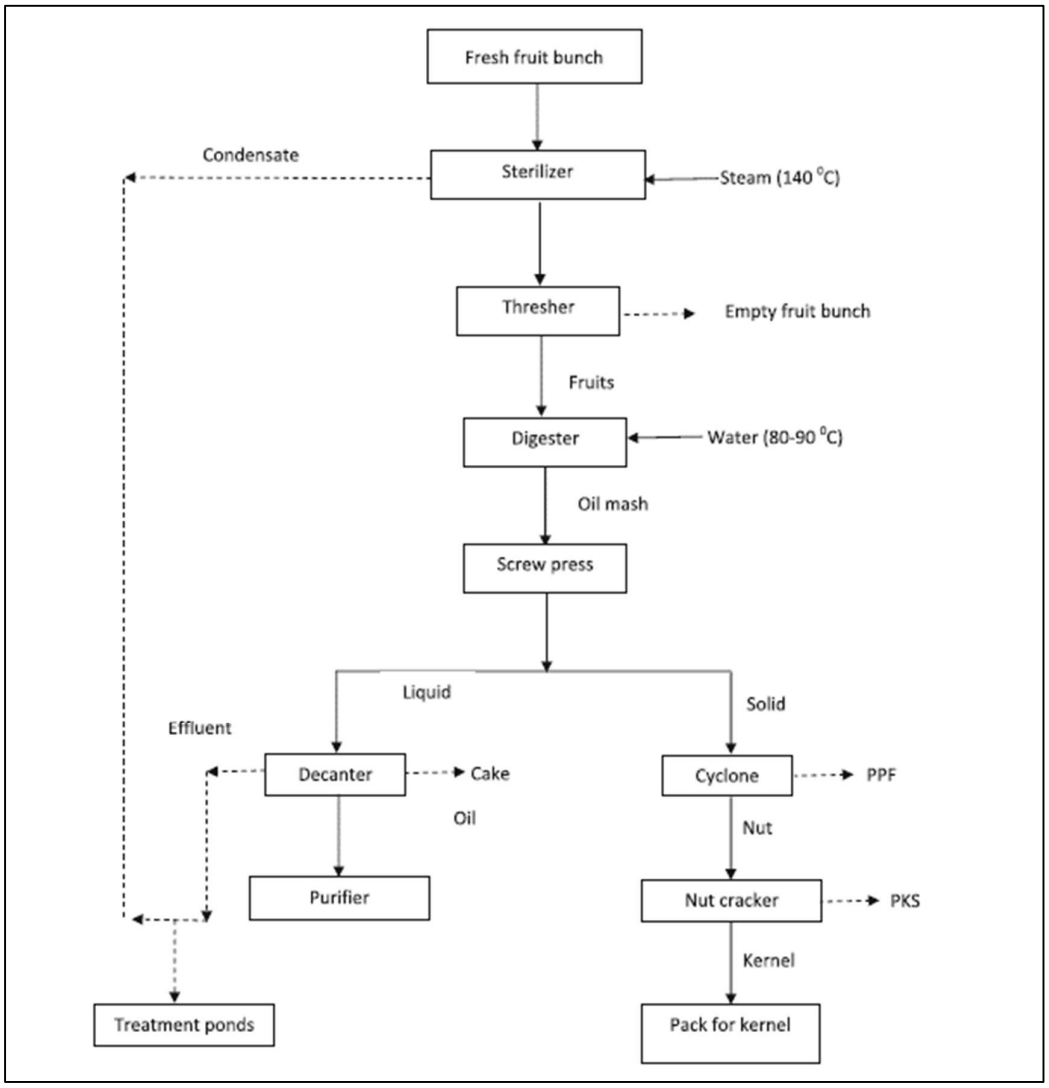


Figure 2.2 Waste Generation Process in Palm Oil Mill (R. P. Singh et al., 2010)

Table 2.1
Waste Generated from Palm Oil Production (Abdullah & Sulaiman, 2013b)

Wastes	**Quantity (ktonnes)**
Fronds	46837
Empty fruit brunches (EFB)	18022
Palm pressed fibres (PPF)	11059
Oil palm trunks (OTP)	10827
Shell	4506

PKC (Figure 2.3) is a secondary product of palm kernel oil extraction, obtained either through mechanical pressing (expeller or screw press) or solvent extraction. Annual production volumes are significant, given Malaysia's scale of palm oil operations. Compositionally, PKC is rich in fibre and protein, contains residual oil, and exhibits specific moisture content and particle size characteristics that make it suitable for processing (Azizi et al., 2021). Despite its nutrient-rich profile, PKC is predominantly used as low-cost animal feed, limiting its market value. This is a missed opportunity, as PKC also contains phenolic compounds with antioxidant, antimicrobial, and other bioactive properties that are highly sought after in the food, pharmaceutical, and cosmetic industries.

Given its abundance in Malaysia and its phytochemical richness, PKC represents a sustainable and underexploited feedstock for high-value product recovery. This study focuses on developing an efficient purification method to recover phenolic compounds from PKC, contributing both to waste valorisation and to the broader goals of sustainable biomass utilisation.



Figure 2.3 Palm Kernel Cake (PKC)

2.3 Phenolic Compounds in PKC

PKC is a solid by-product of palm kernel oil extraction that contains various phytochemicals, including phenolic compounds with strong antioxidant, antimicrobial, and anti-inflammatory properties. In PKC, phenolics occur in both free and bound forms, contributing to its functional and bioactive potential. The phenolic profile of PKC includes p-hydroxybenzoic acid, protocatechuic acid, caffeic acid, ferulic acid, and vanillic acid, with p-hydroxybenzoic acid reported as the predominant phenolic, accounting for a total phenolic content of 18.2% in PKC extract according to Kua et al.

(Kua et al., 2015). The relevance of these phenolic compounds to adsorption lies in their common molecular features rather than their individual identities. Phenolics such as p-hydroxybenzoic acid, protocatechuic acid, caffeic acid, ferulic acid, and vanillic acid share aromatic rings and multiple hydroxyl and carboxyl functional groups, which govern their interaction behaviour during adsorption. These functional groups enable π–π interactions with graphitic domains as well as hydrogen bonding with surface heteroatoms on nitrogen-doped adsorbents.

Compared to other biomass sources, PKC exhibits a distinct phenolic composition and competitive yield. For example, *Centella asiatica L.* contains 122% phenolic acids [40], *Vitis vinifera L*. flavonols range from 112–308% (Gutiérrez-Gamboa et al., 2020), and *Melissa officinalis L*. contains 59% rosmarinic acid (Pistelli et al., 2019). As summarized in Table 2.2, this variation in phenolic yield among biomass sources underscores PKC's viability as a low-cost and abundant feedstock for phenolic recovery.

Table 2.2
Comparison Percentage Yield of Phenolics from Various Biomass Sources

Type of Phenolic	Type of Biomass	% Yield	Reference
Phenolic acids	Centella asiatica L.	122%	(Złotek et al., 2019)
Flavonoids Flavonols	Vitis vinifera L.	112%-308%	(Gutiérrez-Gamboa et al., 2020)
Anthocyanins	Vitis vinifera L. cv. Tinto Cao	47%-82.45%	(R. K. Singh et al., 2020)
Rosmarinic acid	Melissa officinalis L.	59%	(Pistelli et al., 2019)
Resveratrol	Morus alba L.	43%	(Komaikul et al., 2019)
Flavones	Triticum aestivum L.	35%-58%	(Złotek et al., 2019)

2.3.1 Phytochemical Compounds

Phenolic compounds are the main compounds produced during the secondary metabolic process in plants. Phytochemicals are known for their bioactive properties, including antioxidant, antimicrobial, and anti-inflammatory effects. While PKC is often considered a low-value by-product of palm kernel oil extraction and mainly used as animal feed, recent studies highlight its rich phytochemical profile, making it a promising source of compounds for nutraceuticals, functional foods, natural

antioxidants, and environmentally friendly chemical production. This positions PKC as a sustainable feedstock for value-added applications in multiple industries.

The primary phytochemicals in PKC are phenolic compounds, which are well-recognised for their strong antioxidant capacity. In addition, PKC contains antioxidant peptides and protein hydrolysates, both of which contribute to free radical scavenging activity. Other potential phytochemicals reported include tannins (which may contribute to antimicrobial activity), flavonoids (trace levels in some extracts), lignans, and other phenolic derivatives, although data on these compounds remain limited (Albuquerque et al., 2021). Table 2.3 shows the main sources of difference phenolic compounds.

Table 2.3
Main Sources of Difference Phenolic Compounds

Phenolic compounds	**Biomass sources**	**References**
Phenolic acids Hydroxybenzoic acids	Berries, rye, mustard, vegetables, berries, grapes, tea, and wine	(Albuquerque et al., 2021)
Hydroxycinnamic acids	Cereal grains, fruits, mushrooms, rice, coffee, propolis, carrot, coffee, garlic, grapes, spinach, and tomatoes	(Albuquerque et al., 2021)
Flavonoids Flavonols	Cabbage, cauliflower, propolis, spinach, berries, herbs, vegetables, apples, berries, onion, and pears	(Albuquerque et al., 2021)
Flavones	Fruit, vegetables, citrus fruits, broccoli, celery, and green peppers	(Albuquerque et al., 2021)
Flavanols	Berries, cacao, green tea, and grapes	(Albuquerque et al., 2021)
Flavanones	Citrus fruits, and grapefruit	(Albuquerque et al., 2021)
Isoflavones	Soybeans, soy products, berries, grapes, and purple carrot	(Albuquerque et al., 2021)
Tannins Epigallocatechin gallate	Apples, berries, and cacao	(Albuquerque et al., 2021)
Stilbenes Resveratrol	Berries, grapes, and peanuts	(Albuquerque et al., 2021)
Lignans	Flaxseed and sesame	(Albuquerque et al., 2021)

Phenolic compounds dominate PKC's phytochemical composition and are responsible for most of its antioxidant activity. Studies report a Total Phenolic Content (TPC) of around 5.19 mg GAE/g, which is higher than in other palm oil by-products. Specific phenolic acids identified include caffeoylshikimic acid (10,800 mg/kg), p-hydroxybenzoic acid (7,000 mg/kg), and protocatechuic acid (6,000 mg/kg) (Kua et al., 2015). PKC extracts have also been shown to contain hydroxybenzoic acid derivatives, 4H-pyran-4-one, d-glucuronic acid, quinic acid, salicylic acid, and sinapic acid in varying proportions, depending on the extraction method and temperature as depicted in Table 2.4.

Table 2.4
Free Methanol Soluble and Bound Phenolic Of PKC

Content (µg/g of dry weight)

Phenolic	**Free methanol soluble phenolics**		**Cell wall bound phenolics**	**Total**	**Reference**
	25℃	**60℃**			
Caffeic acid	0.60±0.03	1.02±0.05	0.99±0.06	2.61	(Kua et al., 2015)
d-Glucuronic acid	1.01±0.05	Not detected	Not detected	1.01	(Kua et al., 2015)
Ferulic acid	0.63±0.04	0.94±0.02	10.53±0.46	12.10	(Kua et al., 2015)
Glutaric acid	1.45±0.11	2.44±0.14	3.67±0.27	7.56	(Kua et al., 2015)
Protocetechuic acid	25.67±1.69	43.75±3.80	10.68±0.64	80.10	(Kua et al., 2015)
P-Coumaric acid	0.89±0.02	1.65±0.11	7.88±0.53	10.42	(Kua et al., 2015)
P-Hydroxybenzoic acid	99.83±0.69	268.71±2.35	158.67±6.72	527.21	(Kua et al., 2015)

Quinic acid	4.70±0.45	4.99±0.38	Not detected	9.69	(Kua et al., 2015)
Salicylic acid	Not detected	Not detected	0.16±0.04	0.16	(Kua et al., 2015)
Shikimic acid	6.95±0.32	8.93±0.72	1.51±0.38	17.39	(Kua et al., 2015)
Sinapic acid	Not detected	Not detected	1.51±0.06	1.51	(Kua et al., 2015)
Syringic acid	1.15±0.02	1.91±0.07	1.83±0.07	4.89	(Kua et al., 2015)
Vanillic acid	8.20±0.10	15.58±0.25	12.77±0.37	36.55	(Kua et al., 2015)
Total phenolics	151.08	349.92	210.20	711.20	(Kua et al., 2015)
Total phenolics (%)	21.24	49.20	29.56	100	(Kua et al., 2015)

The phytochemical profile of PKC is influenced by several factors. Oil palm variety and genetic differences affect compound concentrations. Processing methods such as mechanical pressing versus solvent extraction impact phenolic yield and composition. Storage conditions, including exposure to oxygen, can lead to oxidation and degradation, reducing biological activity. Despite these insights, there is limited comprehensive profiling of PKC phytochemicals and a lack of correlation studies linking compound concentration to specific biological activities.

Feedstock variability in PKC, arising from differences in oil palm variety, processing conditions, and storage history can influence the concentration and composition of phenolic compounds entering the purification stage. Variations in phenolic content and molecular distribution may affect adsorption performance by altering the availability of aromatic rings and hydroxyl functional groups responsible for π–π interactions and hydrogen bonding with the adsorbent surface. From a process perspective, such variability may lead to fluctuations in adsorption capacity and

breakthrough behaviour, particularly in continuous fixed-bed systems. However, adsorption-based purification offers inherent robustness as adsorbent performance is governed primarily by surface chemistry rather than precise feed composition. Although PKC has traditionally been used as animal feed, it contains abundant phenolic acids and antioxidant peptides, along with minor phytochemicals, offering significant potential for high-value applications in the food, pharmaceutical, and cosmetic industries.

2.3.2 Phenolic Compounds

Phenols are compounds characterized by the presence of an aromatic ring directly bonded to one or more hydroxyl groups. They have resemblance to alcohols with an aliphatic configuration, whereby a hydroxyl group is attached to a carbon chain. Nevertheless, the presence of an aromatic ring, has an impact on the hydrogen atom of the phenolic hydroxyl group as shown Figure 2.4. Due to their instability, phenols exhibit mild acidic properties. The term "phenolic" encompasses a wide range of chemical compounds. Phenolic compounds are categorized into two groups which are simple phenolic molecules and highly polymerized compounds. This classification is based on their structural features, which consist of an aromatic ring with one or more hydroxyl substituents (Kumar et al., 2020). This classification has important implications for extraction and adsorption processes. Simple phenolic compounds possess lower molecular weight and smaller size allowing easier solvent penetration during extraction and faster diffusion into adsorbent pores (Papaoikonomou et al., 2021). In contrast, highly polymerized phenolics are larger and more complex, which can impose mass transfer limitations and restrict access to internal adsorption sites (Saputera et al., 2021). Therefore, molecular size and structural complexity directly influence adsorption efficiency, supporting the use of mesoporous adsorbents such as 3D-N/rGO that provide accessible pore structures and abundant surface active sites for phenolic adsorption.

Structurally, phenolic compounds exhibit distinct variations, leading to their categorization into five major groups: phenolic acids, flavonoids, tannins, stilbenes, and lignans as presents in Figure 2.5 (Albuquerque et al., 2021). Phenolic acids include hydroxybenzoic and hydroxycinnamic acids; flavonoids encompass subclasses such as flavonols, flavones, flavanols, flavanones, and isoflavones tannins can be hydrolysable

or condensed stilbenes are typified by compounds like resveratrol and lignans are characterized by a phenylpropanoid core. These chemicals may be present in a wide range of substances, such as fruits and vegetables.

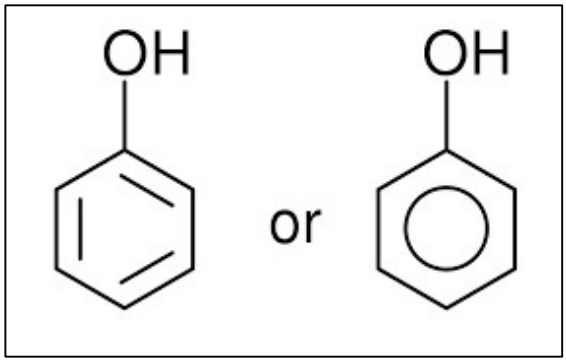


Figure 2.4 Structure of Phenolic Compound (Al Mamari, n.d.)

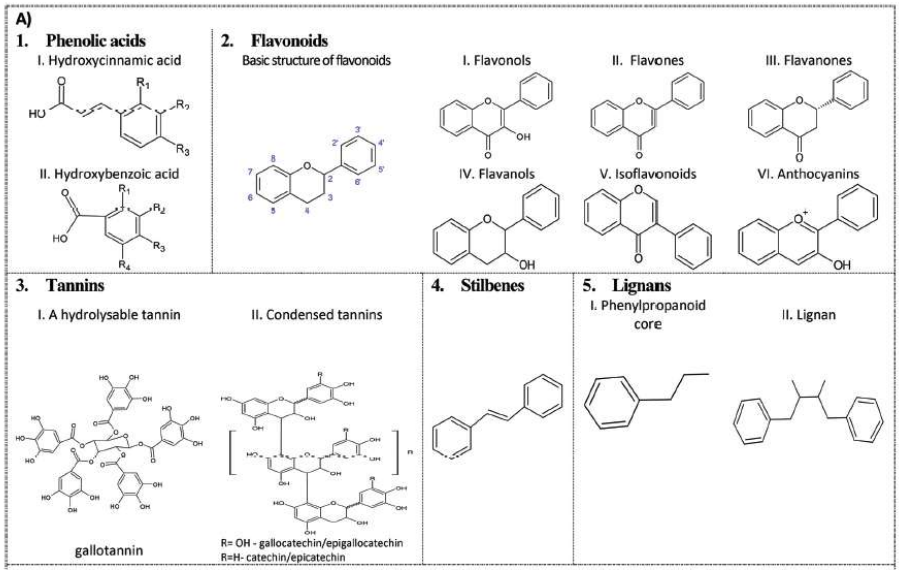


Figure 2.5 Groups of Phenolic Compounds

Table 2.5 summarises the key physical and chemical properties of phenolic compounds that influence their extraction, stability, and purification behaviour. PKC-derived phenolics are predominantly aromatic molecules containing multiple hydroxyl groups, giving rise to moderate polarity, hydrogen-bonding capability, and π-electron–rich structures. These characteristics favour strong interactions with carbon-based adsorbents through π–π stacking between aromatic rings, hydrogen bonding with surface functional groups, and electrostatic interactions influenced by phenolic pKa. The presence and position of hydroxyl groups further govern solubility and adsorption

affinity, making surface chemistry more critical than molecular weight alone. Consequently, the combination of aromatic structure and polar functional groups in PKC phenolics justifies the selection of nitrogen-doped reduced graphene oxide as an effective adsorbent for selective phenolic purification.

Table 2.5
Physical and Chemical Properties of Phenolic Compound

Property	Description	Reference
Physical Properties		
Molecular weight	94.11–500 g/mol (depending on structure, e.g., phenol to complex tannins)	(Sada Khan et al., 2021)
Solubility	Soluble in polar solvents (e.g., water, ethanol, methanol), poor solubility in non-polar solvents	(Ghaffar et al., 2025)
Melting point	Varies widely; simple phenols 40–45 °C, complex phenolics >200 °C	(Lama-Muñoz et al., 2022)
Boiling point	Simple phenols ~181–200 °C; higher for polyphenols	(Cotas et al., 2020)
Chemical Properties		
pKa	8.5–10.0 (weak acids)	(Gopal et al., 2020)
Polarity	High polarity due to hydroxyl group, enhances hydrogen bonding	(Farooq et al., 2021)
Stability	Sensitive to light, oxygen, and heat; prone to oxidation	(Arruda et al., 2020)
Functional groups	Hydroxyl (-OH) attached to aromatic ring; possible methoxy (-OCH_3) and carbonyl groups	(J. Chen et al., 2020)
Colour	Colourless to light yellow in pure form; darkens upon oxidation	(Ercoli et al., 2021)
Antioxidant activity	High due to hydrogen donation from hydroxyl groups	(Farooq et al., 2021)

2.3.3 Application of Phenolic Compounds

Phenolic compounds find use in several industries such as food preservation, food and packaging, cosmetics, and textile sectors due to their inherent antioxidant, antibacterial, and coloration properties. The food industry utilizes the antioxidant and antibacterial properties of phenolic extract derived from Litchi chinensis Sonn as a means of preservation. The addition of pericarp in sheep meat nuggets demonstrated a similar reduction in lipid peroxidation as that seen with the use of BHT (butylated hydroxyl toluene). The cosmetics sector has had parallel growth with the food industry, which has increasingly included natural components in its products. Cosmeceutical formulations use bioactive phenolic chemicals. The absorption of ultraviolet (UV) light is facilitated by the presence of phenolic components. The presence of chromophores within their molecular structure serves to impede the penetration of solar light into the skin. According to a study, the compounds quercetin, resveratrol, and hydroxycinnamic acids have been shown to have a sun protection factor (SPF) ranging from 7 to 30.3 (Albuquerque et al., 2021). Phenolics derived from fruits have been reported to be used in the therapeutic or preventive management of cardiovascular illnesses, colon cancer, and digestive health. The citation provided is in the format of a numerical reference, indicating that the user is referring. In addition, phenolic compounds are used in the production of packaging compositions with antibacterial and antioxidant properties. Anthocyanins, a class of flavonoids known for their antioxidant properties and characteristic pigmentation, have the potential to impede the lipid oxidation process in olive oil when included into its packaging. The textile industry has seen a notable rise in the use of biodegradable phenolic dyes. Oak bark is a source of natural colours, including gallotannin, ellagitannin, quercetin, and extracts from red, black, and green tea. These dyes have been shown to provide protection against ultraviolet (UV) radiation for silk and cotton materials (Carpentieri et al., 2021). Table 2.6 shows the application of phenolic compounds in various industries.

Table 2.6
Application of Phenolic Compound in Various Industries

Phenolic Compound Industrial Application	Effect	Reference
Pharmaceutical Industry	Therapeutic agent for: • Diabetes • Cancer • Neurological disease • Cardiovascular disease	(Albuquerque et al., 2021)
Cosmetic Industry	• Antimicrobial action • Antioxidant action • Anti-inflammatory action • Tyrosinase inhibitor • UV protection	(Albuquerque et al., 2021)
Packaging Industry	• Antioxidant action • Antimicrobial action • Colour indicator for deterioration	(Albuquerque et al., 2021)
Textile Industry	• Natural dye • UV protection • Antimicrobial action • Antifungal action	(Albuquerque et al., 2021)
Food Industry	• Food additives: Natural preservative and natural colorant • Functional ingredient	(Albuquerque et al., 2021)

2.4 Extraction of Phenolic Compounds

Phenolic compounds can be obtained from various biomass sources using different extraction methods, each with its own advantages and limitations. Conventional techniques, such as solvent extraction, Soxhlet extraction, and maceration, are commonly applied due to their simplicity and established protocols, but they are often time-consuming and require large amounts of solvent. In contrast, modern techniques like microwave-assisted extraction (MAE) offer faster processing, higher efficiency, and better yields by enhancing mass transfer and reducing extraction time. Despite these advances, challenges in phenolic compound recovery remain, including the presence of impurities, low extraction yield for certain materials, and the limitations of existing purification approaches.

As summarised in Table 2.7, microwave-assisted extraction (MAE) demonstrates clear advantages over other extraction techniques in terms of extraction time, solvent efficiency, and phenolic yield. MAE achieved the highest total phenolic content (85.64 mg GAE/g) with a significantly shorter extraction time of 2 minutes using an ethanol–water mixture, compared to ultrasound-assisted extraction (UAE), supercritical fluid extraction (SFE), and pressurised liquid extraction (PLE) which required longer processing times (4–210 minutes) and produced lower phenolic yields. The rapid heating and enhanced mass transfer associated with microwave irradiation promote efficient cell wall disruption and phenolic release, while reducing solvent consumption and processing duration. These comparative advantages justify the selection of MAE as the extraction technique in this study, particularly as it provides a high phenolic yield within a short time frame, while subsequent purification is addressed separately using adsorption.

Table 2.7
Different Type of Extraction Method and Percentage Yield of Total Phenolic Content

Extraction Method	Extraction Time (min)	Solvent	Extraction Yield (mg GAE/g)	References
MAE	2	Ethanol:Water: 47:53	85.64	(Osorio-Tobón, 2020)
SFE	210	$scCO_2$:ethanol: 95:5	23	(Osorio-Tobón, 2020)
UAE	4	Ethanol:water: 55:45	54	(Osorio-Tobón, 2020)
PLE	40	Ethanol:water: 75:25	15.9	(Osorio-Tobón, 2020)

2.4.1 Conventional Extraction Techniques

Conventional extraction methods for phenolic compounds primarily rely on solid–liquid extraction, where the desired compounds are separated from plant-based materials into a suitable solvent. Among the most widely used techniques are solvent extraction, Soxhlet extraction, and maceration (Osorio-Tobón, 2020). Solvent

extraction is a relatively simple approach in which the biomass is soaked or stirred in a solvent for a certain duration to allow the dissolution of phenolic compounds (Osorio-Tobón, 2020). Soxhlet extraction, on the other hand, operates through continuous solvent recycling, enabling repeated washing of the sample without the need to replenish fresh solvent (Borenstein et al., 2021). Maceration involves prolonged soaking of the biomass in a solvent at ambient or slightly elevated temperatures, facilitating the diffusion of target compounds into the solvent medium (Kalaskar et al., 2025).

The effectiveness of these methods is strongly influenced by operational parameters such as solvent type, solvent-to-solid ratio, temperature, and extraction time (Luisa et al., 2021). Commonly used solvents include ethanol, methanol, acetone, and water, either individually or in combination, selected based on their polarity to match the solubility characteristics of phenolic compounds (Osorio-Tobón, 2020). While conventional techniques have been extensively applied due to their ease of use, reproducibility, and minimal equipment requirements, they also present notable limitations. These include lengthy extraction times, high solvent and energy consumption, and the potential degradation of thermolabile compounds due to prolonged exposure to heat (Chaves et al., 2020). Furthermore, the selectivity of these methods is often limited, resulting in co-extraction of other plant constituents such as sugars, lipids, and pigments, which may complicate downstream purification (Lee et al., 2021).

2.4.2 Microwave-Assisted Extraction

Among the available techniques, MAE has emerged as one of the most efficient and preferred methods for extracting phenolic compounds due to its ability to reduce extraction time, minimize solvent consumption, increase extraction rates, and improve product quality at a lower operational cost (Gallo et al., 2010). The effectiveness of MAE is largely attributed to the interaction between microwave radiation and the solvent–sample matrix. Microwaves penetrate the sample and cause polar molecules and ionic species within both the solvent and plant material to oscillate rapidly. This oscillation, driven by dipole rotation and ionic conduction, generates localized heating directly inside the matrix rather than relying solely on heat transfer from an external source (Destandau & Michel, 2022).

In solvents such as ethanol, methanol, and water, the absorption of microwave energy depends on their dielectric properties, with high dielectric constant and loss factor facilitating more efficient heating (Destandau & Michel, 2022). This rapid, volumetric heating disrupts plant cell walls, enhances solvent penetration, and accelerates the diffusion of phenolic compounds into the solvent phase. As a result, MAE not only shortens the extraction time but also improves mass transfer efficiency and reduces the degradation of heat-sensitive phenolics compared to prolonged conventional heating (Osorio-Tobón, 2020). Furthermore, the ability to operate at controlled temperatures and pressures allows for selective extraction of target compounds while minimizing co-extraction of impurities. Figure 2.6 presents a schematic diagram of a typical MAE setup.

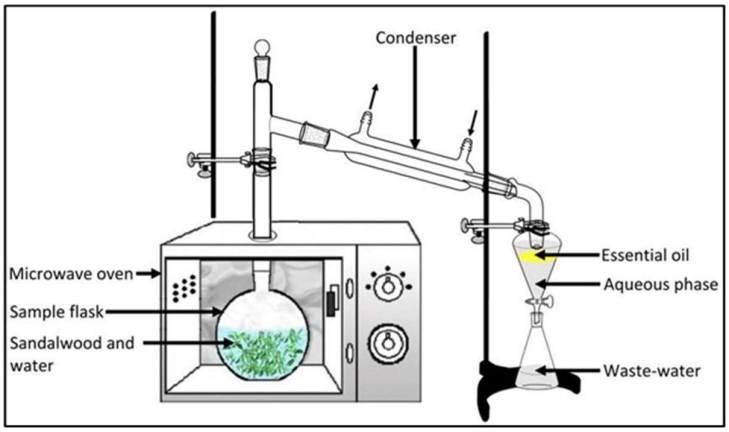


Figure 2.6 Microwave-Assisted Extraction (MAE) (Aparamarta et al., 2022)

The primary determinants impacting the effectiveness of MAE are the ratio of liquid to solid, temperature, microwave power, and extraction time. The recovery of phenolic compounds varies optimally depending on the specific sample and is contingent upon the kind of plant and its active constituent. Extended duration often enhances the solubility of the analyte. Nevertheless, the use of prolonged extraction periods and elevated temperatures often leads to the degradation or undesirable chemical reactions of phenolic compounds, such as enzymatic oxidation (N. M. Saifuddin et al., 2018). Raising the liquid-solid ratio will result in a higher yield of total phenolic content (Tsouko et al., 2019). These results may be attributed to mass transfer mechanisms, namely the enhanced solvent penetration into plant cells, leading to higher release of phenolic chemicals and facilitating their diffusion into the solvent. Table 2.8

displays several types of biomasses and their respective percentage yield extraction of phenolic under three primary parameters of MAE (Tsouko et al., 2019).

Table 2.8
Different Type of Biomass and Percentage Yield of Phenolic Content

Type of biomass	MAE Parameter	Percentage Extraction Yield of Phenolic (%)	References
Peperomia Pellucida	Temperature: 105°C Extraction time: 15 min Microwave power: 850 W	83.33	(Hashim et al., 2020)
Fiddleheads	Liquid-solid ratio: 48.582 Extraction time: 2 min Microwave power: 320W	18.185	(Fabian, 2012)
Pandanus Amaryllifolius	Temperature: 91-92°C Extraction time: 20 min Microwave power: 450W	23.53	(Djenar et al., 2020)
Palm Kernel Cake	Liquid-solid ratio: 7.73:1 Extraction time: 543sec Microwave power: 700 W	31.03	(Tungchaisin et al., 2022)
Melastoma sanguineum fruit	500 W; ~52 °C; ~31% ethanol; ~32 mL/g ratio; 45 min	3.9	(Galal et al., 2019)

2.4.3 Challenges in Phenolic Compound Recovery

Despite the availability of various extraction methods, recovering phenolic compounds from biomass remains a challenge due to multiple factors. One of the most common issues is the presence of impurities such as carbohydrates, proteins, lipids, and pigments, which are often co-extracted along with phenolics. These impurities can reduce the overall purity, complicate downstream analysis, and interfere with bioactivity measurements. In many cases, additional purification steps such as adsorption, liquid–liquid extraction, or membrane separation are necessary. Another key limitation is low extraction yield, especially when phenolics are bound to cell wall components or when extraction parameters are not optimized.

Previous research comparing different extraction methods has highlighted the trade-offs between yield, purity, cost, and scalability as shown in Table 2.9. Advanced techniques like microwave-assisted extraction (MAE) often provide higher yields and

reduced solvent usage, while traditional methods like Soxhlet extraction tend to be less efficient but require simpler equipment.

Table 2.9
Advantages and Disadvantages of Different Extraction Method

Extraction method	Advantages	Disadvantages
Ultrasound Assisted Extraction (UAE)	• Low equipment cost • Low operating temperature • Efficient for thermolabile compounds	• Separation and purification step required • Lack of uniformity in the distribution of ultrasound energy • Large amount of solvent
Microwave Assisted Extraction (MAE)	• High extraction yield • Small equipment size • Low solvent consumption	• High equipment cost • Purification steps required • Very poor efficiency for volatile compounds
Supercritical Fluid Extraction (SFE)	• High extraction yield • Fast extraction • No filtration required	• High equipment cost • Elevated pressure required • Risk of volatile compounds losses
High Pressure Homogenization (HPH)	• High extraction yield • High scalability • Effective in aqueous environments	• Non-selective extraction • Cooling is needed • High energy consumption
Pulsed Electric Fields (PEF)	• Non-destructive • High selectivity • No thermal effect	• Dependence on medium composition (conductivity) • High cost of the equipment

Various extraction techniques provide varying amounts of phenolic compounds. According to Table 2.10, MAE achieved yields of up to 50 mL/g significantly higher than Soxhlet extraction, which produced 7.67 mg GAE/g. Ultrasound-assisted extraction (UAE) and ultrasound/microwave-assisted extraction (UMAE) reported yields of 27.80 mg GAE/g and 20 mL/g, respectively, while subcritical water extraction (SCWE) produced 10–50 mL/g. These findings demonstrate that the MAE approach is the most efficient technique for extracting phenolic compounds from agro-industrial waste, such as PKC.

Table 2.10
Yield of Phenolic Extraction from Different Extraction Method

Extraction Method	Yield Phenolic Extraction	Reference
Ultrasound-Assisted Extraction (UAE)	27.80 mg GAE/g	(Kalia et al., 2008)
Microwave-Assisted Extraction (MAE)	50 mL/g	(Gao et al., 2006)
Ultrasound/Microwave Assisted Extraction (UMAE)	20 mL/g	(Cheng et al., 2011)
Subcritical Water Extraction (SCWE)	10-50 mL/g	(He et al., 2012)
Soxhlet Extraction	7.67 mg GAE/g	(Albayrak et al., 2017b)

2.5 Graphene Oxide

Graphene is a two-dimensional (2D) structure made up of closely spaced, sp2-bonded carbon atoms arranged in a honeycomb lattice (Bellier et al., 2022). Graphene has high modulus, thermal, and electrical conductivity values due to its distinctive structure, which makes it a potential material for several applications. Graphene's chemical functionalization stabilises the material to avoid agglomeration and promotes graphene's dispersion in the polymer matrix. Among the several documented uses of graphene, the most common one is thought to be in the production of nanocomposites, where it is used as an electrically and thermally conductive nanofiller (Bellier et al., 2022). High levels of graphene exfoliation and dispersion in polymer matrices are necessary, nevertheless, in order to get improved electrical and thermal characteristics. One effective method for promoting graphene dispersion in a matrix and stabilising it to avoid agglomeration is chemical functionalization of graphene.

Graphene oxide (GO) is typically synthesised by oxidising graphite using strong oxidising agents and then exfoliating the resulting graphite oxide using either heat treatment or ultrasonic procedures (Bellier et al., 2022). The inclusion of oxygen-containing functional groups, such as hydroxyl, carboxyl, carbonyl, and epoxide, leads to an observed augmentation in the d-spacing of GO. In addition, the presence of oxygen-containing functional groups causes the transformation of planar sp2 oxidised carbon atoms into tetrahedral sp3 by hybridization (Bellier et al., 2022). GO has a high affinity for water due to its strong hydrophilic nature. This is attributed to the presence

of functional groups connected to the basal or edge of the sheets, which facilitate its dispersion in matrices. Furthermore, the existence of oxygen-containing functional groups on the surface of GO results in a very uneven surface, facilitating the bonding between GO and matrixes (Bellier et al., 2022).

2.5.1 GO-Based Adsorbents

Graphene oxide (GO) and GO-based composites have gained significant attention in recent years as highly efficient adsorbents due to their exceptional physicochemical properties such as high surface area, abundant oxygen-containing functional groups, and tunable surface chemistry (Anegbe et al., 2024). These features enhance their interaction with phenolic compounds through mechanisms such as π–π stacking, hydrogen bonding, electrostatic attraction, and hydrophobic interactions. These interaction mechanisms are particularly relevant for PKC phenolics, which possess aromatic rings and hydroxyl groups that favour π–π interactions with graphitic surfaces and hydrogen bonding with surface functional groups (Masoumi et al., 2024). GO can be functionalized with polymers, nanoparticles, or metal oxides to improve selectivity, adsorption capacity, and reusability. Applications of GO-based adsorbents include the removal of dyes, pharmaceuticals, pesticides, and other persistent organic pollutants from water and wastewater (Velusamy et al., 2021). The applications of GO-based adsorbents relevant to phenolic purification because these compounds share common structural features with phenolics, particularly aromatic rings and polar functional groups (Nam et al., 2024). Many dyes and pharmaceuticals contain conjugated aromatic systems similar to phenolic compounds, enabling strong π–π stacking interactions with graphitic surfaces, while their hydroxyl, amine, or carbonyl groups allow hydrogen bonding with oxygen- and nitrogen-containing functionalities on GO.

Table 2.11
GO-Based Adsorbents for Organic Compound Removal

GO-Based Adsorbent	Target Organic Compound	Adsorption Capacity (mg/g)	Reference
Pristine GO	Methylene Blue	714	(Zango et al., 2020)
GO/Fe_3O_4 Nanocomposite	Rhodamine B	277	(Zango et al., 2020)
GO/Chitosan Composite	Bisphenol A	289	(Zango et al., 2020)
Reduced GO (rGO)	Phenol	203	(Zango et al., 2020)
GO/Ag Nanoparticles	Tetracycline	354	(Zango et al., 2020)

GO-based adsorbents demonstrate exceptional adsorption capacities due to their tunable surface chemistry and strong interaction mechanisms with organic molecules as illustrated in Table 2.11. For example, pristine GO shows remarkably high uptake for dyes like methylene blue, while functionalized composites such as GO/chitosan offer enhanced affinity for endocrine-disrupting chemicals like bisphenol A. Magnetic GO composites (e.g., GO/Fe_3O_4) also facilitate easy separation post-treatment, making them attractive for practical applications in wastewater treatment.

2.6 Surface Modification of GO

Graphene oxide (GO) with the chemical formula $C_{54}H_{17}O(OH)_3COOH$ is produced by the oxidation of graphite (Pandey et al., 2022). GO has many functional groups, such as hydroxyl and carboxylic groups at the edges, epoxy groups in the basal planes, as well as phenol and lactone groups . Due to its specific arrangement, GO has amphiphilic characteristics that surpass those of pristine graphene (Pandey et al., 2022). It can be dispersed in polar solvents like water due to its ability to form hydrogen bonds, which is attributed to the presence of hydroxylic and epoxy groups (Pandey et al., 2022). The carbon framework of this chemical may also interact with lipophilic groups. GO is crucial for its amphiphilic characteristics, making it very valuable for biological applications (Ricci et al., 2022). Consequently, there is extensive evidence indicating that materials coated with graphene oxide (GO) improve cell adhesion, proliferation, and differentiation. Due to its properties, GO could connect and collaborate with cells,

growth factors, and hydrophilic substrates to improve the biocompatibility of various cell supports in regenerative medicine.

In this study, surface modification of graphene oxide (GO) was carried out via a one-pot urea-assisted nitrogen doping approach followed by microwave-assisted three-dimensional structuring. Graphene oxide was first prepared using the modified Hummers' method, and nitrogen incorporation was achieved through thermal treatment in the presence of urea, enabling the introduction of nitrogen functionalities into the carbon framework. Different urea loadings were employed to systematically tailor the nitrogen content and surface chemistry of the material. Subsequently, three-dimensional nitrogen-doped reduced graphene oxide (3D-N/rGO) was fabricated through a microwave-assisted self-assembly process using glucose as a cross-linking agent under an inert nitrogen atmosphere. This strategy promoted simultaneous nitrogen doping, partial reduction, and structural reconstruction, transforming layered GO sheets into an interconnected porous three-dimensional network. The combined effect of urea-assisted nitrogen doping and microwave-induced 3D structuring provided synergistic surface modification, enhancing the physicochemical properties of GO and improving its suitability for selective phenolic adsorption in aqueous systems.

There are several limitation and challenges when compared with conventional adsorbents. The synthesis of 3D-N/rGO involves multiple processing steps, including graphene oxide preparation, nitrogen doping, and thermal treatment which can increase material cost and pose challenges for large-scale production relative to low-cost adsorbents such as activated carbon or biomass-derived materials. However, unlike conventional adsorbents like activated carbon that rely primarily on physical adsorption and lack of tunable surface chemistry, 3D-N/rGO exhibits enhanced chemical selectivity through π–π interactions with aromatic phenolic structures and hydrogen bonding facilitated by nitrogen- and oxygen-containing functional groups (Zhang et al., 2019). This selective interaction suppresses the co-adsorption of non-phenolic macronutrients, making 3D-N/rGO more suitable for targeted phenolic purification. In addition, nitrogen doping combined with three-dimensional structuring improves structural stability and adsorption reversibility, partially alleviating concerns related to regeneration and durability.

2.6.1 Hydrophobic Interaction Chromatography (HIC)

The HIC approach utilizes carrier salts with varying polarities, such as ammonium sulphate and sodium chloride, to regulate the affinity of the target components for adsorption onto the hydrophobic adsorbent (de Andrade Lima et al., 2018). Phenolics, known for their significant hydrophobicity, exhibit solubility in polar solvents within supercritical fluid extracts. Similarly, carbohydrates and proteins, characterized by their high hydrophilicity and amphiphilicity, respectively, also demonstrate solubility in these extracts. The constituents mentioned in the extracts are commonly known as 'impurities', thereby providing evidence to support the hypothesis that the hydrophobic adsorption-desorption process is a highly effective method for purifying phenolics. This is because the phenolics become attached to the hydrophobic adsorbent, while the 'impurities' are subsequently separated (de Andrade Lima et al., 2018). To achieve a superior level of purity for the phenolic chemical, it is expected that a hydrophobic adsorption-desorption technique would be used. The procedure presented in this study draws inspiration from the idea of hydrophobic interaction chromatography (HIC). In this approach, the phenolic-rich extract will be adsorbed onto a hydrophobic adsorbent, followed by desorption and subsequent identification using high-performance liquid chromatography (HPLC). The depicted process illustrating the binding of phenolics to hydrophobic adsorbents is shown in Figure 2.7.

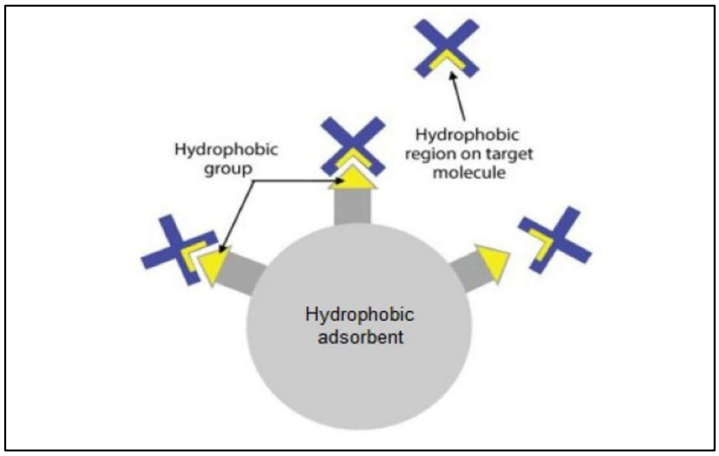


Figure 2.7 Binding of Phenolics to Hydrophobic Adsorbents

Hydrophobic adsorbents may be derived from many materials, such as resins, activated carbon, silica, clay, and graphene oxide (GO). The nanostructure and

physicochemical properties of GO have garnered significant interest in the field of phenolic-rich extract purification. There has been a lack of effort in using GO material for the purification of bioactive extracts. However, the use of GO as a hydrophobic adsorbent for the recovery of phenolic chemicals from industrial wastewater effluent has garnered significant interest (R. Zhao et al., 2021). In their study, Wang et al. successfully achieved the adsorption of phenolic compounds at a rate of 130 mg/g by using a three-dimensional graphene oxide (3D-GO) adsorbent

The 3D-GO adsorbent that was synthesized demonstrated the ability to preserve the interconnectivities of its intimate structure and exhibited a significant increase in active sites and specific surface area. As a result, the adsorption performance was notably enhanced. In addition to the unique architectural features of the 3D GOs, several factors such as electrostatic contact, π-π interaction, hydrophobic effect, hydrogen bond, heteroatom synergy, and the formation of novel active sites played significant roles in the process of immobilization, as seen in Figure 2.8.

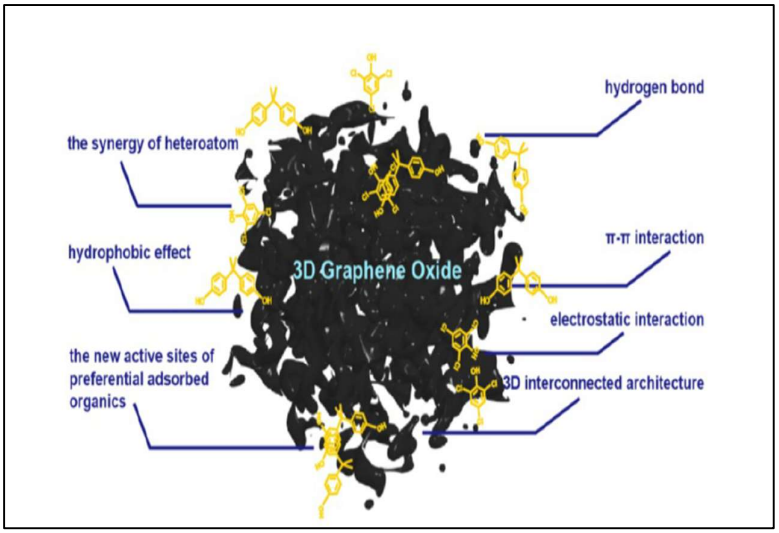


Figure 2.8 Phenolic Compounds Immobilization on 3D-Graphene Oxide

The use of nitrogen-doped reduced GO adsorbent led to a phenolic equilibrium adsorption capacity ranging from 80 to 150 mg/g (R. Zhao et al., 2021). When comparing reduced graphene oxide (rGO) to pure GO, it is observed that rGO exhibits a larger conjugated π area and a higher level of hydrophobicity. The introduction of a nitrogen-containing compound induces nitrogen atoms to selectively replace oxygen-containing functional groups through the process of annealing. This leads to the formation of a three-dimensional hydrophobic nanostructure known as nitrogen-doped

reduced graphene oxide (3D-N/rGO), which exhibits robust hydrophobic and π-π interactions (R. Zhao et al., 2021). The process of nitrogen doping is deemed essential for GO due to its significant impact on the nanostructure properties of the material. According to reports, GO has a significant presence of oxygen-containing functional groups, which exhibit considerable polarity, primarily in the form of negative charges. This polarity enables GO to reject the electronegative charge of phenolic compounds (P. Wang et al., 2019).

In order to confer hydrophobic properties onto graphene oxide GO, the aforementioned limitation may be addressed by the process of reduction or doping of GO with positively charged substances such as chitosan and urea. This approach enables nitrogen doping, therefore diminishing the negative charge associated with GO. The introduction of chitosan or urea during the annealing process leads to the selective substitution of oxygen-containing functional groups by nitrogen atoms. This substitution facilitates the restoration of the conjugated π region, resulting in the formation of a three-dimensional hydrophobic nanostructure known as nitrogen-doped reduced graphene oxide (3D-N-r/GO). The presence of nitrogen atoms in this structure enhances its hydrophobic properties and promotes strong π-π interactions (R. Zhao et al., 2021). The introduction of nitrogen into the three-dimensional graphene oxide (3D-GO) is anticipated to maintain the interconnectivity of the 3D structure, provide a substantial number of active sites, and enhance the specific surface area of the hydrophobic adsorbent. Figure 2.9 shows the synthetic processes and chemical structures of reduced graphene oxide, graphene, and reduced graphene oxide.

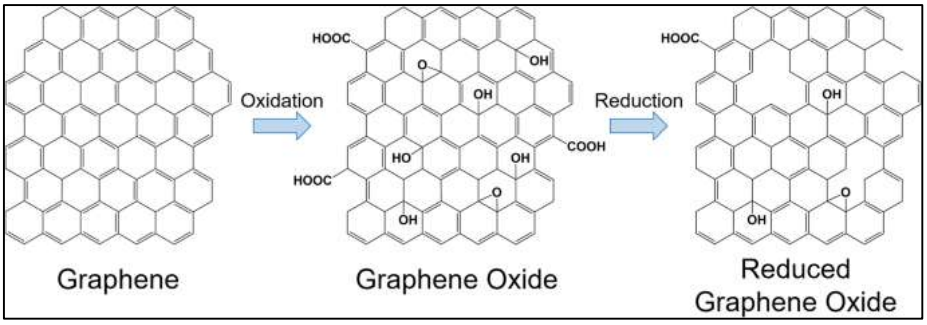


Figure 2.9 The Synthetic Processes and Chemical Structures of Reduced Graphene Oxide, Graphene, and Reduced Graphene Oxide (Bellier et al., 2022)

Although hydrophobic interaction chromatography (HIC) is conventionally employed as a chromatographic separation technique involving salt-mediated binding

and controlled elution, the underlying mechanism of hydrophobic interaction is not limited to chromatographic systems. In this study, the discussion of HIC in Section 2.6.1 is intended to provide the theoretical basis for understanding hydrophobic interaction mechanisms governing phenolic binding. The purification strategy adopted in this work is adsorption-based, which utilises the same hydrophobic interaction principles without the need for high-salt conditions or chromatographic elution. This demonstrates that phenolic compounds preferentially interact with hydrophobic surfaces, and that graphene-based adsorbents with enhanced hydrophobicity and π–π interactions are effective for phenolic immobilisation. Therefore, adsorption was selected as a practical, cost-effective, and scalable alternative to chromatography while remaining conceptually grounded in HIC principles.

2.6.2 Nitrogen doping in rGO

Urea is commonly used as a nitrogen dopant for graphene oxide (GO) to enhance its properties for various applications, including adsorption, catalysis, and energy storage. The process involves heating urea in the presence of graphene oxide, where urea decomposes, releasing ammonia (NH_3) that reacts with the oxygenated groups on the surface of graphene oxide, incorporating nitrogen atoms into the graphene structure (L. Sun, Wang, Tian, Tan, Xie, Shi, Li, & Advances, 2012). This doping introduces nitrogen functional groups such as pyridinic, pyrrolic, and quaternary nitrogen, which improve the material's surface chemistry. Nitrogen doping significantly enhances the adsorption capacity of graphene oxide, as the nitrogen atoms create additional active sites that increase the material's affinity for polar molecules, such as phenolic compounds (H. Zhao et al., 2015). Nitrogen incorporation in nitrogen-doped graphene materials is commonly confirmed using X-ray Photoelectron Spectroscopy (XPS), which enables identification of different nitrogen bonding configurations within the graphene lattice. Previous studies conducted by Kim et al., have reported that the N 1s XPS spectrum of nitrogen-doped reduced graphene oxide typically consists of several characteristic peaks corresponding to pyridinic N (398.1 – 399.3 eV), pyrrolic N (399.8 – 401.2 eV), graphitic N (401.1 – 402.7 eV), and oxidized nitrogen species (402.8 eV) (Kim et al., 2021). These nitrogen functionalities originate from the incorporation of nitrogen atoms into the graphene framework during thermal treatment with nitrogen precursors such as urea, ammonia, or melamine. The presence of these nitrogen

configurations modifies the electronic structure of graphene and introduces additional active sites, which can enhance adsorption interactions and catalytic performance of nitrogen-doped graphene materials (Kim et al., 2021).

Furthermore, nitrogen doping improves the electrical conductivity and stability of graphene oxide by introducing extra charge carriers, which makes the material more efficient in various applications, including sensors and supercapacitors (L. Sun, Wang, Tian, Tan, Xie, Shi, Li, & Advances, 2012). Additionally, nitrogen-doped graphene oxide exhibits improved catalytic properties, which can be useful in applications such as environmental purification, where it can facilitate the removal of pollutants or enhance the recovery of valuable compounds. Urea as a nitrogen source is also cost-effective and environmentally friendly, making it an ideal choice for modifying graphene oxide in sustainable applications. Overall, nitrogen doping of graphene oxide using urea enhances its functional properties, making it a promising material for a wide range of applications, especially in the purification and recovery of phenolic compounds. Table 2.12 shows the different GO-based adsorbent used to remove phenol from aqueous solution.

Table 2.12
Different GO-Based Adsorbent Used to Remove Phenol from Aqueous Solution

GO-Based Adsorbent	Nitrogen Source / Modification	Adsorption Capacity (mg/g)	Target Compound	Reference
N-doped GO (urea)	Urea	241	1-naphthol	(Hashim et al., 2020)
N-doped GO (melamine)	Melamine	198	2-chlorophenol	(Albayrak et al., 2017b)
GO/Fe_3O_4 nanocomposite	Fe_3O_4 nanoparticles	156	Phenol	(Zango et al., 2020)
Sulfonated N-doped GO	Urea + sulfonation	265	4-nitrophenol	(Pandey et al., 2022)
Reduced GO (hydrazine)	Hydrazine	120	Catechol	(Ricci et al., 2022)

Nitrogen-doped GO, particularly using urea, demonstrates superior adsorption capacity compared to many other GO-based adsorbents due to the introduction of active

nitrogen sites (pyridinic, pyrrolic, quaternary), which enhance polar molecule interaction. While melamine-doped GO also shows high adsorption, the slightly lower performance compared to urea-based doping may be due to less uniform nitrogen incorporation. Magnetic GO/Fe_3O_4 composites offer an added benefit of easy separation via magnetic fields but typically have lower adsorption than functionalized nitrogen-doped variants. Sulfonated N-GO achieves the highest adsorption capacities in the table due to the synergistic effect of nitrogen doping and sulfonic acid groups, which enhance electrostatic attraction toward phenolics. Reduced GO prepared with hydrazine has moderate adsorption but lacks the additional functional groups for stronger binding.

Overall, urea-based nitrogen doping offers an optimal balance of performance, cost-effectiveness, and eco-friendliness, making it highly suitable for sustainable phenolic compound recovery applications.

2.6.3 Three-Dimensional (3D) Graphene Structures

In the purification process, the phenolic-rich extract is subjected to filtration via a column that is filled with 3D-N-r-GO. The passage of the extract along the column results in the selective interaction between phenolic chemicals and the adsorbent, resulting in their adsorption. The procedure successfully isolates the phenolic compounds from various contaminants and constituents found in the extract.

Following the process of adsorption, the phenolic compounds may be extracted from the 3D-N/rGO material by using a suitable solvent or employing a desorption technique. The fraction that has been eluted consists of phenolic compounds that have undergone purification and may then undergo further processing or be subjected to analysis in order to determine their quality and concentration. Table 2.13 shows the different adsorbent used to remove phenol from aqueous solution.

Table 2.13
Different Adsorbent Used to Remove Phenol from Aqueous Solution

Adsorbent	Adsorbent Capacity (mg/g)	Reference
M-bentonite	9.9	(Al-Asheh et al., 2003)
AI-Bentonite	8.7	(Al-Asheh et al., 2003)
CTAB-treated bentonite	8.4	(Al-Asheh et al., 2003)
T-bentonite	8.2	(Al-Asheh et al., 2003)
Agro-waste based activated carbon	11.01	(Srihari & Das, 2009)
Graphene oxide nanosheet suspension	1000	(Yu et al., 2016)
Ca-bentonite/chitosan composite	12.496	(Ayoob et al., 2024)
Single wall carbon nanotubes	17.948	(De La Luz-Asunción et al., 2015)
Graphene oxide nanoflak	19-30	(Dakhil & Habib Dakhil, 2013)

Three-dimensional (3D) graphene structures, such as graphene foams, aerogels, and hydrogels, have emerged as advanced materials for adsorption applications due to their interconnected porous networks, high surface area, and excellent mechanical stability. Compared to 2D graphene sheets, 3D structures offer enhanced surface accessibility, reduced aggregation, and easier recovery/reusability after adsorption. Their unique architecture allows efficient mass transfer and rapid adsorption kinetics, making them highly effective for the removal of organic compounds such as dyes, phenols, and antibiotics from aqueous solutions. These properties make 3D graphene materials promising candidates for sustainable water purification systems.

2.7 Purification Technologies

Several techniques have been used to eliminate phenolic compounds from different feed sources. The methods include adsorption, solvent extraction, distillation, Fenton’s procedure, membrane filtering, enzymatic treatment, electrochemical

oxidation, and cloud point extraction. While these methods demonstrate high efficacy in removing phenolic compounds, they are not the most desirable choice due to their drawbacks, including high initial and ongoing expenses, production of secondary pollutants, inability to be reused, and the need for additional treatment to recover phenolic compounds. These limitations hinder their suitability for industrial use. Table 2.14 shows the advantages and disadvantages of different purification method and its efficiency. The purification efficiency refers to the percentage of phenolic compounds successfully recovered or removed from the solution during the purification process (Suliman et al., 2023).

Table 2.14
Advantages and Disadvantages of Different Purification Method and ts Efficiency (Suliman et al., 2023)

Method	Advantages	Disadvantages	Efficiency (%)
Adsorption	• Design simplicity • High sorption capacity • Large surface area for reaction to occur	• High cost for the regeneration system • Low thermal stability • Mechanical weakness	70.7 - 92.5
Solvent extraction	• Easy handling • Low operating cost • Easy to recycle the components involved	• High consumption of energy • Formation of secondary sludge	84.1 - 93.4
Distillation	• Rapid separation • High percentage recovery • Low operating cost	• Need large space for distillation tower • High capital cost	75.0 – 80.0
Fenton's Process	• High efficient at ambient condition of pressure and temperature • No sophisticated equipment needed	• High cost of catalyst synthesis • Narrow optimum pH operating range • Risk associated with handling	98.0 – 99.0
Membrane Filtration	• Mild pressure and temperature required • High operational and maintenance cost • High selectivity	• Membrane fouling •Frequently cleaning procedures • High cake formation	65.0 – 78.1
Enzymatic Treatment	• Rapid process • High selectivity • Cost-saving	• Possibility of enzyme deactivation • Acquired additional	92.3 – 95.0

		additives	
Electrochemical Oxidation	• Operated without the presence of chemical reagent. • Easy to maintain and operate • Eco-friendly method	• Heavily reliant on electrical power • Frequent substitution of electrodes	70.0 - 100
Cloud point extraction	• Biodegradable nature of the extractants • Low energy requirement • Environmental friendly	•Difficulty in automation • Degradation of bioactive compounds • Requirement of further treatment	62.0 – 95.7
Liquid Membrane	• Simple operation • High selectivity • Design simplicity	• Membrane instability • Difficulty in large scale • Lower flux	91.0 – 93.14

The purification of phenolic compounds can be achieved through various methods, each offering distinct operational benefits and limitations. Among the available purification technologies, adsorption has been reported to achieve high purification efficiency due to the strong interactions between phenolic molecules and the active surface sites of adsorbent materials (Suliman et al., 2023). Reported efficiencies for adsorption processes typically range from approximately 70–92%, depending on factors such as surface properties of the adsorbent, operating temperature, and concentration of phenolic compounds. In comparison, solvent extraction techniques may achieve efficiencies ranging from about 84–93%, but these processes often require large amounts of organic solvents and may generate secondary waste streams. Distillation methods, while effective for certain separations, generally exhibit lower efficiency for phenolic purification (approximately 75–80%) and require higher energy input due to the thermal nature of the process. These comparisons indicate that adsorption provides a competitive purification efficiency while maintaining relatively simple operation and lower chemical consumption.

In addition, solvent extraction is widely used due to its ease of handling, relatively low operating cost, and the possibility of recycling solvents (Suliman et al., 2023). However, it often suffers from high energy consumption and the generation of secondary waste streams, such as solvent residues or sludge, which require additional

treatment. Distillation, on the other hand, offers rapid separation and high recovery rates but is associated with high capital costs and the need for large space, making it less practical for small-scale operations (Suliman et al., 2023). Similarly, membrane-based techniques such as membrane filtration and liquid membrane systems exhibit high selectivity and can operate under mild conditions, but they are prone to fouling, membrane instability, and reduced performance over time (Suliman et al., 2023).

Advanced methods such as enzymatic treatment, electrochemical oxidation, and cloud point extraction provide high selectivity, eco-friendly operation, and the potential for lower energy requirements. Nonetheless, these techniques face challenges such as enzyme deactivation, high equipment or catalyst costs, and difficulties in large-scale automation. Fenton's process is recognized for its high efficiency even under ambient conditions, but the high cost of catalysts and narrow pH operating range limit its widespread application (Suliman et al., 2023). In addition, cloud point extraction, despite being environmentally friendly, can lead to the degradation of sensitive bioactive compounds and often requires further downstream purification steps (Suliman et al., 2023).

Among the available techniques, adsorption stands out as a highly promising approach for phenolic compound purification. Its design simplicity, large surface area, and high sorption capacity enable efficient removal of phenolic compounds across a wide range of concentrations. Although the regeneration of adsorbents can be costly and certain materials may exhibit low thermal stability, these limitations are being addressed through the development of advanced adsorbent materials such as functionalized graphene-based composites, which offer improved reusability and selectivity (Suliman et al., 2023). The combination of high efficiency, adaptability to different feedstocks, and potential for scale-up makes adsorption technology a preferable option for sustainable phenolic compound recovery, particularly when integrated with renewable and cost-effective adsorbent materials.

2.7.1 Purification using Adsorption-Desorption Process

Adsorption is a surface phenomenon when atoms, ions, or molecules from a gas, liquid, or dissolved solid stick to the active site of an adsorbent, forming a film of the adsorbate on the adsorbent's surface (Soliman & Moustafa, 2020). The adsorption process may be characterized as the extraction of a material from a liquid or gas by a

solid phase, resulting in a larger concentration or accumulation of the removed adsorbate molecules on the surface of the adsorbent compared to the bulk of the solution. Adsorption has been seen in several systems, including chemical, physical, natural, and biological systems. Furthermore, the adsorption process finds widespread usage in several industrial applications, including heterogeneous catalysts, activated charcoal, adsorption chillers, water purification, and synthetic resins (Soliman & Moustafa, 2020). Figure 2.10 shows the adsorption-desorption combination process of purification.

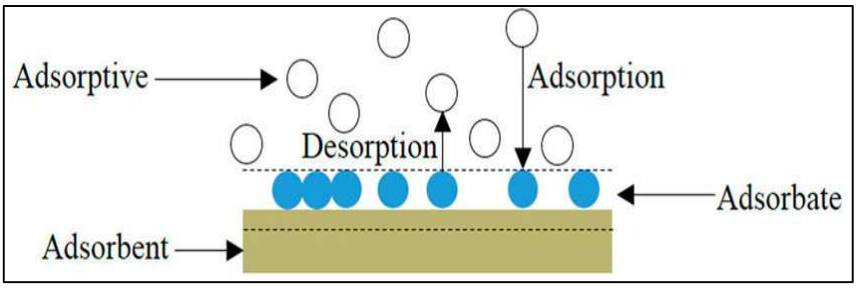


Figure 2.10 Schematic Diagram of Adsorption - Desorption Process (*The General Mechanism of the Adsorption Process. | Download Scientific Diagram*, n.d.)

The adsorption phenomena is characterised by two primary parameters which are adsorbate and adsorbent. On the surface of the adsorbent, the atoms on the outer surface are not completely covered by other atoms of the adsorbent. As a result, they have the ability to attract molecules of adsorbates (Soliman & Moustafa, 2020). The occurrence of the adsorption process is typically due to the difference in environment between the adsorbent atoms on the surface and those in the bulk of the solution. Unlike the surface particles, the bulk particles are surrounded by neighbouring particles from all sides. As a result, the surface molecules have higher energy and residual attractive forces compared to those in the bulk. The force that attracts metal ions to the surface of the adsorbent is known as surface energy, which acts on a per unit surface area basis. The effectiveness of the adsorption process is enhanced by increasing the specific surface area of the adsorbent per unit mass under certain pressure and temperature conditions.

The desorption process, which involves the release of an adsorbate from an adsorbent, is a crucial step in several separation and purification procedures. This process involves the liberation or elimination of molecules that have been adsorbed onto

the surface of the adsorbent, enabling the restoration of the adsorbent and the retrieval of the desired molecules (Ge et al., 2020). Competitive adsorption is a frequently seen process in which a desorption agent and the adsorbed molecules compete for binding sites on the surface of the adsorbent. The desorption agent, often a solvent or chemical compound, has a greater attraction to the adsorbent, causing it to displace and replace the adsorbate. Chemical desorption is a process that modifies the chemical conditions at the locations where adsorption occurs in order to disrupt the interactions between the adsorbent and adsorbate (Ge et al., 2020). This may be accomplished by implementing a chemical desorption agent that interacts with the adsorbed molecules, therefore promoting their liberation. Modifications in physical parameters, such as temperature or pressure, may also influence the desorption process. Elevated temperature supplies the necessary energy to surpass adsorption forces, hence facilitating desorption.

Adsorption column purification is a widely used and efficient method in several sectors for the separation and purification of chemicals from complicated mixtures (Ding et al., 2014). The adsorption column has a densely packed bed of solid material, referred to as the adsorbent, through which the mixture to be cleansed is flowed (Ding et al., 2014). The choice of the adsorbent is crucial since it directly influences the selectivity of adsorption. Typical adsorbent used for adsorption include activated carbon, silica gel, and specialised materials such as zeolites or graphene oxide (GO) (Knaebel, 2016).

During the purification process, the mixture is injected at the uppermost part of the adsorption column. As it passes through the bed, the desired compounds preferentially interact with the adsorbent, sticking to its surface. The interaction is influenced by several forces, including Van der Waals interactions, hydrogen bonding, and electrostatic attractions. The specific forces at play depend on the characteristics of the adsorbent and the molecules being considered as the mixture advances through the column, contaminants and non-target components pass more swiftly through the bed, while the adsorbate remains on the adsorbent surface. The column is engineered to facilitate effective adsorption, ensuring enough duration of interaction between the adsorbent and the mixture.

The adsorption column may be incorporated into a continuous process, and its configuration may vary depending on the specific application, including many columns run in either series or parallel. This approach is extensively used for the purification of compounds in the fields of medicines, chemicals, and environmental remediation. The

effectiveness of the purification process using an adsorption column is impacted by variables such as the rate of flow, height of the bed, and the characteristics of the adsorbate and adsorbent (T. S. Singh & Pant, 2006).

In this study, adsorption–desorption was selected as the purification route following microwave-assisted extraction because it enables selective recovery of phenolic compounds from complex PKC extracts through controlled interaction with the adsorbent surface. The purification performance was systematically evaluated by focusing on key operational parameters which are adsorption temperature, initial phenolic concentration, and adsorbent mass. These variables directly influence adsorption capacity, breakthrough behaviour, and overall phenolic recovery efficiency in the fixed-bed system. Adsorption temperature governs molecular mobility and interaction strength, phenolic concentration determines the mass transfer driving force, and adsorbent mass controls the availability of active binding sites within the column.

2.7.2 Adsorbents in Phenolic Purification

The purification of phenolic compounds from natural sources often involves the use of adsorption techniques due to their efficiency, simplicity, and cost-effectiveness. Adsorbents are critical components of these systems, offering selective binding properties that facilitate the removal of impurities such as proteins, carbohydrates, lipids, and non-phenolic compounds. Numerous materials have been explored for this purpose, including activated carbon, biochar, zeolites, silica gel, and advanced nanomaterials like graphene-based adsorbents. Recent developments in adsorbent technology have focused on enhancing adsorption performance by improving surface area, porosity, and functional group interactions. Among these, three-dimensional nitrogen-doped reduced graphene oxide (3D-N/rGO) has emerged as a promising candidate. The integration of nitrogen doping into reduced graphene oxide enhances its adsorption capacity by introducing active sites for molecular interaction, while the three-dimensional structure maximizes surface area and adsorption efficiency. This study compares various adsorbents, including traditional materials and 3D-N/rGO, to highlight their adsorption capacities, experimental conditions, and suitability for phenolic compound purification. The table below summarizes key adsorbents and their performance metrics. Table 2.15 shows the previous study of adsorption with its adsorption capacity.

Table 2.15
Previous Study of Phenolic Adsorption Using Various Adsorbents

Source of phenolic	Type of Adsorbent	Adsorption capacity (mg/g)	Reference
Bamboo	Biochar's	17	(Zango et al., 2020)
Pine fruit	Biochars	277	(Zango et al., 2020)
Avocado kernel	Activated carbon	3.3	(Zango et al., 2020)
Sugar cane	Activated carbon	27	(Zango et al., 2020)
Banana peel	Activated carbon	2.0	(Zango et al., 2020)
Tea waste	Activated Carbon	132.5	(Zango et al., 2020)
Tetrabromobisphenol	Graphene oxide	10	(Zango et al., 2020)
4-chloro-2-nitrophenol	Graphene	25	(Zango et al., 2020)
2-chlorophenol	Graphene oxide	134	(Zango et al., 2020)
1-naphthanol	Sulfonated graphene	241	(Zango et al., 2020)

Biochar-based adsorbents, derived from sources such as bamboo and pine fruit, demonstrate highly variable capacities, ranging from 17 mg/g for bamboo to an impressive 277 mg/g for pine fruit biochar. This variation can be attributed to differences in surface area, porosity, and the presence of active functional groups, which are influenced by the feedstock composition and pyrolysis conditions. Activated carbon, a widely used commercial adsorbent, also shows a broad capacity range from as low as 2.0 mg/g for banana peel-derived activated carbon to 132.5 mg/g for tea waste-derived activated carbon reflecting the effect of precursor type, activation method, and surface chemistry on adsorption efficiency.

Graphene-based adsorbents exhibit strong potential for phenolic removal due to their high surface area and tunable functional groups. For example, graphene oxide has shown capacities of 10 mg/g for tetrabromobisphenol and up to 134 mg/g for 2-chlorophenol, indicating that adsorption performance is significantly influenced by the molecular structure and polarity of the target phenolic compound. Similarly, functionalized graphene materials such as sulfonated graphene have demonstrated very

high capacities (241 mg/g for 1-naphthanol), suggesting that surface modification can greatly enhance adsorption efficiency by introducing specific binding sites and improving interaction strength. Graphene, in its reduced form, also provides moderate capacity (25 mg/g for 4-chloro-2-nitrophenol) but further modification is often needed to match or surpass the performance of functionalized variants.

Although activated carbon, biochar, and polymeric resins demonstrate considerable adsorption capacities, their performance is often governed primarily by surface area and pore structure with limited control over surface functionality and selectivity. In contrast, 3D-N/rGO offers a combined structural and chemical advantage. The three-dimensional porous architecture enhances mass transfer and minimizes sheet restacking, while nitrogen doping introduces specific functional groups such as pyridinic-N and graphitic-N that promote π–π interactions and hydrogen bonding with aromatic phenolic molecules. Unlike conventional adsorbents that rely largely on physical adsorption, 3D-N/rGO provides tunable surface chemistry, enabling improved selectivity toward phenolic compounds while reducing co-adsorption of non-phenolic constituents. Therefore, within the context of selective phenolic purification rather than bulk contaminant removal, 3D-N/rGO presents a more rational and targeted adsorbent choice for this study.

2.8 Effect of Adsorption Parameters

Adsorption parameters such as pH, temperature, and contact time significantly affect phenolic removal efficiency. Table 2.16 shows the adsorption parameters influencing phenolic compound recovery from different sources. Most studies operate near neutral to slightly acidic pH (5.0–6.5), where phenolic ionization favors adsorption. Lower temperatures (25–30°C) are common to prevent thermal degradation, though some systems use mild heating to improve kinetics. Contact times vary from 30 to 180 minutes depending on the adsorbent surface properties and pore structure.

The mass of the adsorbent is another critical parameter that affects the efficiency of the adsorption process. As the mass of the adsorbent increases, the number of available adsorption sites also increases, which can enhance the overall adsorption capacity. A larger mass of adsorbent generally provides more surface area for phenolic compounds to bind, improving the removal efficiency. A study carried out by Karunarathne et al. investigated the removal of phenol using activated carbon derived

from sugarcane bagasse [68]. In their fixed-bed column experiments, adsorbent dosages of 5 g and 10 g were tested under identical conditions. The results showed a clear improvement in adsorption performance with increased adsorbent mass.

Table 2.16
Adsorption Parameters Influencing Phenolic Compound Recovery from Different Sources

Source of phenolic	Adsorbent	pH	Temp(C)	Contact Time(min)	Absorbent Dose	Reference
Bamboo	Biochar's	6.0	25	60	2.0	(Zango et al., 2020)
Pine fruit	Biochars	5.5	30	120	1.5	(Zango et al., 2020)
Avocado kernel	Activated carbon	6.5	25	90	3.0	(Zango et al., 2020)
Sugar cane	Activated carbon	6.0	40	60	2.5	(Zango et al., 2020)
Tea waste	Activated Carbon	5.0	25	30	2.0	(Zango et al., 2020)
2-chlorophenol	Graphene oxide	6.0	25	45	1.0	(Zango et al., 2020)
1-naphthanol	Sulfonated graphene	5.5	30	60	0.8	(Zango et al., 2020)
Olive mill wastewater	Zeolite	7.0	40	180	2.5	(Zango et al., 2020)
Coffee pulp extract	Chitosan-based composite	6.0	25	60	1.2	(Zango et al., 2020)

The effects of adsorption parameters such as temperature, concentration, and adsorbent mass play a critical role in the development of efficient adsorption systems. These variables have been shown to significantly influence the adsorption capacity, equilibrium behavior, and the potential for adsorbent regeneration. Temperature plays a critical role in influencing both the kinetics and thermodynamics of the adsorption process. As temperature increases, changes in adsorption rate and capacity can occur

due to variations in adsorbate diffusivity and the interaction strength between adsorbate and adsorbent. A study involving eggshells as adsorbents for ferric ions carried out by N. Yeddou et al. in Figure 2.11 shows the effect of temperature over a range of 20℃ to 50℃ (Yeddou & Bensmaili, 2007). Based on Figure 2.11, the equilibrium adsorption capacity (q_e) and the sorption rate constant decreased with increasing temperature from 20°C to 50°C (Yeddou & Bensmaili, 2007). This decline was attributed to increased solubility of the target compound (ferric carbonate), which reduced the driving force for adsorption and potentially enhanced desorption at elevated temperatures. Among the three temperatures, the highest adsorption capacity was observed at 20°C, followed by 30°C and 50°C. The observed decrease in adsorption capacity at elevated temperatures could be attributed to the weakening of physical interactions, such as van der Waals forces or hydrogen bonding, which typically govern physisorption (Yeddou & Bensmaili, 2007).

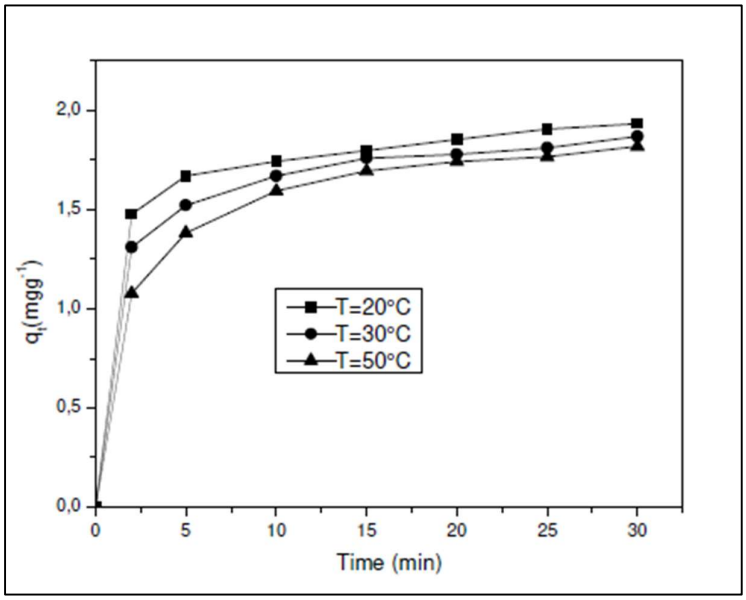


Figure 2.11 Effect of Temperature (Yeddou & Bensmaili, 2007)

The initial concentration of phenolic compounds is a key parameter that directly influences the adsorption behaviour, particularly the adsorption capacity, mass transfer rate, and breakthrough characteristics in column systems. As the driving force for diffusion increases with concentration, more adsorbate molecules are available to interact with the active sites of the adsorbent. Figure 2.12 illustrated the effect of inlet concentration at 0.5 and 1.5 mg/mL under constant bed height and flow rate conditions

(Babu & Gupta, 2005). The study conducted by Babu B et al., demonstrated that increasing the inlet concentration reduced the breakthrough time from 2525 to 2275 seconds (without velocity variation), and from 1875 to 1575 seconds (with velocity variation) (Babu & Gupta, 2005). The steeper breakthrough curves at higher concentrations indicate faster saturation of the adsorbent bed due to a more pronounced concentration gradient across the pores, although the external mass transfer resistance may slightly increase at elevated concentrations.

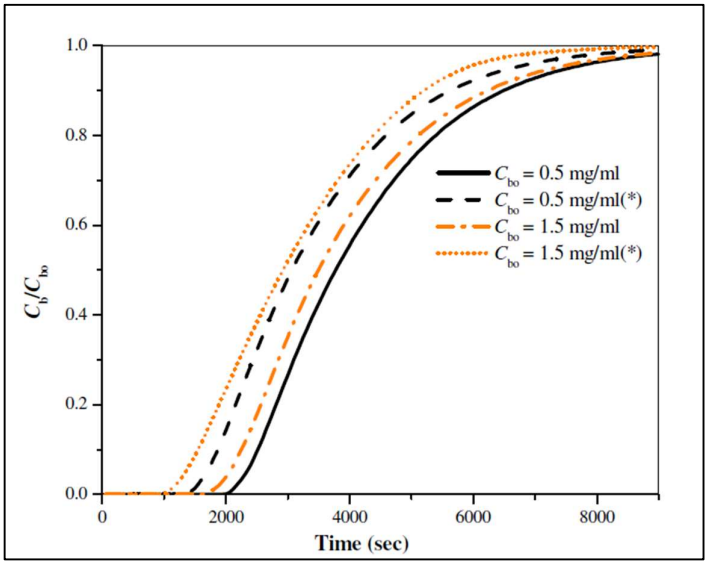


Figure 2.12 Effect of Concentration (Babu & Gupta, 2005)

The mass of the adsorbent is another critical parameter that affects the efficiency of the adsorption process. As the mass of the adsorbent increases, the number of available adsorption sites also increases, which can enhance the overall adsorption capacity. A larger mass of adsorbent generally provides more surface area for phenolic compounds to bind, improving the removal efficiency. A study carried out by Karunarathne et al. investigated the removal of phenol using activated carbon derived from sugarcane bagasse (Karunarathne & Amarasinghe, 2013). In their fixed-bed column experiments, adsorbent dosages of 5 g and 10 g were tested under identical conditions. The results showed a clear improvement in adsorption performance with increased adsorbent mass. Based on Figure 2.13, the breakthrough time increased from 15 minutes at 5 g to 80 minutes at 10 g, while the amount of phenol adsorbed at breakthrough also rose significantly. Similarly, the total amount of phenol adsorbed at full bed exhaustion increased from 60.11 mg (12.02 mg/g) to 123.38 mg (12.34 mg/g),

indicating enhanced overall bed capacity. This improvement is attributed to the higher availability of active sites and the extended contact time resulting from the increased bed height (Karunarathne & Amarasinghe, 2013). Consequently, the mass transfer zone broadens, allowing more complete adsorption before breakthrough occurs. However, it is also important to consider that excessive adsorbent loading may lead to underutilization due to site aggregation or limited solute diffusion. Thus, optimizing adsorbent mass is essential for maximizing performance while maintaining operational efficiency.

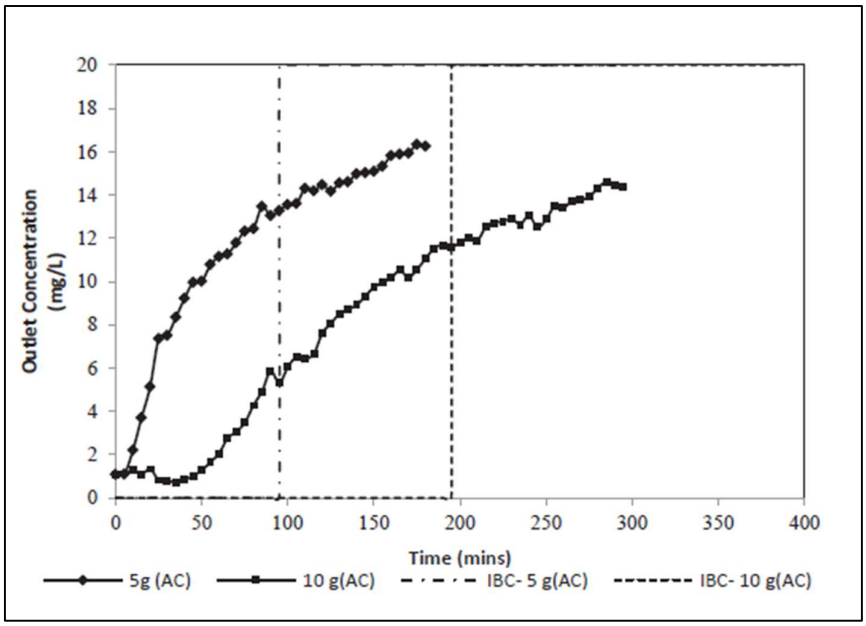


Figure 2.13 Breakthrough Curve at Varying Adsorbent Masses (Karunarathne & Amarasinghe, 2013)

In the present study, adsorption temperature, initial phenolic concentration, and adsorbent mass were systematically investigated as the key operational parameters influencing phenolic recovery using 3D-N/rGO. Adsorption temperature was evaluated to determine its influence on thermodynamic behaviour and adsorption capacity, while initial phenolic concentration was varied to assess mass transfer driving force and breakthrough characteristics in the fixed-bed system. Additionally, the effect of adsorbent mass was examined to evaluate site availability, breakthrough time, and overall adsorption efficiency. These parameters were selected based on their direct impact on adsorption capacity, equilibrium behaviour, and column performance, which

are the primary focus of this research. The detailed experimental findings and optimization results are discussed in Chapter 4.

2.9 Adsorption Isotherms Models

The adsorption isotherm was defined as the relation between the equilibrium concentration of the adsorbate in the liquid phase and the amount of adsorbate adsorbed on the solid adsorbent at a fixed temperature. The models can supply the adsorption mechanism, surface characteristics, and the interaction force between adsorptive and adsorbent. The most frequently used isotherms models are Langmuir, Freundlich and Temkin, which represents different types of adsorption behaviour.

For Langmuir isotherm, monolayer adsorption on the homogenous surface having finite number and same type of sites is considered. This was interpreted to mean that there is no more adsorption the moment the site is occupied. This model is only appropriate for systems in which chemisorption is predominant. Li et al. found that the adsorption of phenol on graphene conformed to the Langmuir model, indicating that the saturation point of the adsorption of the phenolate would be reached at monomolecular adsorption and the uniform adsorption surface had high adsorption capacity and affinity for phenolic molecules (Y. Li et al., 2012). Similarly, Zaini et al. observed the Elovich model fitted the adsorption of phenol on activated carbon, prepared from palm kernel shell, very well, implying the presence of an equal Langmuir sites and monolayer coverage of phenol on the surface (Zaini et al., 2023). The Freundlich isotherm, however, is an empirical model expressing that adsorption occurs on a heterogeneous surface with sites of different energy. It is capable of multilayer adsorption and is more applicable to natural and modified bio-adsorbents. Ayoob et al. observed an appropriate equilibrium Freundlich isotherm model was obtained for phenol adsorption on GO-bentonite nanocomposites, suggesting the heterogeneity on the surface and various affinity sites (Ayoob et al., 2024). This was supported by Srihari and Das, who reported a similar trend in their nonconventional activated carbon from agro-waste and, this, suggest that adsorption strength decreases with increase of surface coverage (Srihari & Das, 2009).

The Temkin isotherm considers the adsorbate−adsorbate interaction and assumes that the heat of adsorption diminishes linearly with the increase of surface coverage. Zhao et al. reported that the Temkin model fitting was also suitable for

AHGO-N 2 with adsorbed molecules and a homogeneous distribution of the binding energies up to a certain point (R. Zhao et al., 2021). The adsorption isotherms are of great importance for the optimization of adsorption performances, prediction of the systems, and design of effective processes, for purification of phenolic compounds in the industry.

Table 2.17
Isotherm Studies on The Adsorption of Phenolic Compounds Using Various Adsorbents

Adsorbent	Isotherm Model	Adsorption Capacity (mg/g)	R^2 Value	Reference
Activated carbon (olive mill wastewater)	Langmuir	52.4	0.996	(Y. Li et al., 2012)
Biochar from bamboo	Freundlich	17.0	0.972	(Hashim et al., 2020)
Graphene oxide nanoflakes	Langmuir	30.0	0.987	(Al-Asheh et al., 2003)
Tea waste-based activated carbon	Freundlich	132.5	0.980	(Mourão et al., 2006)
Nitrogen-doped reduced graphene oxide (3D-N/rGO)	Langmuir and Temkin	147.8	0.991 / 0.982	(Ricci et al., 2022)
Sulfonated graphene	Freundlich	241.0	0.984	(Mourão et al., 2006)
Palm kernel shell activated carbon	Langmuir	93.2	0.989	(Zaini et al., 2023)
GO-bentonite nanocomposite	Langmuir and Freundlich	123.8	0.990 / 0.974	(Ayoob et al., 2024)
Single-walled carbon nanotubes	Langmuir	17.95	0.995	(H. Zhao et al., 2015)
Agro-waste activated carbon (Hemidesmus indicus)	Freundlich	370.37	0.920	(Bellier et al., 2022)

2.9.1 Langmuir Isotherm Model

The Langmuir isotherm, which assumes the adsorption of a single layer on a uniform surface, and the Freundlich isotherm, which accounts for the adsorption of many layers on a non-uniform surface, are often used (Zaini et al., 2023). The Langmuir model is used to ascertain the utmost adsorption capability, whilst the Freundlich model delineates the adsorption intensity and surface heterogeneity. The experimental data may be used to determine the adsorption process and the contact forces between phenol and graphene by fitting them to these isotherm models. The Langmuir isotherm model can be represented as (Kaveh et al., 2024):

$$\frac{C_e}{q_e} = \frac{C_e}{q_{max}} P + \frac{1}{K_L q_{max}} \tag{2.1}$$

where q_{max} is the maximum adsorption capacity, K_L is langmuir constant related to the rate of adsorption, C_e is equilibrium concentration (mgL^{-1}) and q_e is adsorption capacity at equilibrium.

2.9.2 Freundlich Isotherm Model

The Freundlich isotherm model is a mathematical equation used to elucidate heterogeneous systems. The adsorbent's absorption capacity is not limited and may be used in the low to medium range of adsorbate concentration. The mathematical representation of the Freundlich equation is expressed in a linear form as follows (Kaveh et al., 2024):

$$\ln q_e = ln\ k_F + \frac{1}{n} \ln C_e \tag{2.2}$$

where q_e is the adsorption capacity at equilibrium, k_F is Freundlich constant for measure of adsorption capacity, n is Freundlich constant for relative favourability of the adsorption process and C_e is equilibrium concentration (mg/L)

2.9.3 Temkin Isotherm Model

The Temkin isotherm model assumes that the heat of adsorption of all molecules in the layer decreases linearly with coverage due to adsorbate–adsorbent interactions. It also presumes a uniform distribution of binding energies up to some maximum binding energy. Unlike the Langmuir model, Temkin incorporates the effects of indirect adsorbate–adsorbent interactions into its equation. The linear form of the Temkin equation is given as (Dada et al., 2012):

$$q_e = B \ln A + B \ln C_e \tag{2.3}$$

where qe is the adsorption capacity at equilibrium (mg/g), Ce is the equilibrium concentration of the adsorbate (mg/L), A is the Temkin isotherm equilibrium binding constant (L/g) related to the maximum binding energy, and B= RT/b is a constant related to the heat of adsorption (J/mol), with R being the universal gas constant (8.314 J/mol·K), T the absolute temperature (K), and b the Temkin constant related to adsorption heat.

2.9.4 Dubinin-Radushkevich

The Dubinin–Radushkevich (D–R) isotherm model is used to describe adsorption on both homogeneous and heterogeneous surfaces. Unlike the Langmuir model, it does not assume a uniform surface or constant adsorption potential. The D–R model is generally applied to distinguish between physical and chemical adsorption based on the mean free energy of adsorption. Its linear form is expressed as (Dada et al., 2012):

$$\ln q_e = \ln q_m + \beta \varepsilon^2 \tag{2.4}$$

where qe is the adsorption capacity at equilibrium (mol/g), qm is the theoretical saturation capacity (mol/g), β is a constant related to the mean free energy of adsorption (mol^2/J^2) and ε is the Polanyi potential, calculated as:

$$\varepsilon = RT \ln\left(1 + \frac{1}{C_e}\right) \tag{2.5}$$

The mean free energy (E) of adsorption can be determined using:

$$E = \frac{1}{\sqrt{2\beta}} \tag{2.6}$$

where this parameter differentiate between physisorption (E < 8 kJ/mol) and chemisorption (E > 8 kJ/mol)

2.9.5 Redlich-Peterson

The Redlich–Peterson (R–P) isotherm model is a hybrid model that incorporates elements from both the Langmuir and Freundlich isotherms. It can be applied to homogeneous or heterogeneous systems and does not strictly follow a monolayer adsorption assumption. The non-linear form of the model is expressed as (Mourão et al., 2006):

$$\ln\left(\frac{K_R C_e}{q_e} - 1\right) = \beta \ln C_e \tag{2.7}$$

where qe is the adsorption capacity at equilibrium (mg/g), Ce is the equilibrium concentration of the adsorbate (mg/L), K_R is the R-P isotherm constant (L/g), β is the exponent between 0 and 1 (indicates the degree of heterogeneity).

In this study, the experimental adsorption data of phenolic compounds onto 3D-N/rGO were fitted using the Langmuir, Freundlich, Dubinin–Radushkevich (D–R), and Redlich–Peterson isotherm models. These models were selected to represent both homogeneous and heterogeneous adsorption behaviours expected for nitrogen-doped

graphene materials. The Langmuir model was applied to evaluate possible monolayer adsorption on relatively uniform active sites created by graphitic domains and nitrogen functionalities. In contrast, the Freundlich model accounts for surface heterogeneity and multilayer adsorption which is consistent with the defect-rich and chemically diverse surface of 3D-N/rGO containing pyridinic, pyrrolic, and graphitic nitrogen sites. The D–R model was used to estimate the mean adsorption energy and to distinguish between physical and chemical adsorption mechanisms providing insight into the interaction strength between phenolic molecules and the modified graphene surface. The Redlich–Peterson model, a hybrid of Langmuir and Freundlich equations was employed to further validate the adsorption behaviour under non-ideal conditions. The selection of these models therefore aligns with the physicochemical characteristics of 3D-N/rGO which exhibits a partially restored graphitic structure combined with heterogeneous nitrogen-containing active sites, making it necessary to evaluate both monolayer and heterogeneous adsorption mechanisms.

2.10 Adsorption Thermodynamics

The thermodynamic approach is an essential tool to get insight into the nature, feasibility and the energetic of adsorption stages. Important thermodynamic parameters showing if the adsorption is spontaneous, endothermic, exothermic also if entropy tends to become greater at the solid-liquid interface. In this regard, evident information is available from Gibbs free energy change (ΔG°), as well as enthalpy change (ΔH°) and entropy change(ΔS°). Such parameters are commonly determined from the equilibrium data at various temperatures by the van't Hoff equation.

Negative ΔG° value indicates natural change (Δ process at the prevailing conditions. If ΔH° is positive, it suggests endothermic adsorption: adsorption is favored at higher temperatures. In the absence of a heat flow, the bow is entirely positive except in the case of the former, where it is negative. A positive ΔS° value indicates an increase in randomness at the solid−liquid interface, as in the case where the adsorbate molecules replace water molecules on the surface of the adsorbent.

The thermodynamic nature of phenol adsorption on different adsorbents has been extensively investigated. Li et al. noted that the adsorption of phenol onto graphene was an exothermic and spontaneous process, and that the ΔG° decreased with increase in temperature, while the ΔH° was determined to be 25.3 kJ/mol, suggesting physical

adsorption, although there was most likely chemisorption as well (Y. Li et al., 2012). In a related study, Zaini et al. for activated carbon prepared from palm kernel shell, the positive value of ΔH° (+22.6 kJ/mol) and ΔS° (+107.4 J/mol·K) show the increased disorder and the favorable adsorption at higher temperature (Zaini et al., 2023).

Ayoob et al. found that GO-bentonite nanocomposites also had spontaneous adsorption, which ΔG° values in the range of −13.7 to −15.9 kJ/mol and ΔH° +28.5 kJ/mol indicated that endothermic and chemisorption occurred (Ayoob et al., 2024). Zhao et al. verified those observations in the case of nitrogen-doped reduced graphene oxide (N-rGO), with high ΔH° values and strong adsorbate interactions (Ricci et al., 2022). As a whole, the thermodynamic studies not only confirm the energy feasibility of adsorptive removal but also suggest desirable conditions for adsorber operating. Such knowledge is critical to the design and fabrication of efficient adsorbent materials in water treatment and pollutant removal apparatus.

Table 2.18
Thermodynamic Parameters for Adsorption of Phenolic Compounds Using Various Adsorbents

Adsorbent	**ΔG° (kJ/mol)**	**ΔH° (kJ/mol)**	**ΔS° (J/mol·K)**	**Adsorption Nature**	**Reference**
Graphene	-12.5 to -18.4	+25.3	+135.2	Spontaneous, endothermic	(Y. Li et al., 2012)
GO-bentonite nanocomposite	-13.7 to -15.9	+28.5	+140.6	Spontaneous, endothermic	(Ayoob et al., 2024)
Nitrogen-doped reduced graphene oxide (3D-N/rGO)	-14.7 to -19.0	+31.4	+152.6	Spontaneous, endothermic	(Ricci et al., 2022)
Activated carbon (olive mill wastewater)	-11.2 to -13.5	+21.8	+120.5	Spontaneous, endothermic	(Y. Li et al., 2012)
Sulfonated graphene	-10.6 to -16.7	+27.1	+136.8	Spontaneous, endothermic	(Hashim et al., 2020)
Biochar from bamboo	-7.5 to -10.2	+18.9	+94.5	Spontaneous, endothermic	(Hashim et al., 2020)

Carbon nanotubes	-9.4 to -12.1	+24.7	+112.8	Spontaneous, endothermic	(H. Zhao et al., 2015)

2.10.1 Van't Hoff Equation

Gaining comprehension of the thermodynamics of the adsorption process provides vital data about the spontaneity, feasibility, and energetics of the interaction. The Gibbs free energy (ΔG), enthalpy (ΔH), and entropy (ΔS) are fundamental thermodynamic parameters. A negative change in Gibbs free energy (ΔG) shows that the process is spontaneous. On the other hand, changes in enthalpy (ΔH) and entropy (ΔS) provide information on whether the adsorption process is endothermic or exothermic, and the level of randomness at the solid-liquid interface, respectively (Y. Li et al., 2012). Thermodynamic analysis helps to forecast the stability of the adsorbate-adsorbent complex and understand the influence of temperature on the adsorption behaviour.

$$\Delta G^o = -RT \ln K \tag{2.8}$$

$$\Delta G^o = \Delta H^{o-} T\Delta S^o \tag{2.9}$$

$$\ln K = \frac{\Delta S^o}{R} - \frac{\Delta H^o}{RT} \tag{2.10}$$

$$K = \frac{Q_e}{C_e} \tag{2.11}$$

where T is absolute temperature (K) and R is gas constant (8.314×10^{-3} kJ/ Kmol). The plot of ln K versus 1/T is linear with the slope and the intercept giving the values of ΔH^o and ΔS^o

In this study, the thermodynamic parameters ΔG°, ΔH°, and ΔS° were evaluated to understand the nature of the adsorption process. The Gibbs free energy change (ΔG°) indicates the spontaneity of adsorption, where a negative ΔG° value confirms that the process occurs spontaneously under the studied conditions. The enthalpy change (ΔH°) describes the heat effect of adsorption and determines whether the process is endothermic (ΔH° > 0) or exothermic (ΔH° < 0). Meanwhile, the entropy change (ΔS°) reflects the degree of randomness or disorder at the solid–liquid interface during

adsorption. A positive ΔS° suggests increased randomness, whereas a negative value indicates a decrease in system disorder.

2.11 Adsorption Kinetics

The adsorption kinetics is one of the most important parameters for solute uptakes rate and possible adsorption mechanism. Investigations into kinetic models could help to recognize whether the controlling are surface adsorption, chemical binding, or diffusion inside the framework of the adsorbent. The pseudo-first-order, pseudo-second-order, intraparticle diffusion, and Elovich models are the most frequently used models. It is well known that pseudo second-order kinetic model is generally acceptable to describe adsorption of chemisorption mechanism.

The pseudo-first-order equation developed by Lagergren considers that the rate of occupation of adsorption sites is directly proportional to the number of unoccupied sites. While this model is appropriate for some systems, it shows weak performance in predicting the whole adsorption trajectory for phenolic compounds. On the other hand, the pseudo-second-order model will better fit the actual data if the adsorption process is dominated by chemical reaction such as electron sharing and exchanging. For instance, Li et al. reported that the adsorption of phenol on graphene was satisfactorily fit by the pseudo-second-order kinetic model with a high correlation coefficient, which suggested that chemisorption was the controlling process (Y. Li et al., 2012).

Zaini et al.(Zaini et al., 2023). also observed a good fit for the pseudo-second-order model and concluded that fast adsorption took place at the beginning of the adsorption process, which was controlled by abundant active sites of the PKS-derived activated carbon. The same result was obtained by Ayoob et al. in their research on GO-bentonite nanocomposites, and the kinetic data fitted the pseudo-second-order model very well, confirming that the predominant role was played by the chemical bonding formed between phenol and the adsorbent surface groups (Ayoob et al., 2024).

Intraparticle had diffusion effect on the adsorption rate in some systems, but it was not the only rate controlling phenomenon. Zhao et al. found that although pore-filling contributed to the adsorption process, surface chemisorption was the dominant mechanism especially in the case of nitrogen-doped reduced graphene oxide (Ricci et al., 2022). In brief, the kinetic studies provide essential information about the kinetics

of adsorption, which guide the development of efficient adsorbents and optimum conditions to remove phenolic pollutants.

Table 2.19
Kinetic Parameters for Adsorption of Phenolic Compounds Using Various Adsorbents

Adsorbent	Adsorbate / Conditions	Best-fit Kinetic Model	Rate Constant (k)	R^2 Value	Reference
Graphene	Phenol; 20–100 mg/L; pH 6.5; 25 °C	Pseudo-second-order	0.015 g/mg·min	>0.990	(Y. Li et al., 2012)
GO-bentonite nanocomposite	Phenol; 50–300 mg/L; 25 °C	Pseudo-second-order	0.013 g/mg·min	0.981	(Ayoob et al., 2024)
Activated carbon from olive mill wastewater	Phenol; 25 °C; agitation 200 rpm	Pseudo-second-order	0.022 g/mg·min	0.993	(Y. Li et al., 2012)
Sulfonated graphene	Phenol; batch; 5 h contact time	Pseudo-second-order	0.018 g/mg·min	0.970	(Hashim et al., 2020)
Bamboo biochar	Phenol; 100 mg/L; 300 min contact time	Pseudo-second-order	0.008 g/mg·min	0.960	(Hashim et al., 2020)
Carbon nanotubes	Phenol; pH 5–7; 25 °C	Pseudo-second-order	0.021 g/mg·min	0.988	(H. Zhao et al., 2015)
Agro-waste activated carbon (Hemidesmus indicus)	Phenol; 10–500 mg/L; contact time 180 min	Pseudo-first-order	0.0003 g/mg·min	0.970	(Bellier et al., 2022)
Tea waste activated carbon	Phenol; 50–300 mg/L; pH 4–9; 25 °C	Pseudo-second-order	0.014 g/mg·min	0.980	(Hashim et al., 2020)
Nitrogen-doped rGO	Phenol; 50–250 mg/L; 25 °C	Pseudo-second-	0.017 g/mg·min	>0.990	(Ricci et al., 2022)

order

2.11.1 Pseudo-First Order

The pseudo-first-order model, proposed by Lagergren, assumes that the rate of adsorption is directly proportional to the difference between the equilibrium adsorption capacity qe and the adsorption capacity at time t (Kaveh et al., 2024). The linearized form is:

$$\ln(q_e - q_t) = ln\, q_e - k_1 t \tag{2.12}$$

where qt is adsorbed analyte at time t (min), qe is adsorbed analyte at equilibrium and k1 is pseudo-first order rate constant (min^{-1})

2.11.2 Pseudo-Second Order

The pseudo-second-order model assumes that chemisorption is the rate-limiting step, involving valence forces through the sharing or exchange of electrons (Kaveh et al., 2024). The linearized form is:

$$\frac{t}{q_t} = \frac{t}{q_e} + \frac{1}{k_2 q_e^2} \tag{2.13}$$

where qt is adsorbed analyte at time t (min), qe is adsorbed analyte at equilibrium and k2 is pseudo-second order rate constant (g mg^{-1} min^{-1})

CHAPTER 3
RESEARCH METHODOLOGY

3.1 Overview of Research Methodology

This chapter presents an overview of the research methodology employed to achieve the objectives of this study, which focuses on the synthesis of three-dimensional nitrogen-doped reduced graphene oxide (3D-N/rGO) and its application for enhanced phenolic recovery from palm kernel cake (PKC) extracts obtained via microwave-assisted extraction (MAE). The methodology was systematically structured to ensure that each research objective was addressed using appropriate experimental and analytical approaches.

The first research objective, which aims to synthesize and optimize 3D-N/rGO adsorbents with varying urea loadings, was addressed through a one-pot hydrothermal synthesis method followed by batch adsorption–desorption purification experiments. Batch purification was employed to evaluate the adsorption and desorption performance of 3D-N/rGO prepared with different urea loadings and to identify the optimal nitrogen-doping level for phenolic recovery. Comprehensive characterization using Fourier Transform Infrared Spectroscopy (FTIR), N_2 adsorption–desorption analysis, Thermogravimetric Analysis (TGA), High-Resolution Transmission Electron Microscopy (HRTEM), and X-ray Photoelectron Spectroscopy (XPS) was conducted to correlate the structural and surface properties of the 3D-N/rGO adsorbents with their adsorption performance. The purified phenolic compounds were subsequently characterised through total phenolic content (TPC) determination, liquid chromatography–mass spectrometry (LC–MS), and macro- and micronutrient analyses to evaluate their compositional properties.

The second research objective, which investigates the effect of adsorption process parameters on phenolic purification, was examined using a continuous fixed-bed adsorption system. Key operating parameters, including adsorption temperature, phenolic concentration, and adsorbent mass, were systematically varied to evaluate their influence on breakthrough behaviour, adsorption capacity, and recovery efficiency.

The third research objective, which focuses on elucidating the adsorption mechanism of phenolic compounds onto the optimized 3D-N/rGO adsorbent, was

achieved through kinetic, isotherm, and thermodynamic analyses. Experimental data were analysed using pseudo-first-order and pseudo-second-order kinetic models, Langmuir, Freundlich, Temkin, Dubinin–Radushkevich, and Redlich–Peterson isotherm models, as well as thermodynamic evaluation using the Van't Hoff equation.

3.2 Materials and Chemicals

Table 3.1 shows the list of chemicals used and its description throughout the research study.

Table 3.1
The Chemicals Used for Research Study

Materials/Chemicals	Purity/Quantity	Brand	Description
Palm Kernel Cake	5kg	-	Act as the raw materials and is in powdery form
Ethanol	96%	Emsure Merck	Act as a co-solvent
Silica gel	100 g	-	To prevent moisture in dried PKC
Graphite powder	1kg	Sigma-Aldrich	To synthesize GO using Modified Hummer's Method
Liquid Nitrogen Gas	1 gas	Alpha gas	Adsorption and desorption of N2 gas
Urea Powder	100g	Sigma Aldrich	To synthesize N-rGO
Potassium Permanganate	500g	Sigma Aldrich	To synthesize GO using Modified Hummer's Method
Sodium Nitrate	500g	Qrec	To synthesize GO using Modified Hummer's Method
Hydrochloric Acid	37%	Qrec	To synthesize GO using Modified Hummer's Method
Sulphuric Acid	98%	Qrec	To synthesize GO using Modified Hummer's Method
Hydrogen Peroxide	30%	Qrec	To synthesize GO using Modified Hummer's Method
Deionized water	100%	-	This solvent was chosen because it has better purity compared to distilled water

3.3 Equipment and Apparatus

Table 3.2 shows the list of apparatus involved and its description:

Table 3.2
The Apparatus Used for Research Study

Apparatus	Description	Location
Analytical Balance	To weight the sample	UiTM Pulau Pinang
Grinder	To grind the sample into powder form	UiTM Pulau Pinang
Sieve shaker	To sieve the grinded sample into desired size	UiTM Pulau Pinang
Oven	To remove moisture content in PKC	UiTM Pulau Pinang
Rotary Evaporator	To separate ethanol from extracted oil	UiTM Pulau Pinang
Microwave-Assisted Extraction (MAE)	To heat solvent in contact with sample	UiTM Pulau Pinang
UV-Vis Spectrophotometer	To determine total protein content in phenolic rich extract	UiTM Pulau Pinang
Liquid Chromatography Mass Spectrophotometer (LC-MS)	To analyse the available bioactive compounds (phenolic) in the purified extracted PKC after purification	Institut Farmaseutikal Dan Nutraseutikal Malaysia (IPharm)
X-ray Photoelectron Spectroscopy (XPS)	Identify the element, chemical state, overall electronic structures, and density of the electron states of hydrophobic adsorbent	Universiti Sains Malaysia (USM)
Thermogravimetric Analyser (TGA)	Determination of temperature resistance of hydrophobic adsorbent	UiTM Pulau Pinang
Fourier Transform Infrared Spectroscopy (FTIR)	Functional groups identification for hydrophobic	Universiti Sains Malaysia (USM)
High-Resolution Transmission Electron Microscope (HRTEM)	Determination of high resolution of morphology and microscopic structure of hydrophobic adsorbent (3D-N/rGO)	Universiti Sains Malaysia (USM)
N_2 Adsorption-Desorption	To determine the specific surface area and porosity of hydrophobic adsorbent (3D-N/rGO)	UiTM Pulau Pinang

3.4 Experiment Process Flowchart

This section presents the experimental process flowchart outlining the overall research methodology in this study.

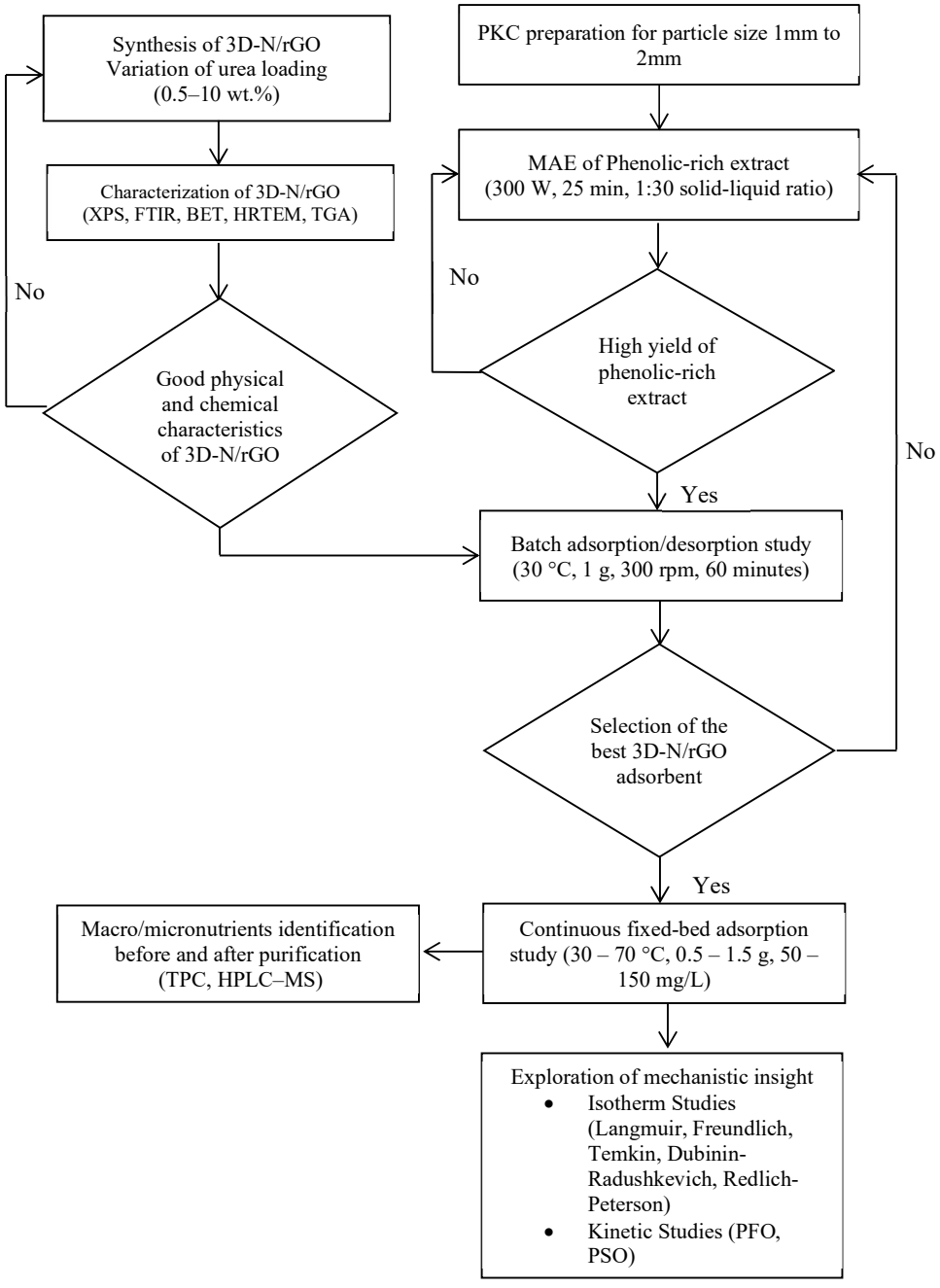


Figure 3.1 Experimental Flowchart for Overall Research Objectives

3.5 Preparation of Palm Kernel Cake (PKC)

The PKC was acquired from a local supplier. The PKC was washed thoroughly with distilled water to remove residual particulate matter. Then, the PKC were dried at 40°C for 48 hours in an universal oven (Memmert UN 110 plus).



Plate 3.1 Oven Used to Dry PKC



Plate 3.2 PKC After Drying

Once dried, the PKC was pulverized into a fine powder using a grinder (Heavy duty grinder 2500 g stainless steel) until a uniform powdery consistency was achieved. The powder was then sieved to obtain particles within the size range of 0.5 to 1 mm. A total of 10 g of the ground PKC was weighed using an analytical balance and subsequently placed into an empty tea bag (Bradley, 2007).

3.6 Microwave-Assisted Extraction (MAE) of Phenolic-rich Compounds From PKC

Figure 3.2 shows the schematic diagram of MAE that was performed using a modified microwave (Samsung MS23K3513AK). The actual experimental setup is provided in Appendix A1. A 10 g of PKC sample was placed into round bottom flask followed by the addition of 300 mL of ethanol as a co-solvent. Ethanol was selected as the extraction solvent based on its proven selectivity and extraction efficiency for phenolic compounds from palm kernel cake (PKC) under microwave-assisted extraction (MAE) conditions. In a previous study conducted by , ethanol demonstrated the highest extraction yield (45%) and total phenolic content (0.086 mg GAE/g dry oil) when compared to methanol and water under identical MAE operating parameters,

confirming its suitability for phenolic recovery from PKC (Rosli, Mohamad Nor, et al., 2025).

The round bottom flask was then placed inside the microwave cavity and connected to a condenser that were attached with water inlet and outlet hoses to allow continuous cooling during extraction. The condenser was used to condense ethanol vapour generated during microwave heating and return it to the extraction flask, enabling reflux under controlled conditions. Continuous water circulation ensured efficient condensation, minimised solvent loss, and maintained consistent extraction conditions throughout the MAE process. The procedure has been conducted with constant parameters which were extraction time 25 minutes, microwave power 300 W and solid-to-liquid ratio of 10 to 1:30 (Doulabi et al., 2020; Oufighou et al., 2025; Tan et al., 2025). The microwave-assisted extraction (MAE) parameters applied in this study were determined and validated based on experimental investigation conducted in a previous study by Rosli et al. The effects of microwave power (300, 450, and 600 W) and extraction time (10–25 minutes) on total phenolic content (TPC), antioxidant activity (AOA), and extraction kinetics of phenolic compounds from palm kernel cake (PKC) were comprehensively evaluated. The results demonstrated that an extraction time of 25 minutes at a microwave power of 300 W yielded the highest TPC (1.715 mg GAE/g dry oil) and AOA (186.03 g AAE/mL), while higher microwave powers led to a decline in phenolic recovery due to thermal degradation of heat-sensitive compounds (Rosli, Mohd Ariff, et al., 2025). Similar microwave-assisted extraction conditions have also been reported in previous studies conducted by Oufighou et al., where phenolic compounds were effectively extracted using ethanol as solvent with microwave power around 300 W (Oufighou et al., 2024).

Following the extraction process, the mixture of the extracted sample and ethanol was separated using a rotary evaporator (Buchi Rotavapor R-215 model). To accurately determine the mass of the extracted PKC oil, the evaporator flask was initially weighed before adding the sample. After ethanol was removed through evaporation, the flask was weighed again. The difference in weight represented the mass of the pure PKC oil, ensuring precise measurement after solvent removal. This step is essential to ensure that the final mass measurement reflects only the oil obtained after ethanol removal, excluding the weight of the flask itself. By subtracting the initial empty flask weight from the post-evaporation weight, a precise determination of oil yield can be achieved, which is crucial for evaluating extraction efficiency and enabling reliable

comparisons between different experimental runs. The weight of PKC oil can be calculated using Equation (3.1).

$$\text{Weight oil extract} = \text{Weight flask after rotavap} - \text{Weight empty flask} \quad (3.1)$$

where the unit for the weight of PKC oil and flask in (g).

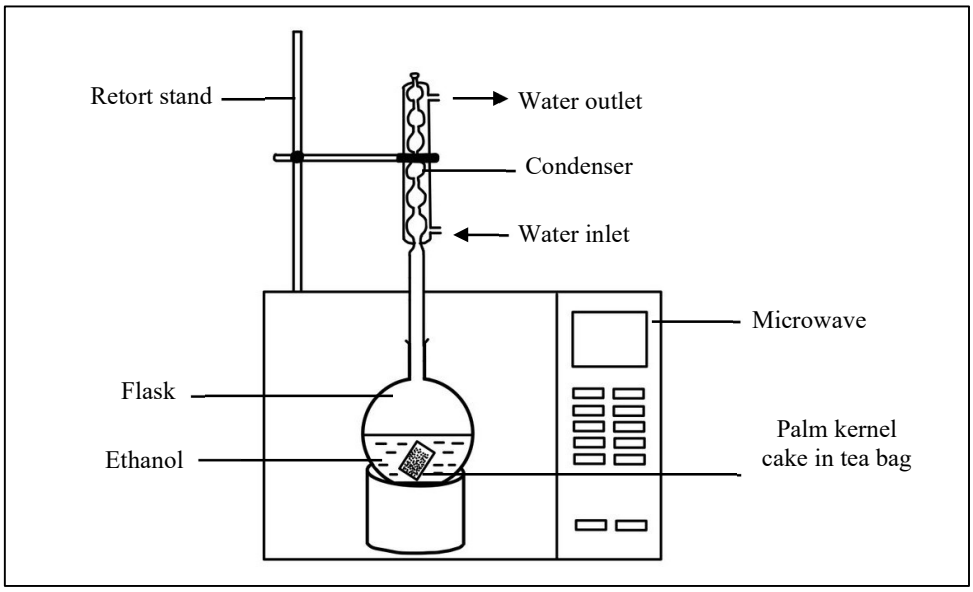


Figure 3.2 Schematic Diagram of MAE

3.7 Preparation of 3-Dimensional Nitrogen-Doped Reduced Graphene Oxide (3D-N/rGO) Adsorbent

The preparation of 3D-N/rGO involved a two-step synthesis process: the initial production of graphene oxide (GO) via the modified Hummers' method, followed by the nitrogen doping and reduction process to form the three-dimensional nitrogen-doped reduced graphene oxide structure. The GO synthesis provided an oxidized layered material with abundant oxygen-containing functional groups, which served as active sites for subsequent nitrogen doping. In the second stage, a nitrogen-rich precursor was introduced under controlled thermal and chemical conditions to achieve both reduction and nitrogen incorporation, resulting in a 3D porous architecture. This structure was designed to enhance surface area, improve adsorption affinity, and provide abundant

active sites, making the adsorbent suitable for efficient phenolic compound recovery in fixed-bed adsorption studies.

3.7.1 Synthesis of Graphene Oxide using Modified Hummer's Method

Graphene oxide (GO) was synthesized from graphite powder using the modified Hummers' method (L. Sun, Wang, Tian, Tan, Xie, Shi, Li, & Fu, 2012). The modified Hummers' method was selected in this study due to its practicality, reproducibility, and ability to produce graphene oxide (GO) with consistent oxidation and suitable surface functionalisation. As reported by Hasanli et al., the modified Hummers' approach offers a shorter synthesis duration and a simpler experimental procedure compared to other graphite oxidation routes, while producing GO with well-defined oxygen-containing functional groups confirmed by XRD, SEM, and FTIR analyses (Abdelhamid & Hussein, 2021). Initially, 2.5 g of graphite powder was dispersed in 60 mL of concentrated sulphuric acid (H_2SO_4), followed by the gradual addition of 1.25 g of sodium nitrate ($NaNO_3$). The mixture was stirred vigorously in an ice-water bath at 0–10 °C for 1 h. Subsequently, 7.5 g of potassium permanganate ($KMnO_4$) was added slowly to prevent a rapid temperature rise, maintaining the suspension temperature below 20 °C under continuous stirring for 1 h. The reaction mixture was then stirred at room temperature overnight until a brownish suspension was obtained.

Next, 135 mL of deionized (DI) water was added slowly, and the mixture was heated to 60 °C in an oil bath for 1 h, followed by cooling to room temperature. Subsequently, 25 mL of hydrogen peroxide (H_2O_2) was added to terminate the reaction, resulting in a colour change from brown to golden yellow. The suspension was filtered and washed twice with 400 mL of hydrochloric acid (HCl) to remove residual metal ions, followed by three rinses with DI water until the pH approached 5–6. Finally, the GO product was dried in an oven at 60 °C prior to further use.

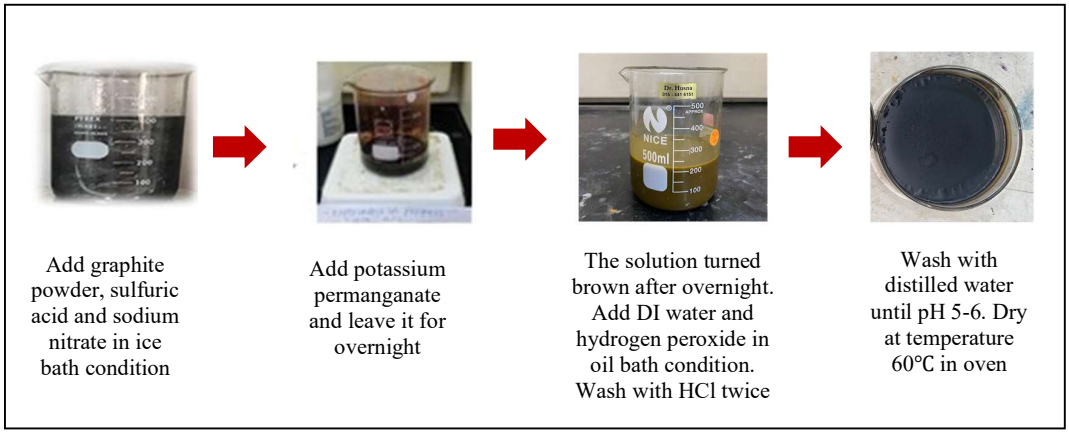


Plate 3.3 Synthesis GO Using Modified Hummer Method (Pandey et al., 2022)

3.7.2 Synthesis of 3D-N/rGO Adsorbent

The synthesis of nitrogen-doped reduced graphene oxide (N/rGO) is accomplished using a one-pot synthesis. This approach involves the combination of a 1g of GO that was previously synthesized using the modified Hummer's method with 0.005 g of urea and mixed in with 100 mL of distilled water to produce urea loading at 0.5 wt. % (S. Li et al., 2023). The mixture is stirred for 1 hour at 200 rpm in a room temperature After 1 hour, the mixture was dried in an oven at temperature of 100℃ for 24 hours (S. Li et al., 2023). The dried N/rGO then was pulverized using mortar and pestle. In this synthesis, the urea loading varies according to 0.5, 2, 5, 8 and 10 wt. %. The selected range provides a controlled comparison from low nitrogen loading (0.5 wt.%) to higher nitrogen loading (10 wt.%), which may increase nitrogen functional group incorporation and defect density, thereby influencing surface chemistry and adsorption behaviour. The optimal urea loading was subsequently determined based on batch adsorption–desorption purification performance and comprehensive material characterization, enabling selection of the most suitable nitrogen-doping level for phenolic recovery.

The synthesis of the 3D-N/rGO was carried out by mixed 1 g of glucose and 1 g of 0.5 wt.% urea loading N/rGO in round bottom quartz flask (Lu et al., 2023). The powder mixture then exposed to microwave heating at microwave power of 850 W for 30 minutes with a continuous of nitrogen gas flow of 150 mL/min supplied into the round-bottom flask to provide an inert atmosphere during synthesis (Zhou et al., 2020). After 30 minutes, the black foam-like substances that have produced will be collected.

This synthesis was repeated for others urea loading which were 2, 5, 8 and 10 wt. % which are here after denoted as 0.5, 2, 5, 8 and 10% 3D-N/rGO respectively.

3.8 Purification of Phenolic Extract using 3D-N/rGO

3.8.1 Purification via Batch Adsorption

Batch adsorption experiments were conducted using a modified method to evaluate the performance of 3D-N-rGO with varying urea loadings at 0.5, 2, 5, 8, and 10 wt.% in adsorbing phenolic compounds extracted from palm kernel cake (PKC). Batch adsorption was selected as the primary purification approach due to its effectiveness for preliminary screening and comparative evaluation of adsorbent performance under controlled conditions. In this study, batch adsorption was employed to fulfil Research Objective 1 by facilitating the selection of the optimal urea loading that yields the highest adsorption capacity. The adsorbent identified under batch conditions was subsequently applied in Research Objective 2 for fixed-bed purification studies. Compared with alternative purification techniques such as chromatography, membrane separation or liquid–liquid extraction, batch adsorption provides a simpler and more cost-effective method with lower operational complexity and reduced solvent consumption.

The phenolic extracts, initially obtained using ethanol, were separated via rotary evaporation and subsequently re-dissolved in ethanol for use. Each adsorption test involved mixing 1 g of the adsorbent with the phenolic solution in 250 mL conical flasks, which were sealed with parafilm and agitated at 300 rpm for 60 minutes at 30 °C (Ali et al., 2022; Darla et al., 2023). The selection of operational parameters was influenced by the limitations of the available equipment to ensure consistent and reproducible results. After the adsorption process, the mixtures were filtered to separate the spent adsorbent, while the filtrate containing unadsorbed components was collected and labeled as impurities. For the desorption step, the recovered adsorbents were immersed in 50 mL of acetone under identical stirring and temperature conditions. The concentrations of phenolic compounds before and after both adsorption and desorption were determined using the Folin-Ciocalteu assay, as described in Section 3.9.1. All experiments were performed in triplicate to ensure reproducibility and statistical reliability of the results. Adsorption capacity, removal efficiency, desorption capacity,

and desorption ratio were calculated based on Equations (3.2), (3.3), and (3.4) respectively (Cao et al., 2024).

$$\text{Adsorption capacity, } Q_e \text{ (mg/g)} = \frac{(C_i - C_f)V_s}{m} \quad (3.2)$$

$$\text{Adsorption Effieciency, } R_e \text{ (\%)} = \frac{(C_i - C_f)}{C_i} \times 100\% \quad (3.3)$$

$$\text{Desorption capacity, } Q_d \text{ (mg/g)} = \frac{C_d V_d}{m} \quad (3.4)$$

where C_i (mg/L) is initial concentration of extracted sample, C_f (mg/L) is final concentration, C_d (mg/L) is the sample concentration in the desorption solution, V_s (L) is the sample solution during adsorption process, V_d (L) is the sample solution volume during desorption process and m (g) is mass adsorbent was used.

3.8.2 Purification via Fixed Bed Adsorption

Fixed-bed adsorption was selected as the final purification strategy in this study to evaluate the dynamic adsorption behaviour of the optimised 3D-N/rGO adsorbent under continuous-flow conditions, which more closely resemble practical and industrial purification processes. A continuous fixed-bed column setup (3" x 24" Glass Chromatography Column–Medium Frit–10 Micron) was utilized to carry out the adsorption of phenolic compounds using a hydrophobic nanostructured 3D-N/rGO adsorbent (T. Van Chen et al., 2025). A flow adaptor was newly installed at the top of the column, and a variable-speed peristaltic pump was employed to control the flow rate, minimize bed dispersion, and prevent adsorbent loss. Prior to the adsorption process, the column was equilibrated with pure ethanol for 30 minutes (Nikolaeva et al., 2021). Subsequently, the 3D-N/rGO adsorbent exhibiting the highest adsorption capacity identified from batch studies was selected to assess its performance under varying conditions which was the 10% 3D-N/rGO.

In this study, the adsorption process parameters that will be conduct were adsorption temperatures (30, 40, 50, 60 and 70°C), initial phenolic concentrations (50, 70, 90, 120, and 150 mg/L), and adsorbent masses (0.50, 0.75, 1.0, 1.25, and 1.50 g) (Dargahi et al., 2023; Mamman et al., 2024). The selection of parameters were selected

with consideration of the performance boundaries of the available column configuration and equipment, thereby ensuring reliable operation and reproducible data acquisition. The key operating parameters in the fixed-bed adsorption study were selected to evaluate adsorption behaviour under controlled and practically relevant conditions. Adsorption temperature and initial phenolic concentration were varied to examine adsorption kinetics, thermodynamic behaviour, and isotherm characteristics, while the mass of adsorbent was adjusted to assess its effect on adsorption capacity and breakthrough behaviour.

A fixed volume of 250 mL phenolic solution was maintained for all experiments, with a flow rate set at 4.17 mL/min. The flow rate and solution volume were kept constant to ensure stable hydrodynamic conditions and consistent mass transfer during column operation. The samples were collected at regular 5-minute intervals for a total duration of 60 minutes. Upon completion, the concentrations of phenolic compounds before and after adsorption and desorption were determined using the Folin-Ciocalteu assay, as detailed in Section 3.9.1. Adsorption capacity, removal efficiency, and desorption capacity were calculated using Equations (3.2), (3.3), and (3.4) respectively. The schematic diagram of the experimental setup is illustrated in Figure 3.3.

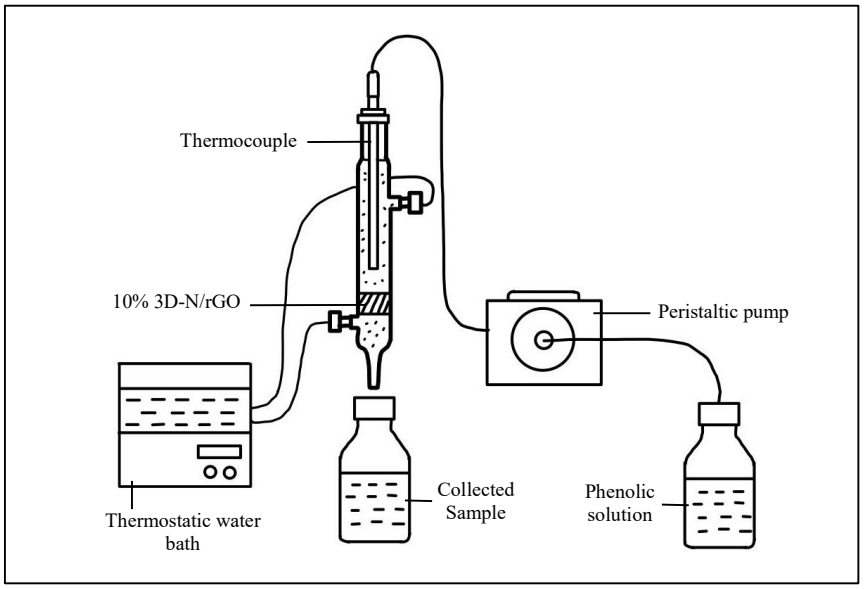


Figure 3.3 Schematic Diagram of Continuous Fixed-Bed Column

3.9 Phenolic Compounds Identification

3.9.1 Total Phenolic Content (TPC)

Total phenolic content (TPC) is measure using Folin-Ciocalteu. Dissolving 0.5 g gallic acid in 10 mL ethanol yielded a standard solution. Once the solution was in a 100-mL volumetric flask, the rest will fill with distilled water. Gallic acid solutions in ethanol were produced as per usual technique at 50, 100, 250, and 500 mg/L. Using different micropipette tips for each gallic acid concentration is essential while doing tests. To create 5 test tubes, 0.2 mL of 0.2N Folin-Ciocalteu reagent, 3.16 mL of distilled water, 0.6 mL of sodium carbonate (7.5%, w/v), and 40µL of gallic acid will be add with varying concentrations. Then, the mixture is rapidly mix and incubate for 2 hours at dark room temperature. Gallic acid will be replaced with ethanol for blank sample. Replaced gallic acid with the extracted sample for analysis. To ensure accuracy, the tests is repeat for three times. A double-beam UV-Vis spectrophotometer measure absorbance at 765 nm and compared it to gallic acid calibration curves. The absorbance was measured against an ethanol blank. Results were reported as mg gallic acid equivalents (GAE) per L (Jovanović et al., 2022).

The extracts were analysed to determine the TPC, which was then measured and reported as mg of gallic acid equivalents (GAE) per g of bio-oil (mg/g). Therefore, the total phenolic content may be calculated using the Equation (3.5) (Cao et al., 2024):

$$\text{Total Phenolic Content, C} = c\frac{V}{m} \tag{3.5}$$

where C (mg GAE/g bio-oil) is total phenolic content, c (mg/mL) is concentration of gallic acid from calibration curve, V (mL) is volume of extracted sample, and m (g) is the mass extract.

3.9.2 Liquid Chromatography Mass Spectrophotometer (LC-MS)

The identification and quantification of phenolic compounds were performed using an Agilent Q-TOF LC-MS/MS system (Model G6540B) equipped with a Dual AJS ESI (electrospray ionization) source operating in negative ion mode for phenolic

sample after purification. Chromatographic separation was carried out using a reversed-phase column at 40 °C. The mobile phase consisted of solvent A (0.1% formic acid in water) and solvent B (0.1% formic acid in acetonitrile). A gradient elution was employed starting from 95% A and 5% B at 0.00 min to 5% A and 95% B at 20.00 min, held until 25.00 min, and reverted to initial conditions at 30.00 min. The flow rate was maintained at 0.3 mL/min with a total run time of 30 minutes. The injection volume was 2 µL using a flush port needle wash for 5 seconds.

For the mass spectrometry conditions, the capillary voltage was set to 3500 V with a nozzle voltage of 1000 V. The drying gas temperature and sheath gas temperature were maintained at 350 °C, each with a flow rate of 12 L/min. The nebulizer pressure was set at 40 psig. The fragmentor voltage was 175 V, skimmer at 65 V, and octopole RF peak at 750 V. Data acquisition was conducted in AutoMS² mode with a mass range of m/z 100–1100 for both MS and MS/MS scans. The MS scan rate was 2 spectra/sec, while MS/MS was 4 spectra/sec with a medium isolation width (4 amu). Collision energy was fixed at 10 eV. Reference masses (m/z 112.9856, 119.0363, and 1033.9881) were used for continuous mass axis calibration throughout the analysis (Lippa et al., 2022; Sittipod et al., 2020).

3.9.3 Macro and Micronutrient

The macronutrient and micronutrient compositions of the phenolic compound before and after purification using 3D-N/rGO were determined following standard analytical methods. Moisture content was measured by weighing 2 g of sample into a pre-dried dish (W_1), drying at 135 °C until a constant weight (W_2) was obtained, and calculating the percentage moisture based on weight loss. Protein content was determined via the Kjeldahl method, where 1 g of sample was digested with potassium sulphate, copper sulphate, and sulphuric acid at 410 °C, distilled after neutralization with NaOH, and titrated with standardized NaOH solution. Carbohydrate content was calculated by difference, subtracting the sum of measured moisture, protein, and fat contents from 100 g, although fat was not measured in this study. Glucose content was analyzed using HPLC by dissolving 4 g of sample in distilled water, sonicating, diluting with acetonitrile, filtering, and injecting into an NH_2 column with an acetonitrile–water mobile phase (75:25 v/v) at a flow rate of 1 mL/min, with refractive index detection.

3.10 Characterization of 3D-N/rGO Adsorbent

3.10.1 Thermal Gravimetric Analysis (TGA)

The thermal stability of the adsorbent was evaluated using thermogravimetric analysis (TGA) conducted with a Thermal Advantage Q Series (TA 1000) instrument. TGA is a thermal analysis method that monitors changes in a material's physical and chemical properties as a function of temperature or time, typically under controlled heating or atmospheric conditions. The synthesized 3D-N/rGO samples with various urea loadings (0.5, 2, 5, 8, and 10 wt.%) were heated up to 700 °C at a rate of 10 °C/min in an air atmosphere. For comparison, graphene oxide (GO), prepared via Hummer's method, was subjected to heating up to 1000 °C at a slower rate of 5 °C/min under dry air conditions.

3.10.2 N_2 Adsorption-Desorption

The nitrogen (N_2) adsorption-desorption analysis was performed using a Micromeritics ASAP 2020 instrument. This technique was employed to characterize the adsorbent in terms of its surface area, pore volume, and pore size distribution. The BET method was specifically applied to determine the surface area due to its suitability for such measurements. To gain deeper insight into the pore structure, the Density Functional Theory (DFT) method was utilized for detailed pore size distribution analysis. The porosity and surface characteristics of graphene oxide (GO) and 3D nitrogen-doped reduced graphene oxide (3D-N/rGO) with varying urea loadings (0.5, 2, 5, 8, and 10 wt.%) were evaluated to support the adsorption-desorption performance and efficiency findings obtained from the batch adsorption studies described in Section 3.10.1. Prior to analysis, all 3D-N/rGO samples were degassed at 150 °C with a ramp rate of 5 °C/min for 24 hours by using a slit-shaped pore model.

3.10.3 High Resolution Transmission Electron Microscope (HRTEM)

The morphological and structural features of the synthesized 3D-N/rGO were examined using a Twin S, Tecnai, FEI High Resolution Transmission Electron Microscope (HRTEM), operated at an accelerating voltage of 200 kV (Aagaard et al., 2020). A small quantity of the sample was dispersed in deionized water and ultrasonicated to achieve a uniform suspension. A drop of this suspension was then placed onto a 300-mesh carbon-coated copper grid (Gras et al., 2011). The grid was subsequently dried under vacuum to ensure proper adherence and reduce contamination. HRTEM imaging provided detailed information on the internal structure, including lattice fringes, layer arrangement, and crystalline properties of the 3D-N/rGO material.

3.10.4 Fourier Transform Infrared Spectroscopy (FTIR)

The identification of functional groups in GO and 3D-N/rGO samples with varying urea loadings (0.5, 2, 5, 8, and 10 wt.%) was performed using Fourier Transform Infrared (FTIR) spectroscopy. This technique enables the detection of specific chemical bonds through their characteristic vibrational frequencies. The analysis was carried out using a Thermo Scientific Nicolet iS10 FTIR spectrometer, operating across a wavenumber range of 4000 to 400 cm^{-1}. This range is suitable for identifying a variety of functional groups, including hydroxyl, carbonyl, and amine groups. The instrument was set to a resolution of 16 to ensure clear distinction between absorption peaks. For sample preparation, approximately 1 to 2 mg of sample was thoroughly mixed with around 100 mg of dry potassium bromide (KBr) powder and pressed into a transparent pellet using a hydraulic press (Subramaniam et al., 2024). The use of KBr, which is transparent in the infrared region, allows accurate analysis in transmission mode (Subramaniam et al., 2024). This method enabled a detailed examination of the chemical structure, confirming the presence of functional groups such as N–H and C=O, and provided insights into the effectiveness of nitrogen doping through urea incorporation.

3.10.5 X-Ray Photoelectron Spectroscopy (XPS)

X-ray photoelectron spectroscopy (XPS) analysis, including both wide and high-resolution narrow scans, was conducted using an AXIS Ultra DLD spectrometer (Kratos, UK) at the Science and Engineering Research Centre (SERC), Universiti Sains Malaysia (USM). The instrument was equipped with an Al Kα monochromatic X-ray source (1486.6 eV) operated at 9 mA emission current and 12 kV anode high voltage. Spectra were collected over a 300 μm × 700 μm area under ultra-high vacuum conditions (7.6×10^{-9} torr) using a multichannel plate and delay line detector (DLD). The analysis was performed in hybrid lens mode with a slot aperture, while the analyser operated in fixed analyser transmission (FAT) mode with a pass energy of 160 eV for survey scans and 20 eV for high-resolution scans. Each scan was repeated a minimum of three times to ensure data accuracy. Charge neutralization was applied using a low-energy electron gun within the magnetic lens field. Data processing and peak deconvolution were carried out using Vision software (Vision Manager and Vision Processing), with background subtraction performed using the linear method. All binding energies were calibrated against the C 1s peak of adventitious carbon at 284.6 eV.

3.11 Mechanistic Insight Exploration

To elucidate the adsorption behaviour of phenolic compounds onto 3D nitrogen-doped reduced graphene oxide (3D-N-rGO), a mechanistic study was conducted comprising isotherm, kinetic, and thermodynamic analyses.

3.11.1 Isotherm Analysis

The equilibrium adsorption data were fitted to various isotherm models, namely Langmuir, Freundlich, Dubinin–Radushkevich (D–R), and Redlich–Peterson, to describe the interaction between the adsorbate and the adsorbent surface. The Langmuir model assumes monolayer adsorption on a homogeneous surface, and the key parameters include the maximum adsorption capacityand the Langmuir constant (KL), which reflects adsorption affinity. The Freundlich model describes adsorption on heterogeneous surfaces, with the Freundlich constants KF (adsorption capacity and

adsorption intensity) The D–R model provides information about adsorption energy, while the Redlich–Peterson model combines features of both Langmuir and Freundlich models. Linearized equations and corresponding plots for each model are summarized in Table 3.3.

3.11.2 Kinetic Analysis

Kinetic modelling was performed using pseudo-first-order and pseudo-second-order equations to determine the adsorption rate and potential rate-limiting steps. The pseudo-first-order model uses the rate constant k1 and equilibrium adsorption capacity qe to describe adsorption dependent on the number of unoccupied sites. The pseudo-second-order model considers the adsorption rate proportional to the square of the number of unoccupied sites, with the rate constant k2 and equilibrium adsorption capacity qe as key parameters. All equation for kinetic study were summarized in Table 3.3.

3.11.3 Thermodynamics

Thermodynamic parameters, including the Gibbs free energy change, enthalpy change, and entropy change, were calculated to assess the feasibility, spontaneity, and heat exchange associated with the adsorption process. The Gibbs free energy change was calculated using $\Delta G\circ = -RT \ln K_c$, where Kc is the equilibrium constant, R is the universal gas constant, and T is the absolute temperature. The enthalpy and entropy changes were obtained from the Van't Hoff equation shown in Table 3.3.

Table 3.3
Summary of Mechanistic Insight Study

Type of Models	Linear Equation	Plot	References
Isotherm Study			
Langmuir Isotherm	$\frac{C_e}{q_e} = \frac{1}{Q_m K_L} + \frac{1}{Q_m} C_e$	$\frac{C_e}{q_e}\ vs\ C_e$	(Dada et al., 2012)
Freundlich Isotherm	$\log q_e = \log K_F + \frac{1}{n} \log C_e$	$\log q_e\ vs \log C_e$	(Dada et al., 2012)
Temkin	$q_e = B \ln A_t + B \ln C_e$	q_e vs $\ln C_e$	(Dada et al., 2012)

Dubinin-Radushkevic	$\ln q_e = \ln q_m - \beta\varepsilon^2$	$\ln q_e \; vs \; \varepsilon^2$	(Dada et al., 2012)
Redlich Peterson	$\ln\left(\frac{K_R C_e}{q_e} - 1\right) = \beta \ln C_e$	$\ln\left(\frac{K_R C_e}{q_e} - 1\right) \; vs \; \ln C_e$	(Mourão et al., 2006)
Thermodynamic Study			
Van't Hoff Equation	$\Delta G^o = -RT \ln K_c$ $\Delta G^o = \Delta H^o - T\Delta S^o$		(Haydari et al., 2023)
	$\ln K_c = -\frac{\Delta H^o}{RT} + \frac{\Delta S^o}{R}$	$\ln K_c \; vs \; \frac{1}{T}$	(Haydari et al., 2023)
	$k_c = \frac{q_e}{C_e}$		(Haydari et al., 2023)
Kinetic Study			
Pseudo-First Order	$\log(q_e - q_t) = \log q_e - \frac{k_1}{2.303} t$	$\log(q_e - q_t) \; vs \; t$	(Haydari et al., 2023)
Pseudo-Second Order	$\frac{t}{q_t} = \frac{1}{k_2 q_e^2} + \frac{t}{q_e}$	$\frac{t}{q_t} \; vs \; t$	(Haydari et al., 2023)

CHAPTER 4
RESULTS AND DISCUSSION

4.1 Introduction

This chapter presents and discusses the experimental findings of the study, focusing on the effects of extraction conditions, adsorbent characteristics, and adsorption performance in both batch and fixed-bed column systems. The results are organised according to key parameters, including nitrogen doping ratios, temperature, initial phenolic concentration, and adsorbent mass, with data supported by relevant figures, tables, and model analysis to highlight observed trends. Comparative discussion with previous studies is incorporated to validate the outcomes and provide practical context. By systematically examining these factors, this chapter aims to identify optimal conditions for maximising phenolic recovery and adsorption efficiency while offering insights into the underlying adsorption mechanisms, beginning with batch adsorption–desorption using 3D-N/rGO with varying urea ratios.

4.2 Batch Adsorption–Desorption Purification of Phenolic Compounds Using 3D-N/rGO with Varying Urea Ratios

This section examines the purification performance of 3D-N/rGO synthesised with different urea loadings (0.5, 2, 5, 8, and 10 wt.%) in removing phenolic compounds from palm kernel cake (PKC) extracts through batch adsorption–desorption experiments. Batch adsorption–desorption experiments were employed as an initial screening approach to identify the optimal urea loading that provides the highest adsorption capacity and purification efficiency, in accordance with Research Objective 1. The urea loadings were selected to represent increasing nitrogen incorporation, allowing assessment of how different nitrogen contents affect surface functionality, adsorption affinity, and purification efficiency. The nitrogen doping can enhance phenolic adsorption through the introduction of surface defects, heteroatom active sites, and π–π and hydrogen-bonding interactions, while excessively high doping levels may reduce adsorption performance due to partial pore blockage or structural disruption.

The adsorbent mass, contact time, agitation speed, and temperature were kept constant based on equipment limitations, ensuring fair comparison across samples. The purification efficiency was evaluated by measuring the total phenolic content (TPC) before and after adsorption using the Folin–Ciocalteu assay, enabling the calculation of adsorption and desorption capacities. Figure 4.1 presents the initial and final TPC values for each urea loading, providing a direct comparison of the adsorbent's performance at different nitrogen-doping levels.

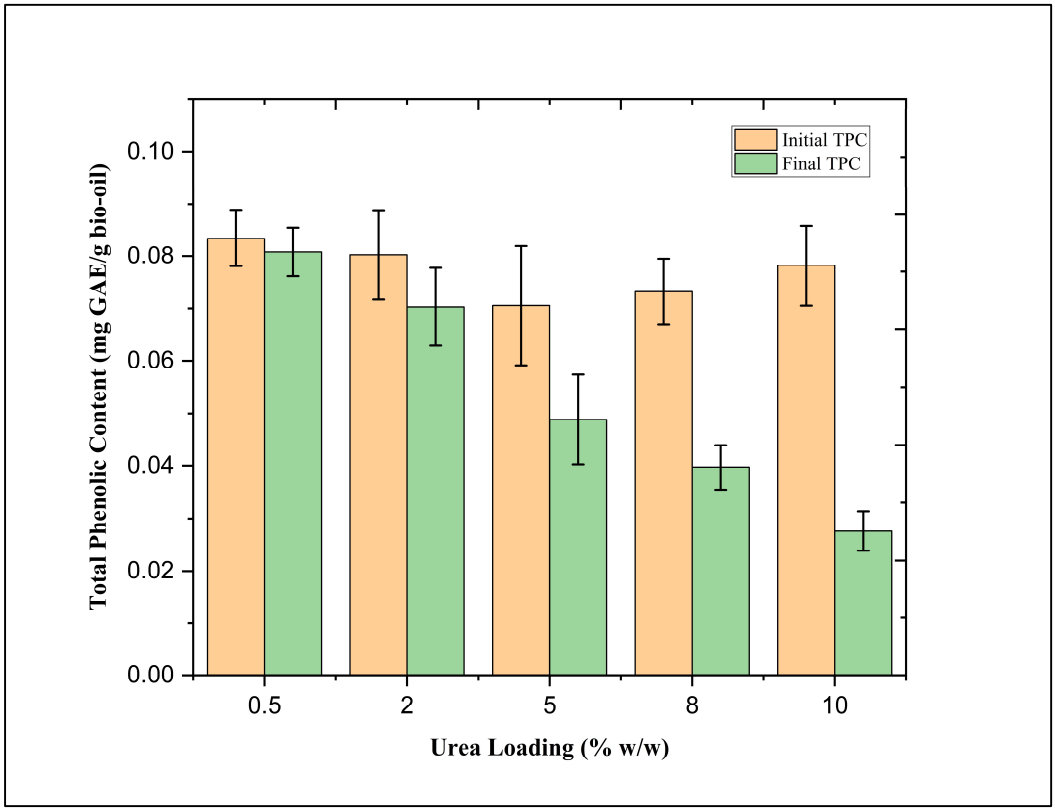


Figure 4.1 Effect of Urea Loading on TPC Before and After Purification

Among the various doping levels tested, the highest initial TPC was recorded at 0.5% urea loading (0.0835 mg GAE/g bio-oil), with only a slight decrease to 0.0808 mg GAE/g bio-oil after purification. This minimal reduction indicates that the adsorbent at this doping level exhibited the lowest adsorption efficiency towards phenolic compounds, likely due to insufficient nitrogen incorporation, which limits the number of active adsorption sites on the graphene structure. In contrast, the lowest final TPC was observed at 10% urea loading, decreasing from an initial TPC of 0.07982 mg GAE/g bio-oil to 0.0276 mg GAE/g bio-oil, indicating the highest adsorption efficiency. The significant reduction at this doping level suggests that a higher amount of urea

effectively enhanced the surface functionality of the 3D-N/rGO through increased nitrogen doping, which promoted stronger interactions such as hydrogen bonding and π–π stacking with phenolic molecules. Therefore, while lower urea loadings showed minimal removal, the 10% urea loading demonstrated the most effective purification performance.

The observed enhancement in phenolic removal at higher urea loading levels corresponds well with previous research. Sun et al. (2012) (L. Sun, Wang, Tian, Tan, Xie, Shi, Li, & Fu, 2012) reported that nitrogen-doped graphene synthesized via hydrothermal reaction with urea exhibited superior surface functionality and polarity, facilitating stronger interactions with phenolic compounds through π–π stacking and hydrogen bonding. Similarly, Zhao et al. (2021) (R. Zhao et al., 2021) confirmed the efficient removal of phenol using nitrogen-doped reduced graphene oxide, attributing the improvement to the presence of nitrogenous active sites such as pyridinic-N and graphitic-N. Supporting this, Saifuddin et al. (2014) (N. Saifuddin et al., 2014) demonstrated that the use of nitrogen-rich precursors enhanced phenolic compound recovery from palm oil mill effluent by improving surface affinity and adsorption kinetics. These findings validate the improved adsorption performance observed in this study at 10% urea doping, where higher nitrogen content likely contributed to the increased availability of active adsorption sites.

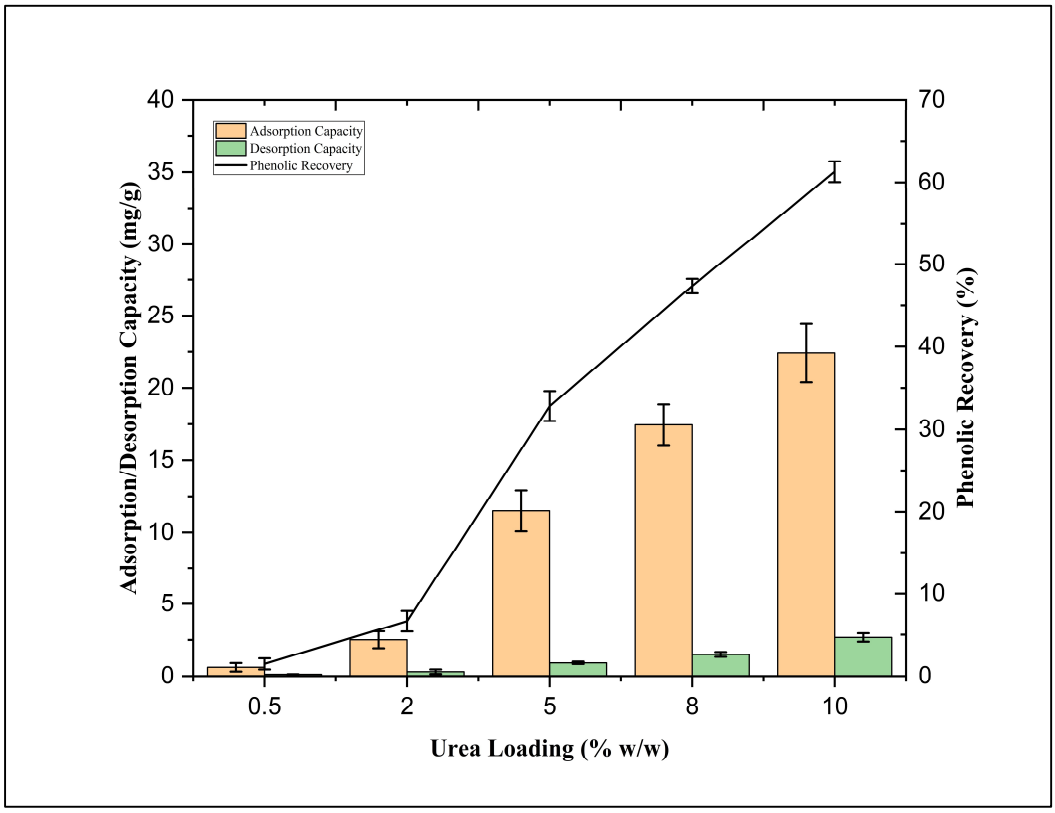


Figure 4.2 Effect of Urea Loading on The Adsorption and Desorption of Phenolic Compounds

Figure 4.2 illustrates the effect of urea loading on the adsorption and desorption capacities of 3D-N/rGO, as well as the corresponding phenolic recovery percentage. A clear trend is observed where increasing urea loading from 0.5 wt.% to 10 wt.% significantly enhances the adsorption capacity, which rises sharply from below 1 mg/g to approximately 23 mg/g. The enhanced adsorption performance observed at higher urea loadings particularly at 10 wt.% 3D-N/rGO is strongly supported by the XPS results as discussed in subsection 4.3.2. The survey spectra (Figure 4.7) confirm the successful incorporation of nitrogen into the graphene framework, as evidenced by the appearance of N 1s peaks in 3D-N/rGO that are absent in pristine GO. High-resolution N 1s spectra reveal the presence of pyridinic-N, pyrrolic-N, and graphitic-N species in the doped samples, with a clearer and more intense contribution of pyridinic and graphitic nitrogen after purification. These nitrogen functionalities are known to act as active adsorption sites, enhancing interaction with phenolic compounds through π–π interactions, hydrogen bonding, and polar interactions. In addition, BET analysis discussed in subsection 4.3.1 (Figure 4.4 and Table 4.3), shows a progressive decrease in surface area with increasing urea loading, from 46.61 m^2/g at 0.5 wt.% to 15.11 m^2/g

at 10 wt.%, the adsorption capacity increased significantly. This indicates that nitrogen functional group rather than surface area dominate phenolic adsorption. The reduction in surface area is attributed to partial pore blockage and aggregation of graphene sheets caused by excessive urea decomposition at higher loadings. However, XPS results demonstrate that higher urea loading simultaneously increases nitrogen-containing functional groups, which compensate for the loss of surface area by providing stronger and more selective adsorption sites.

In parallel, the phenolic recovery percentage also increases consistently with urea content, reaching over 60% at 10% urea loading, further confirming the enhanced adsorption efficiency. However, despite the increase in adsorption, the desorption capacity remains relatively low across all doping levels, with only a slight increase observed at higher loadings. The low desorption capacity observed across all urea loadings can be explained by the strong binding interactions between phenolic compounds and nitrogen-functionalised graphene surfaces. The dominance of pyridinic-N and graphitic-N species, together with reduced oxygenated groups after purification, suggests that phenolic adsorption is governed by relatively strong π–π stacking and hydrogen-bonding interactions. Overall, the data highlight 10% urea loading as the most effective condition for maximizing both adsorption performance and phenolic recovery.

The increasing adsorption capacity and phenolic recovery with higher urea loading observed in this study is well supported by previous literature. Liu et al. (2020) reported that nitrogen doping into three-dimensional graphene-based materials enhances surface polarity and active sites, resulting in improved adsorption of phenolic compounds. Patel (2019) (Patel, 2019) highlighted that nitrogen-rich modifications increase the efficiency of fixed-bed systems by promoting stronger adsorbate–adsorbent interactions and better binding behavior. Furthermore, Yeddou and Bensmaili (2007) (Yeddou & Bensmaili, 2007) emphasized that surface functionalization enhances the adsorption efficiency of phenol onto carbon materials, especially when the dopant introduces polar or basic groups to the adsorbent surface. These findings are in line with the current results, where 10% urea doping yielded the highest adsorption and phenolic recovery due to optimal nitrogen incorporation.

4.2.1 Liquid Chromatography-Mass Spectrometry (LC-MS) Analysis

The synthesized 3D-N/rGO adsorbent possesses structural and chemical properties that support its application for phenolic compound purification. The three-dimensional porous network provides a high surface area with interconnected channels that facilitate efficient molecular diffusion and improve accessibility to adsorption sites. Nitrogen doping within the graphene framework, including pyridinic-N, pyrrolic-N, and graphitic-N, enhances interactions with aromatic phenolic structures through π–π interactions, while oxygen-containing functional groups such as hydroxyl, carbonyl, and carboxyl groups contribute to hydrogen bonding and electrostatic interactions with phenolic molecules. These combined physicochemical characteristics promote selective adsorption of phenolic compounds while reducing non-polar lipid impurities present in the crude extract. To evaluate the effectiveness of the purification process, liquid chromatography–mass spectrometry (LC–MS) analysis was conducted to compare the chemical profiles of the extract before and after purification.

Table 4.1
Identified Compounds in The Extract Before and After Purification Using 3D-N/rGO Adsorbent Based on LC-MS Analysis

Compound	**Before Purification**		**After Purification**	
	RT (min)	**m/z**	**RT (min)**	**m/z**
2,3-Dihydroxy stearic acid	12.74	316.261	ND	ND
3R-methyl-undecanoic acid	15.09	200.177	ND	ND
2-ethyl-dodecanoic acid	17.30	228.209	ND	ND
10z, 12z-octadecadienoic acid	18.43	280.241	ND	ND
Palmitic acid	19.37	256.240	ND	ND
C18:1n-13 (oleic acid isomer)	19.77	282.256	ND	ND
11, 15-dimethyl-hexadecanoic acid	21.19	284.272	ND	ND
Phenolic ring fragment	0.69	130.966	2.21	130.966
Phenolic acid fragment	3.68	174.956	3.91	174.956

Polyphenol fragment	4.79	304.914	5.05	304.914

ND. : Not Detected

The LC–MS analysis of the extract before purification revealed several compounds predominantly associated with fatty acid derivatives and lipid-related components as summarized in Table 4.1 which are common fatty acids found in plant-based materials. For example, 2,3-dihydroxystearic acid was detected at RT 12.74 min with m/z 316.261, indicating the presence of hydroxylated fatty acid derivatives in the crude extract. Similarly, 3R-methyl-undecanoic acid was observed at RT 15.09 min (m/z 200.177) and 2-ethyl-dodecanoic acid at RT 17.30 min (m/z 228.209), both representing branched-chain fatty acid structures. In addition, 10z,12z-octadecadienoic acid appeared at RT 18.43 min with m/z 280.241, while palmitic acid, a common saturated fatty acid in plant matrices, was detected at RT 19.37 min (m/z 256.240). The compound C18:1n-13 (oleic acid isomer) was also identified at RT 19.77 min with m/z 282.256, together with 11,15-dimethyl-hexadecanoic acid at RT 21.19 min (m/z 284.272). These compounds are primarily long-chain fatty acids or lipid derivatives, indicating that the crude extract contains a complex mixture of hydrophobic lipid components prior to purification. The presence of these lipid compounds may interfere with the detection and enrichment of phenolic compounds due to their non-polar characteristics.

After purification using the 3D-N/rGO adsorbent, the LC–MS analysis of showed a noticeable reduction or not detected in the previously detected lipid-related compounds. As shown in Table 4.1, the fatty acids detected in the crude extract, including 2,3-dihydroxystearic acid (RT 12.74 min, m/z 316.261), 3R-methyl-undecanoic acid (RT 15.09 min, m/z 200.177), 2-ethyl-dodecanoic acid (RT 17.30 min, m/z 228.209), 10z,12z-octadecadienoic acid (RT 18.43 min, m/z 280.241), palmitic acid (RT 19.37 min, m/z 256.240), C18:1n-13 (RT 19.77 min, m/z 282.256) and 11,15-dimethyl-hexadecanoic acid (RT 21.19 min, m/z 284.272), were not detected after purification. This observation suggests that the 3D-N/rGO adsorbent effectively removed hydrophobic lipid impurities from the extract.

The disappearance of long-chain fatty acid signals and the increased prominence of lower molecular weight fragment ions suggest that the purification process selectively enriched polar phenolic constituents while eliminating non-polar lipid impurities. Such purification is essential for improving the detection sensitivity and

structural characterization of phenolic compounds in complex plant extracts. This observation is further supported by the Total Phenolic Content (TPC) results in section 4.2, where the phenolic content of the bio-oil decreased after purification with the 3D-N/rGO adsorbent. The reduction in TPC indicates that phenolic compounds were effectively adsorbed onto the 3D-N/rGO surface during the purification process.

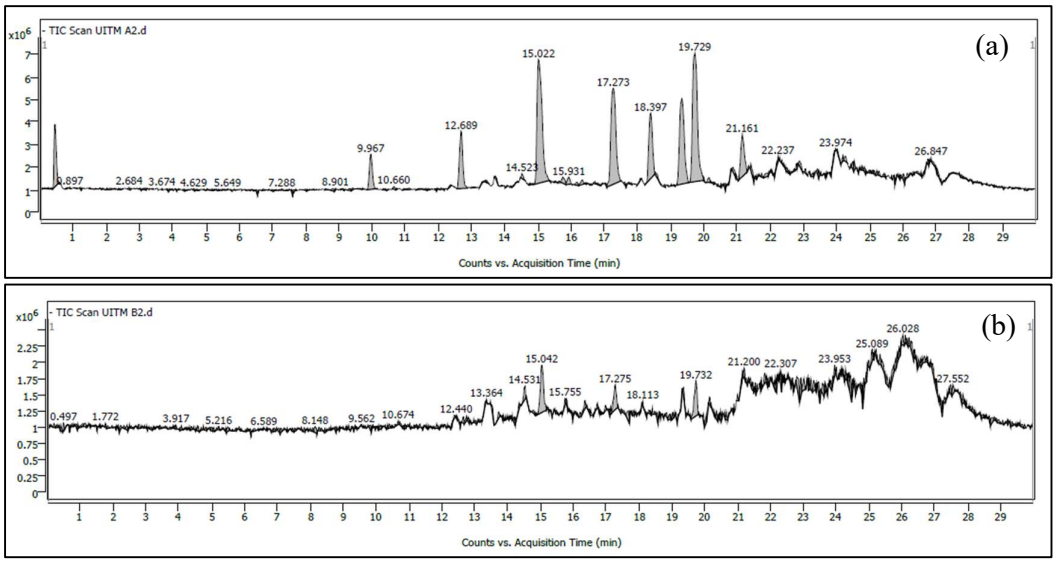


Figure 4.3 LC-MS Chromatograph Results (a) Before Purification and (b) After Purification

The comparison of the LC–MS chromatographs before and after purification is presented in Figure 4.3. In Figure 4.3a, several prominent peaks were observed across the retention time range of approximately 12–21 min, corresponding to the lipid-related compounds identified in Table 4.1, such as fatty acid derivatives including 2,3-dihydroxystearic acid, palmitic acid, and other long-chain fatty acids. These peaks indicate the presence of hydrophobic lipid components in the untreated extract. After purification using the 3D-N/rGO adsorbent, the chromatograph result Figure 4.3b showed a noticeable reduction in the intensity and number of these peaks. The disappearance of several peaks in the 12–21 min retention time region further confirms that the purification process effectively removed lipid-related impurities from the extract.

In addition, several fragment ions within the m/z range of 150–600 were observed particularly m/z 130, 174 and 304, which are commonly associated with phenolic ring, phenolic acid and polyphenol fragments respectively (Mohamed Yunus

et al., 2021). For example, the fragment ion m/z 130.966 was detected at a retention time of 0.69 min (before) and 2.21 min (after), while the fragment m/z 174.956 appeared at approximately 3.68 min (before) and 3.91 min (after), and m/z 304.914 was detected at around 4.79 min (before) and 5.05 min (after). A study conducted by Amirhossein Sharifi-Rad et al. (2021) demonstrated that phenolic acids such as caffeic acid, chlorogenic acid, and ferulic acid produce characteristic fragment ions within the m/z range of 127–179, which result from the fragmentation of phenolic ring structures during MS/MS analysis (Sharifi-Rad et al., 2021). In the same study, flavonoid compounds including taxifolin and isorhamnetin were reported to generate fragment ions around m/z 300–303, which are comparable to the m/z 304 fragment detected in this study (Sharifi-Rad et al., 2021).

Another study reported by Maha A. M. El-Shazly et al. (2022), also revealed comparable fragmentation pathways for phenolic compounds (El-Shazly et al., 2022). Their study showed that phenolic acids such as caffeic acid and cinnamic acid commonly produce fragment ions in the m/z 129–135 region, which correspond to the aromatic phenolic rings during MS/MS analysis. In addition, phenolic acid derivatives including ferulic acid and caffeoylquinic acid derivatives generate fragments around m/z 173–179, representing typical phenolic acid fragmentation patterns (El-Shazly et al., 2022). Moreover, flavonoid compounds such as taxifolin, isorhamnetin and luteolin were found to yield fragment ions near m/z 300, resulting from the breakdown of flavonoid aglycone structures (El-Shazly et al., 2022). These reported fragments are consistent with the m/z 304 fragment detected further indicating the presence of phenolic-related constituents in the extract.

4.2.2 Macro and Micronutrient

Table 4.2 presents the macronutrient and micronutrient composition of the phenolic extracts before adsorption, after desorption, and the corresponding purification factor (PF) values obtained using 3D-N/rGO adsorbent. The macronutrients measured include carbohydrate, protein, moisture, and glucose content, while the micronutrients are represented by the total phenolic content (TPC). The PF, calculated as the ratio between the concentration in the desorbed fraction and that in the feed solution prior to adsorption, provides an indication of the effectiveness of the purification process. This

comparison allows for the evaluation of the adsorbent's ability to selectively retain and recover phenolic compounds while removing non-target components.

Table 4.2
The Macro and Micro-Nutrients Composition of Phenolic Compound Before and After Purification Using 3D/N/rGO Adsorbent

	Composition	Before Adsorption	Desorption	Purification Factor (PF)
Macronutrients	Carbohydrate (g/100g)	1.5	0.0	0.0
	Protein (g/100g)	0.2	0.1	0.5
	Moisture (g/100g)	98.3	99.9	1.016
	Glucose (% w/w)	ND < 0.1	ND < 0.1	0.0
Micronutrients	Total Phenolic Content (mg GAE/g bio-oil)	0.094	0.068	0.723

PF: Purification factor (the ratio between the value in the desorption and those values before adsorption), N.d. (not detected)

Among the macronutrients, carbohydrates and proteins were slightly present before adsorption (1.5 g/100 g and 0.2 g/100 g, respectively), but their values dropped significantly or were completely removed after desorption, resulting in purification factors of 0.0 and 0.5, respectively. The selective removal behaviour observed among different macronutrients can be attributed to the distinct physicochemical properties and interaction mechanisms of each component with the 3D-N/rGO adsorbent. Carbohydrates, which are predominantly hydrophilic and lack aromatic structures, exhibit weak affinity towards the hydrophobic and π-electron–rich surface of 3D-N/rGO (Wei et al., 2020). As a result, carbohydrates are minimally retained on the adsorbent surface and are effectively removed during adsorption and subsequent washing steps, leading to their complete absence in the desorbed fraction. In contrast, proteins contain a heterogeneous distribution of functional groups including aromatic amino acid residues (Dunham et al., 2021). This allow interaction with nitrogen-doped graphene surfaces through hydrogen bonding, electrostatic attraction, and π–π interactions. Consequently, a fraction of protein molecules remains associated with the adsorbent, while the remainder is removed during desorption, resulting in partial rather than complete removal.

The fat and ash content were consistently absent in both stages, while moisture content slightly increased from 98.3 to 99.9 g/100 g, yielding a PF of 1.016, likely due to minor fluctuations during processing. Glucose remained undetectable (ND < 0.1%) throughout, indicating no significant interference. For micronutrients, the total phenolic content (TPC) decreased from 0.094 to 0.068 mg GAE/g bio-oil after desorption, corresponding to a PF of 0.723. Although a purification factor (PF) of 0.723 indicates successful recovery of a substantial fraction of phenolic compounds, it also reflects an approximate 28% loss during the adsorption–desorption process. This loss can be attributed primarily to irreversible or strongly bound phenolic species that remain retained on the 3D-N/rGO surface after desorption. Strong π–π interactions between the aromatic rings of phenolic compounds and the graphene framework, together with hydrogen bonding involving nitrogen-containing functional groups, can limit complete phenolic release under the desorption conditions.

This value suggests that a considerable portion of phenolics was successfully recovered after purification, while unwanted macronutrients were mostly removed. Overall, the data confirm that 3D-N/rGO effectively enhanced the selectivity towards phenolic compounds while minimizing co-extraction of non-phenolic nutrients. This finding aligns with previous research demonstrating that nitrogen-doped reduced graphene oxide (N-rGO) exhibits a high affinity for phenolic compounds due to the presence of nitrogen functional groups, which facilitate π–π interactions and hydrogen bonding with phenolic molecules. For instance, a study by Li et al. (2012) reported that N-RGO strongly adsorbed bisphenols, enhancing its performance in removing phenolic compounds from aqueous solutions (Y. Li et al., 2012).

4.3 Characterization of Hydrophobic Nanostructure 3D-N/rGO Adsorbent

4.3.1 Physical Stability and Surface Characteristics

Figure 4.4 and Table 4.3 collectively present the thermogravimetric analysis (TGA) and proximate analysis of graphene oxide (GO) and 3D nitrogen-doped reduced graphene oxide (3D-N/rGO) synthesised with varying urea loadings (0.5, 2, 5%, 8, and 10 w.%). The proximate analysis quantifies the contributions of moisture content, volatile matter, fixed carbon, and ash content, providing quantitative support for the thermal stability trends observed in the TGA curves. TGA was performed to evaluate

the thermal stability and decomposition behaviour of the materials, which can be correlated to their structural integrity and nitrogen doping level. The weight loss patterns observed reflect moisture evaporation, decomposition of labile oxygen-containing groups, and breakdown of the carbon framework at elevated temperatures. By comparing the thermal profiles of GO and the doped 3D-N/rGO samples, the influence of nitrogen incorporation on enhancing thermal stability can be assessed.

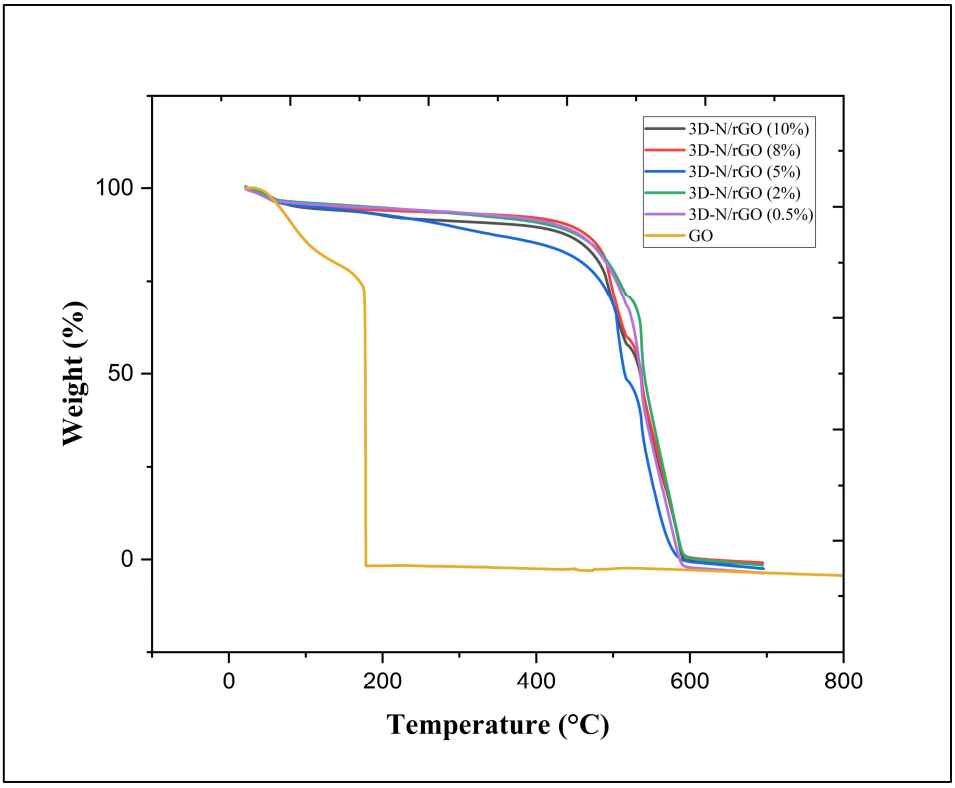


Figure 4.4 TGA Curves of GO and 3D-N/rGO at Different Urea Loading

Table 4.3
Proximate Analysis of GO and 3D-N/rGO at Different Urea Loading

Samples	Moisture Content (%)	Volatile Matter (%)	Fixed Carbon (%)	Ash Content (%)
GO	21.33	78.67	0.00	0.00
3D-N/rGO (0.5%)	4.04	95.96	0.00	0.00
3D-N/rGO (2%)	4.38	95.08	0.54	0.00
3D-N/rGO (5%)	5.01	94.99	0.00	0.00
3D-N/rGO (8%)	4.99	94.31	0.69	0.00
3D-N/rGO (10%)	5.63	94.37	0.00	0.00

Graphene oxide (GO) exhibited a high moisture content of 21.33%, reflecting the strong hydrophilicity associated with abundant oxygen-containing functional groups such as hydroxyl, epoxy, and carboxyl moieties. This is consistent with the sharp and rapid weight loss observed in the TGA curve at approximately 200 °C, which corresponds to the decomposition of these labile oxygen functionalities. The absence of fixed carbon and residual mass in GO indicates poor thermal stability and extensive structural degradation at relatively low temperatures.

In contrast, all 3D-N/rGO samples demonstrated substantially lower moisture contents (4.04–5.63%), indicating effective reduction of oxygenated groups and decreased hydrophilicity following nitrogen doping and thermal treatment. The volatile matter content remained high (>94%) for all doped samples, reflecting the decomposition of surface functional groups over a broader temperature range, as observed in the gradual weight-loss profiles between approximately 200 °C and 600 °C in the TGA curves.

Notably, samples with higher urea loadings exhibited increased thermal resistance, as evidenced by the delayed onset of major decomposition and higher residual mass at elevated temperatures. The 2% and 8% 3D-N/rGO samples showed measurable fixed carbon contents of 0.54% and 0.69%, respectively, indicating improved structural integrity and partial preservation of the carbon framework after thermal treatment. Although the fixed carbon values appear low overall, their presence

exclusively in nitrogen-doped samples confirms that nitrogen incorporation contributes to enhanced thermal robustness compared to GO.

The 10% 3D-N/rGO sample displayed the highest residual weight at 600 °C in the TGA curve, despite a lower measured BET surface area reported. This behaviour suggests the formation of thermally stable nitrogen functionalities and cross-linked carbon structures arising from higher urea decomposition and nitrogen incorporation. Stronger C–N bonding and reduced oxygen content suppress rapid thermal degradation and delay framework collapse at elevated temperatures (Wu et al., 2022). These results show the successful formation of nitrogen-doped rGO and demonstrate that increasing urea loading not only modifies chemical composition but also enhances the thermal stability of the adsorbent material.

Figure 4.5 presents the nitrogen adsorption–desorption isotherms of 3D nitrogen-doped reduced graphene oxide (3D-N/rGO) prepared with varying urea loadings (0.5, 2, 5%, 8, and 10 w.%) determined by Brunauer–Emmett–Teller (BET) analysis. The isotherms exhibit a typical type IV pattern with an H3 hysteresis loop, characteristic of mesoporous materials, indicating the presence of slit-shaped pores formed by the stacking of graphene layers. These results provide insight into how urea loading modulates surface area and porosity, which are critical factors in adsorption performance.

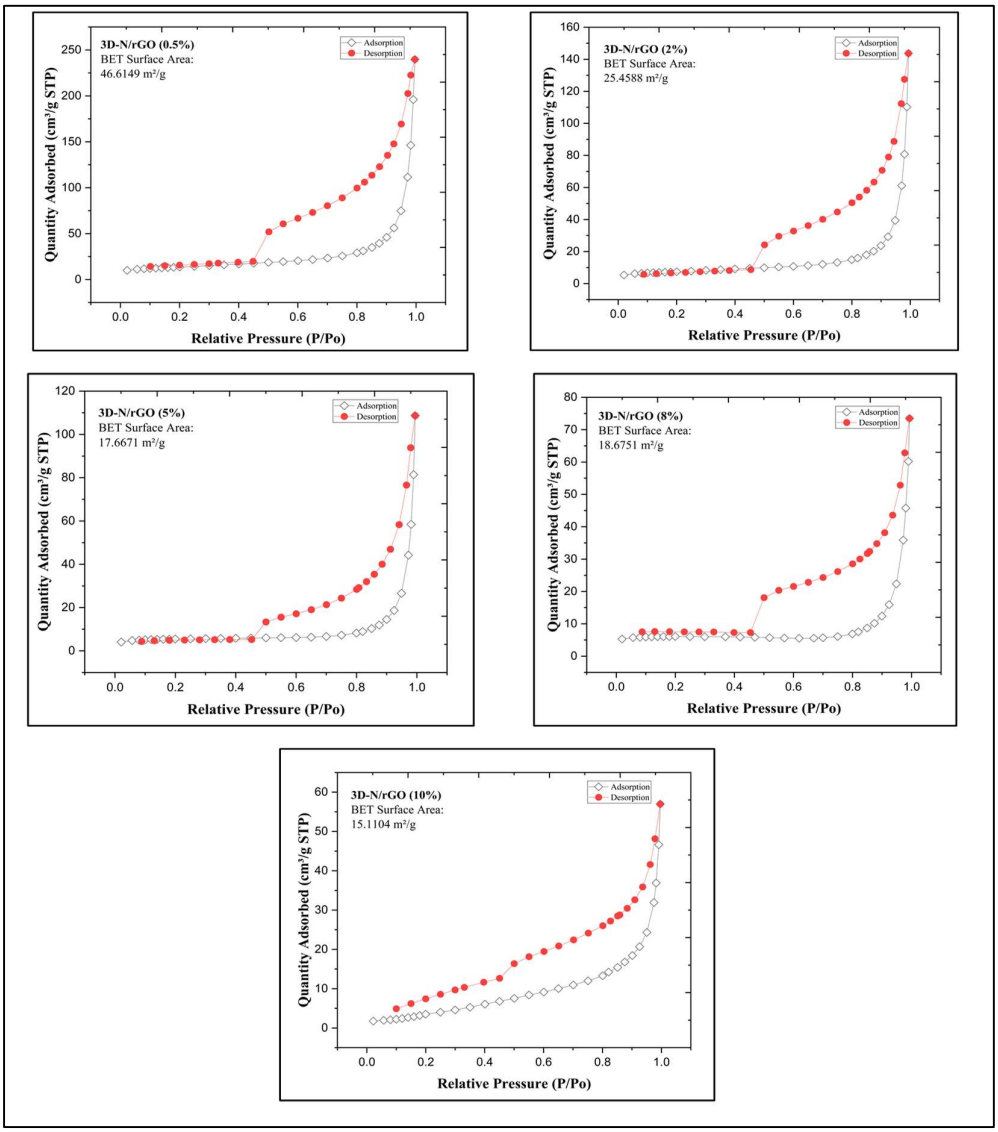


Figure 4.5 BET Analysis of 3D-N/rGO With Different Urea Loading

Table 4.4
Summary of BET Analysis

Urea Loading of 3D-N/rGO (%)	Surface Area (m^2/g)	Pore Volume (cm^3/g)	Pore Size ($\AA$)
0.5	46.6149	0.370716	318.1092
2	25.4588	0.222263	349.2128
5	17.6671	0.168063	380.5101
8	18.6751	0.113658	243.4431
10	15.1104	0.088144	233.3348

Table 4.4 shows the summary of BET analysis. The 3D-N/rGO sample doped with 0.5% urea exhibited the highest BET surface area of 46.6149 m^2/g, reflecting the presence of well-developed porosity and limited pore obstruction during synthesis. As the urea loading increased, a clear decreasing trend in surface area was observed. The surface area dropped to 25.4588 m^2/g at 2% loading, followed by further reductions to 17.6671 m^2/g (5%), 18.6751 m^2/g (8%), and ultimately 15.1104 m^2/g at 10% urea loading.

This reduction in surface area with increasing nitrogen content may be due to the excessive urea during synthesis that led to pore blockage or collapse of the 3D graphene network (Zhang et al., 2019). The thermal decomposition of urea at high loadings may produce excessive gaseous by-products or cross-linking between graphene sheets, which can promote aggregation and reduce the accessibility of internal pores (Zeng & Pan, 2022).

Despite the decline in surface area, the adsorption capacity and phenolic recovery increased with higher urea loading, with 10% 3D-N/rGO exhibiting the highest adsorption performance. This inverse relationship demonstrates that surface area is not the dominant factor governing phenolic adsorption efficiency. Instead, the enhancement in adsorption performance is attributed primarily to changes in surface chemistry induced by nitrogen doping. XPS analysis discussed confirmed that higher urea loadings resulted in increased incorporation of nitrogen functional groups, particularly pyridinic-N and graphitic-N species. These nitrogen functionalities introduce electron-rich active sites that strengthen π–π interactions, and hydrogen bonding between the adsorbent surface and phenolic molecules. In addition, FTIR analysis further supports the surface modification by showing changes in oxygen-containing functional groups and the appearance of nitrogen-related vibrations after nitrogen doping. These combined results indicate that the improved adsorption performance is mainly governed by the modification of surface functional groups rather than surface area alone. A more detailed discussion of the XPS and FTIR characterization results is presented in subsection 4.3.2.

This observed decline in BET surface area with increasing urea loading is consistent with the findings of Khojasteh et al., (2018) (Khojasteh et al., 2018) who reported that excessive urea in the solid-phase synthesis of nitrogen-doped graphene led to aggregation and partial collapse of the porous network due to the generation of gaseous by-products during thermal treatment. Despite the reduction in surface area,

their study highlighted a significant enhancement in adsorption performance, attributed to the introduction of nitrogen functionalities such as pyridinic and graphitic nitrogen species. These active sites were found to play a pivotal role in improving the interaction between the adsorbent and target molecules. Such findings support the notion that surface chemistry rather than surface area alone drives the superior adsorption capability of 3D-N/rGO, particularly in the context of phenolic compound purification.

Figure 4.6 shows the morphological characteristics of graphene oxide (GO) and three-dimensional nitrogen-doped reduced graphene oxide (3D-N/rGO) were investigated using High Resolution Transmission Electron Microscopy (HRTEM). Images (a) and (b) depict GO at different magnifications, revealing randomly stacked, wrinkled, and partially transparent sheet-like structures, which are typical features of exfoliated graphene oxide layers. The presence of disordered and aggregated flakes indicates the successful oxidation and exfoliation of graphite into GO, consistent with previous reports (James et al., 2013).

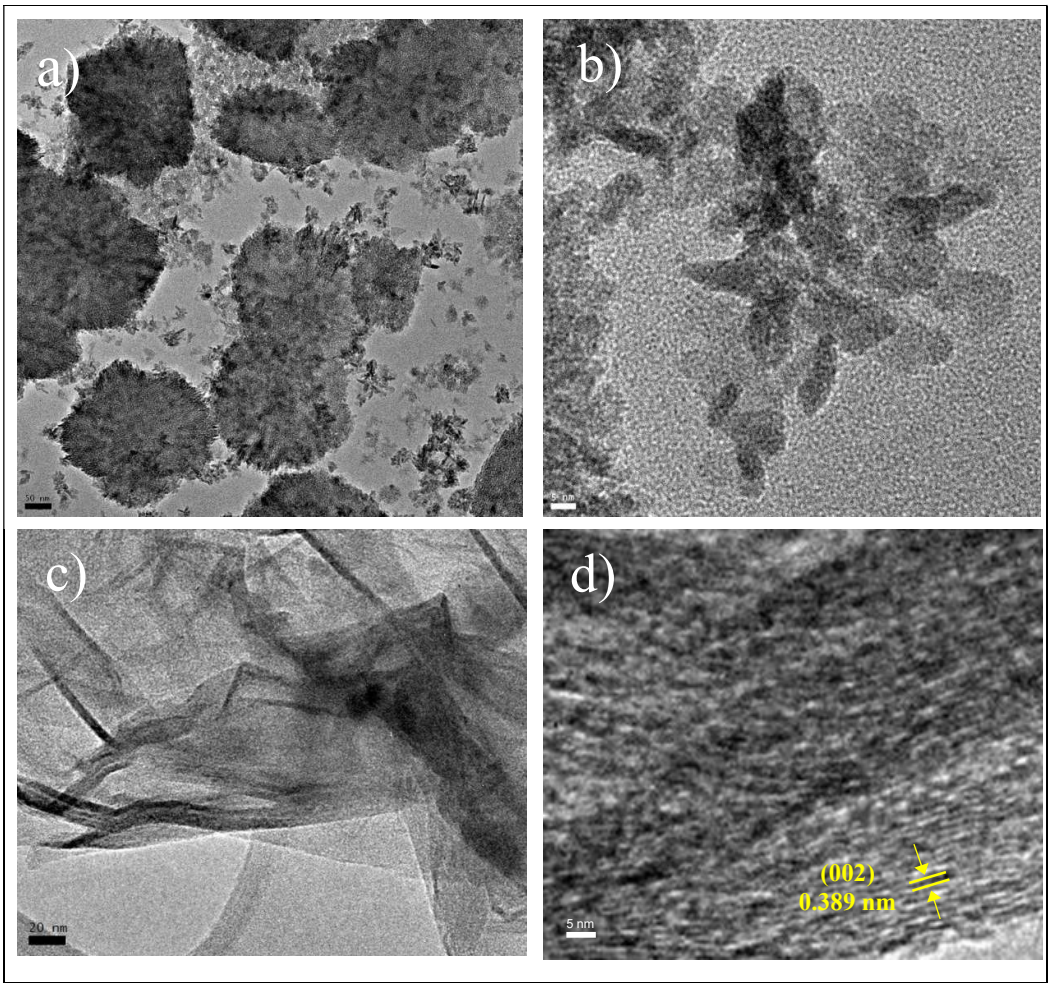


Figure 4.6 HRTEM Images; (a-b) GO at Different Magnification and (c-d) 3D-N/rGO at Different Magnification.

In contrast, images (c) and (d) show the morphology of 3D-N/rGO after nitrogen doping and reduction. Image (c) highlights the thin, interconnected layers forming a crumpled 3D network, suggesting enhanced surface roughness and the creation of porous architecture due to nitrogen incorporation and structural reassembly during thermal treatment (Kaniyoor et al., 2011). This wrinkled and folded morphology facilitates high surface area and abundant active sites, which are beneficial for adsorption applications.

Notably, image (d) displays lattice fringes with an interlayer spacing of approximately 0.389 nm, corresponding to the (002) plane of graphitic carbon. This spacing is slightly larger than pristine graphite (0.34 nm), indicating partial restoration of graphitic domains and the presence of structural defects induced by nitrogen doping (Chi et al., 2023). The clear lattice structure confirms the crystalline nature of the reduced graphene layers, and the expanded spacing may be attributed to the

incorporation of nitrogen atoms or residual oxygen-containing groups. These structural defects are known to act as active adsorption sites by enhancing π–π interactions and hydrogen bonding with aromatic phenolic molecules.

The presence of nitrogen-induced defects and enlarged interlayer spacing facilitates improved accessibility of phenolic compounds to the internal graphene layers, thereby strengthening adsorbate–adsorbent interactions. Pyridinic and graphitic nitrogen species as identified in XPS analysis, further contribute to increased electron density and polarity at defect sites, enhancing the affinity towards phenolic hydroxyl groups. In addition, BET analysis (Table 4.4) shows that increasing urea loading resulted in a gradual decrease in surface area from 46.61 m^2/g (0.5 %) to 15.11 m^2/g (10 %), accompanied by a reduction in pore volume from 0.3707 to 0.0881 cm^3/g and a decrease in pore size from 318 Å to 233 Å. These changes associated with structural rearrangement and partial restacking of graphene sheets after nitrogen incorporation which is consistent with the structural defects and layer modification observed in HRTEM analysis. Despite the reduction in surface area and pore structure parameters, the 10 wt.% 3D-N/rGO exhibited the highest adsorption performance indicating that phenolic adsorption in this system is governed more strongly by surface chemical functionality introduced through nitrogen doping rather than by surface area alone.

These morphological features are consistent with previous studies. Feng et al. (2015) (Feng et al., 2021) reported wrinkled and interconnected graphene nanosheets with visible lattice fringes in their 3D-rGO structures, promoting porosity and adsorption potential. In agreement, Hou et al. (2016) (Hou et al., 2016) found that nitrogen incorporation led to crumpled morphologies and structural distortions that improved adsorption performance. The observed 0.389 nm spacing in this study reflects partial graphitic restoration and doping-induced disorder, confirming successful synthesis of 3D-N/rGO with favorable traits for phenolic compound purification. In the context of phenolic purification, these structural attributes are critical, as they promote effective binding and retention of phenolic compounds during the adsorption process, thereby improving the overall purification efficiency.

4.3.2 Functional Groups and Surface Chemistry

Figure 4.7 displays the FTIR spectra of GO and 3D-N/rGO synthesized with varying urea loadings (0.5%–10%), highlighting the structural changes and functional groups present in the materials.

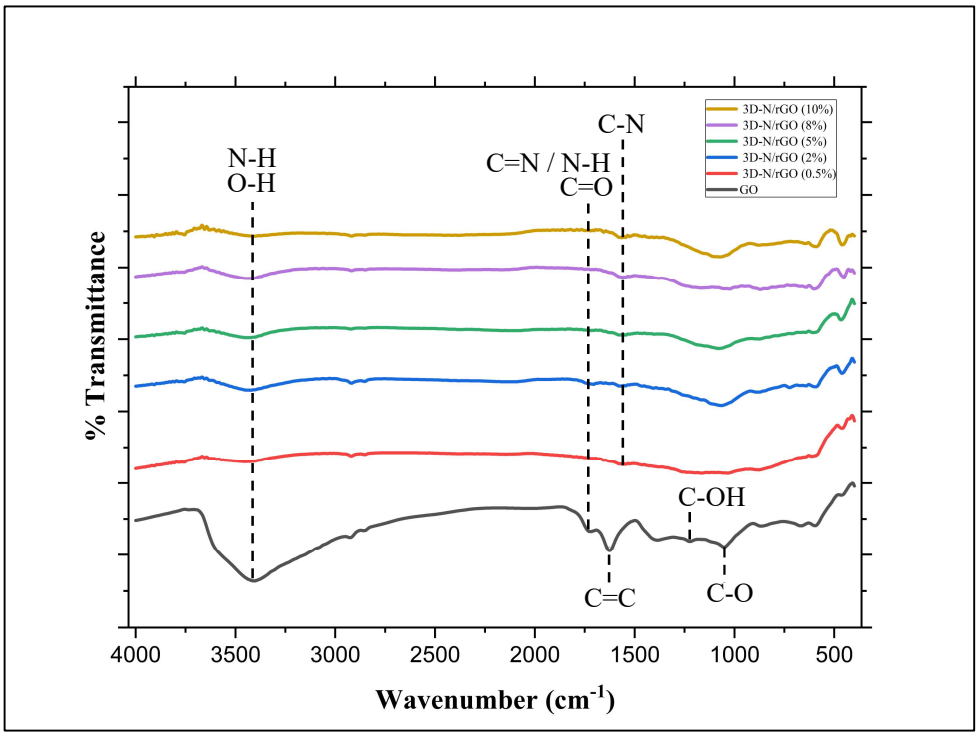


Figure 4.7 FTIR of GO and 3D-N/rGO at Different Urea Loading

In the spectrum of pristine GO exhibits strong and broad peaks that can be observed around 3400 cm^{-1} corresponding to O–H stretching vibrations. A distinct peak near 1720 cm^{-1} attributed to C=O stretching of carboxyl groups (Song et al., 2021). The peaks around 1620 cm^{-1} corresponds to C=C skeletal vibrations of sp^2 carbon with possible contribution from absorbed water bending (Arsalani et al., 2018). Additional peaks observed at approximately 1220 cm^{-1} and 1050 cm^{-1} are associated with C–OH stretching and C–O stretching of epoxy or alkoxy groups, respectively (Arsalani et al., 2018). These oxygen-containing functional groups confirm the successful oxidation of graphite and indicate the presence of abundant hydrophilic sites, which can interact with phenolic hydroxyl groups through hydrogen bonding during purification. However, the high oxygen content also means fewer exposed graphitic domains, potentially limiting π–π stacking interactions with the aromatic rings of phenolic compounds.

Upon nitrogen doping via urea, significant changes were observed in the spectra of 3D-N/rGO. The intensity of the oxygen-related peaks decreased gradually with increasing urea content, indicating partial reduction of GO and removal of oxygen functionalities during thermal treatment. Simultaneously, the appearance of new or shifted bands particularly in the regions around 1550–1650 cm^{-1} and 1380–1450 cm^{-1} suggest the incorporation of nitrogen-containing groups such as C–N, C=N, N–H bending, and possibly pyridinic or pyrrolic nitrogen. These nitrogen functionalities introduce additional active sites that can form strong hydrogen bonds with hydroxyl groups in phenolics, complementing π–π interactions and enhancing both adsorption strength and selectivity during purification.

Among the doped samples, the 10 wt.% urea-loaded 3D-N/rGO exhibited the greatest reduction of oxygen peaks and the most pronounced nitrogen-related features, indicating optimal surface chemistry for phenolic recovery. The combination of restored graphitic domains for π–π stacking and nitrogen-based sites for hydrogen bonding maximises the adsorption affinity towards phenolic compounds.

Figure 4.8 shows the surface chemical composition and bonding states of GO and 3D-N/rGO before and after purification were analyzed using X-ray Photoelectron Spectroscopy (XPS).

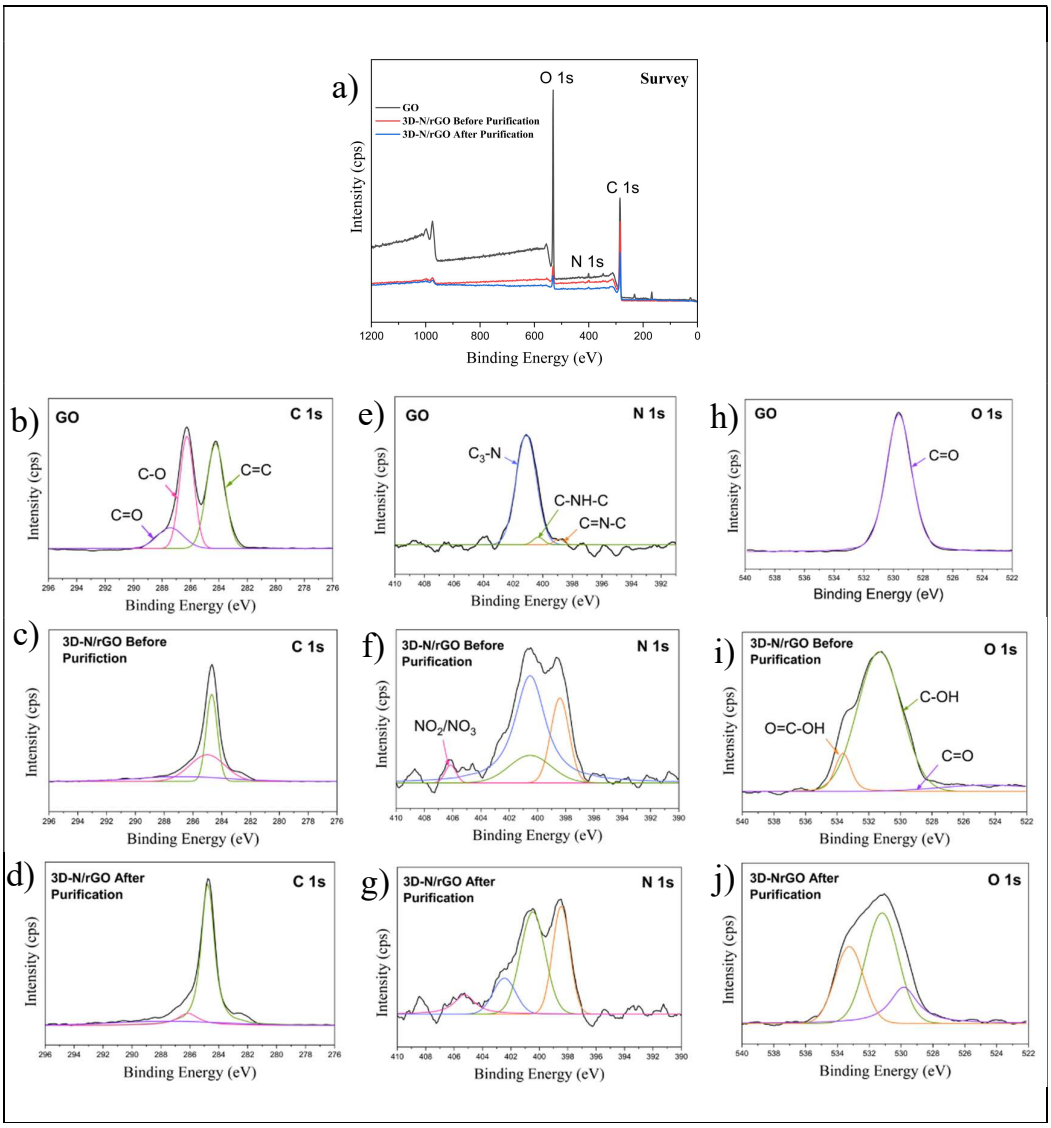


Figure 4.8 XPS Survey Spectrum of GO and 3D/rGO Before and After Purification; (a) Survey Scan, (b-d) C 1s Spectra, (e-g) N 1s Spectra and (h-j) O 1s Spectra

The survey spectrum (Figure 4.8 a) confirms the presence of the key elements C 1s (284 eV), O 1s (531 eV), and N 1s (400 eV) (Galal et al., 2019; Zhou et al., 2018). As expected, nitrogen peaks are absent in GO but become prominent in 3D-N/rGO, indicating successful nitrogen doping following thermal treatment with urea.

The high-resolution C 1s spectra (Figures 4.8 b–d) show distinct variations in bonding environments. For GO (Figure 4.8 b), peaks corresponding to C=C (284.6 eV), C–O (286.7 eV), and C=O (288.4 eV) were observed, reflecting high oxidation states due to oxygen-containing functional groups. In 3D-N/rGO before purification (Figure 4.8 c), the intensity of oxygenated groups decreased, suggesting partial reduction, while the dominant C–C peak increased, indicating partial restoration of graphitic domains. After purification (Figure 4.8 d), the C 1s spectrum further sharpens, with the C–C peak becoming more dominant, confirming enhanced graphitization and reduced oxygen functionalities key for improving electrical and adsorption properties.

The N 1s spectra (Figures 4.8 e–g) provide insight into the nitrogen bonding configurations in the doped samples. No signal was observed for GO, while the spectrum for 3D-N/rGO before purification (Figure 4.8 f) shows the presence of pyridinic-N (C=N–C, 398.3 eV), pyrrolic-N (C–NH–C, 399.8 eV), graphitic-N (C_3–N, 401.0 eV), and oxidized N species such as NO_2/NO_3 (402.8 eV). After purification (Figure 4.8 g), the nitrogen peaks become more defined, with a notable reduction in oxidized nitrogen species and increased intensity of pyridinic and graphitic N, which are known to enhance adsorptive and electrochemical properties. The different nitrogen configurations identified in the N 1s spectra contribute distinctively to the adsorption behaviour of phenolic compounds. Pyridinic nitrogen, located at the edges or defect sites of the graphene lattice, provides electron-rich sites that can strongly interact with the aromatic rings of phenolic compounds through π–π interactions, thereby enhancing adsorption affinity (Hossain et al., 2024). Graphitic nitrogen, incorporated within the carbon lattice, improves the electron density and hydrophobic character of the graphene surface which further facilitates π–π stacking with phenolic molecules (D. Wang et al., 2023). In contrast, pyrrolic nitrogen is primarily associated with structural defects and contributes less directly to adsorption interactions due to its involvement in five-membered ring structures (Hossain et al., 2024). Based on the increased intensity of pyridinic and graphitic nitrogen observed after purification, these two nitrogen species are considered the dominant contributors to phenolic adsorption in this study as they provide favorable electronic environments and active sites for selective phenolic binding.

The O 1s spectra (Figures 4.8 h–j) further reflect changes in oxygen-containing groups. For GO (Figure 4.7 h), a dominant peak at 531.5 eV corresponds to C=O, indicating a high oxidation state. In 3D-N/rGO before purification (Figure 4.7 i),

additional peaks assigned to C–OH (532.7 eV) and O=C–OH (533.8 eV) appear, showing diverse surface oxygen functionalities. After purification (Figure 4.8 j), the C=O peak shifts slightly with reduced intensity of O=C–OH, indicating the removal of residual oxygen groups and improved structural integrity of the reduced graphene framework.

Similar findings were reported by Yang et al. (2020) (Shi et al., 2022b), who observed an increase in pyridinic and graphitic nitrogen species after thermal treatment of nitrogen-doped graphene oxide, which enhanced the material's electronic properties and adsorption potential . In agreement with this, Zhang et al. (2019) (Zhang et al., 2019) reported that nitrogen doping via urea introduced functional groups such as C=N–C and C_3–N, which were clearly distinguished in the N 1s spectra and contributed to selective adsorption interactions .

4.4 Continuous Fixed-Bed Purification of Phenolic Compounds Using 3D-N/rGO Adsorbent

In this fixed-bed adsorption study, the 3D-N/rGO adsorbent synthesized with 10% urea loading was selected, as it demonstrated the highest adsorption efficiency during batch adsorption–desorption experiments. This ratio exhibited enhanced nitrogen doping, which improved surface functionality and facilitated stronger interactions with phenolic compounds. Using the 10% urea-loaded adsorbent allowed for a more effective evaluation of continuous purification performance under varying operational conditions.

4.4.1 Effect of Adsorption Temperature

Figure 4.9 presents the breakthrough curves obtained at different adsorption temperatures from range of 30 °C to 70 °C for the continuous fixed-bed purification of phenolic compounds using 3D-N/rGO with 10% urea loading. The curves illustrate the relationship between the normalized outlet concentration (Ci/Co) and time, providing insight into how temperature influences the adsorption dynamics within the column.

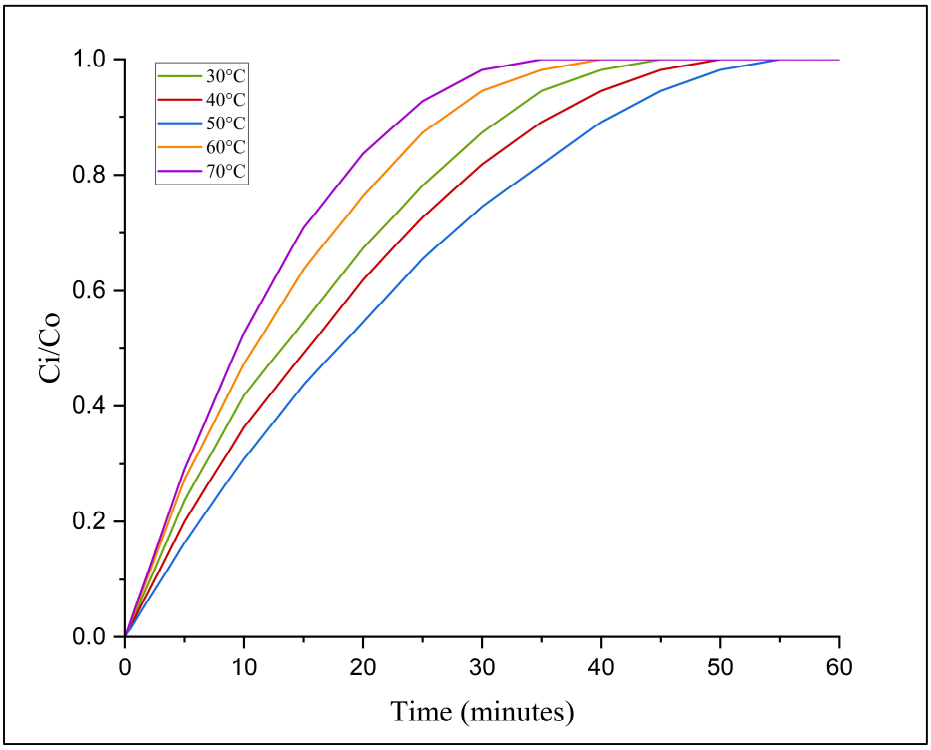


Figure 4.9 Breakthrough Curve at Different Temperatures

Table 4.5
Effect of Temperature on Adsorption Capacity of 3D-N/rGO Adsorbents

Temperature (℃)	Breakthrough Time (minutes)	Adsorption Capacity (mg/g)	Total Adsorption Capacity (mg/g)
30	2.12	0.8840	63.6364
40	2.50	1.0425	74.0909
50	3.06	1.2771	87.7273
60	1.83	0.7632	51.3636
70	1.72	0.7172	43.1818

The breakthrough curves (Figure 4.9) and adsorption data (

Table 4.5) clearly indicate that temperature significantly affects the dynamic adsorption behaviour. At 50°C, the column exhibited the longest breakthrough time (3.06 minutes) and the highest total adsorption capacity (87.73 mg/g). This implies that the adsorbent achieved its highest removal efficiency at this temperature. The enhanced performance is likely attributed to the improved diffusion rate of phenolic molecules and increased interaction strength with the 3D-N/rGO surface (Kong et al., 2022).

Moderate thermal energy at 50°C may have facilitated better molecular transport into the porous structure of the adsorbent, thus enhancing active site accessibility.

In comparison, lower temperatures such as 30°C and 40°C resulted in shorter breakthrough times (2.12 min and 2.50 min) and lower total adsorption capacities (63.64 mg/g and 74.09 mg/g, respectively). The reduced adsorption performance at these temperatures is associated with limited diffusion and kinetic energy of the phenolic molecules, which may have hindered the transport of solutes to the adsorption sites within the column (Solomakou et al., 2023).

At higher temperatures which are 60°C and 70°C, both breakthrough time and adsorption capacity declined markedly. The breakthrough times were shortened to 1.83 minutes and 1.72 minutes, while the total adsorption capacities dropped to 51.36 mg/g and 43.18 mg/g, respectively. These happened because of excessive temperature may promote desorption or reduce the affinity between the phenolic molecules and the adsorbent surface (Soto et al., 2011). Thermal agitation at elevated temperatures can weaken the interaction forces such as hydrogen bonding or π–π interactions, thereby reducing the overall adsorption performance.

The observed optimum adsorption at 50 °C aligns with findings by Yeddou and Bensmaili (2007) (Yeddou & Bensmaili, 2007), who reported that moderate thermal energy enhances sorbate diffusion and accessibility to active sites in porous adsorbents. Similarly, Babu and Gupta (2005) (Babu & Gupta, 2005) emphasized that temperature variations significantly influence breakthrough behavior, with optimal adsorption occurring before thermal agitation begins to disrupt adsorbate-adsorbent interactions. At elevated temperatures (60–70 °C), the decline in capacity in this study can be attributed to reduced sorption affinity and possible desorption, consistent with the decrease in sorption observed in thermodynamic analyses of low-cost biosorbents. These comparisons reinforce that 50 °C provides a thermal balance, enhancing kinetic mobility while preserving adsorptive interactions.

The observed optimum adsorption performance at 50 °C can be further explained by thermodynamic analysis presented in Section 4.5.2. The positive enthalpy change (ΔH° = +13.06 kJ/mol) obtained from the Van't Hoff plot confirms that the adsorption of phenolic compounds onto 3D-N/rGO is an endothermic process, indicating that increasing temperature initially enhances adsorption by improving molecular diffusion and activation of adsorption sites. This is consistent with the increase in adsorption capacity from 30 °C to 50 °C. However, although the Gibbs free

energy change (ΔG°) remained negative at higher temperatures, indicating a spontaneous process, the decline in adsorption capacity at 60–70 °C suggests that excessive thermal energy weakens adsorbate–adsorbent interactions, such as hydrogen bonding and π–π interactions, leading to partial desorption and reduced breakthrough time. Therefore, 50 °C represents an optimal balance between enhanced diffusion kinetics and stable adsorption interactions, resulting in maximum adsorption efficiency under dynamic fixed-bed conditions.

Overall, among the tested temperatures, 50 °C was identified as the optimal condition for phenolic compound adsorption onto 3D-N/rGO in the fixed-bed column. This temperature provided the most favourable balance between breakthrough time and adsorption capacity, indicating efficient interaction between the adsorbate and adsorbent. The results suggest that moderate heating enhances phenolic removal without inducing significant desorption or weakening of intermolecular forces.

4.4.2 Effect of Phenolic Concentration

Figure 4.10 illustrates the breakthrough curves obtained at different initial phenolic concentrations from 50 mg/L to 150 mg/L using 3D-N/rGO with 10% urea loading in a continuous fixed-bed system. The curves plot Ci/Co against time, enabling a direct comparison of how feed concentration influences adsorption dynamics. This analysis provides insight into mass transfer behavior, adsorption site saturation, and the overall efficiency of the column under varying solute concentrations.

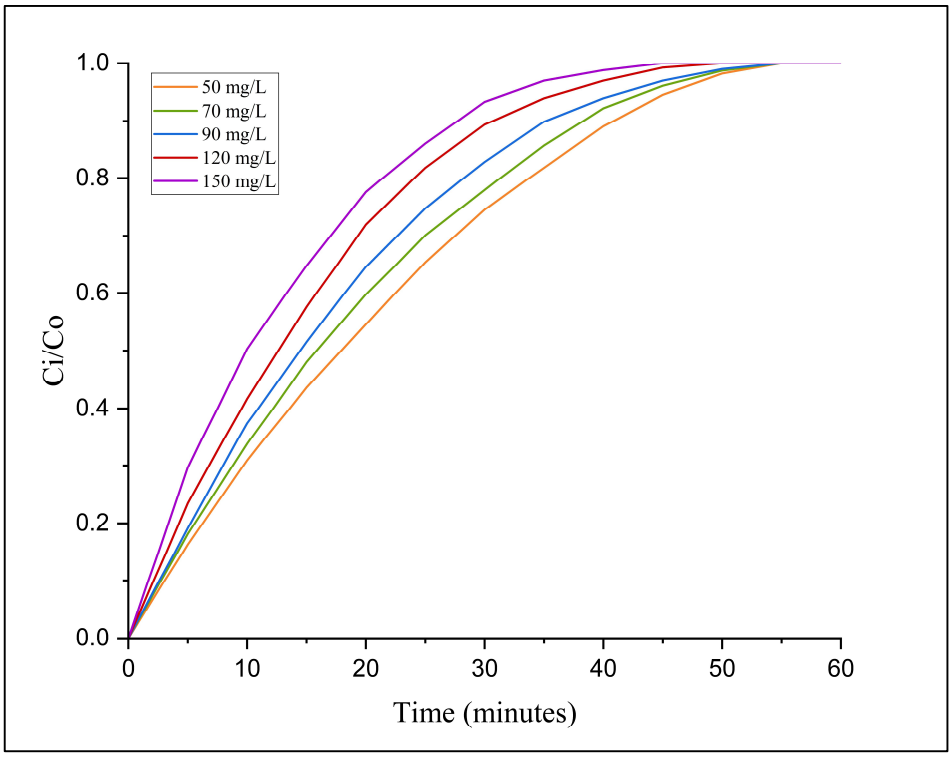


Figure 4.10 Breakthrough Curve at Different Concentration

Table 4.6
Effect of Concentration on Adsorption Capacity of 3D-N/rGO Adsorbents

Concentration (mg/L)	Breakthrough Time (minutes)	Adsorption Capacity (mg/g)	Total Adsorption Capacity (mg/g)
50	3.06	1.2771	87.7273
70	2.75	1.6055	111.8182
90	2.61	1.9604	130.4545
120	2.13	2.1305	146.3636
150	1.68	2.1032	151.8182

As shown in Figure 4.10, increasing the influent phenolic concentration led to earlier breakthrough and steeper breakthrough curves. This is supported by the data in Table 4.6 where the breakthrough time decreased progressively from 3.06 minutes at 50 mg/L to 1.68 minutes at 150 mg/L, indicating faster saturation of the adsorbent bed at higher solute loading.

Although breakthrough occurred earlier at higher inlet phenolic concentrations, the total adsorption capacity increased with increasing concentration which is characteristic of fixed-bed adsorption systems and can be explained by mass transfer zone (MTZ) dynamics. At higher influent concentrations, the larger concentration gradient between the bulk solution and the adsorbent surface provides a stronger driving force for mass transfer, enhancing diffusion of phenolic molecules into the pores of 3D-N/rGO and increasing the amount adsorbed per unit mass of adsorbent. However, this accelerated mass transfer also causes faster saturation of active sites resulting in a narrower and more rapidly propagating MTZ and consequently, shorter breakthrough times [151]. This explains why the total adsorption capacity increased from 87.73 mg/g at 50 mg/L to 151.82 mg/g at 150 mg/L, while the breakthrough time decreased from 3.06 min to 1.68 min. The slight reduction in breakthrough adsorption capacity at the highest concentration suggests early bed saturation and reduced adsorbent utilisation under high solute loading which highlighting the trade-off between adsorption capacity and column service time in continuous fixed-bed operation.

However, the breakthrough adsorption capacity increased up to 120 mg/L (2.1305 mg/g) but slightly declined at 150 mg/L (2.1032 mg/g), suggesting a possible

limitation in adsorbent accessibility or early saturation under higher loading conditions. This implies that while higher concentrations improve total capacity, they may also result in quicker column exhaustion, reducing the efficiency of continuous operation (Baur et al., 2016).

The observed increase in total adsorption capacity with higher phenolic concentrations agrees with the study by Foo and Hameed (2010) (Foo et al., 2010), who reported that elevated solute concentrations enhance the mass transfer driving force, thus facilitating greater uptake by the adsorbent. Similarly, Wang et al. (2013) (H. Wang et al., 2013) found that higher concentrations led to steeper breakthrough curves and shorter breakthrough times due to faster saturation of adsorption sites. These findings support the current observation where 3D-N/rGO exhibited higher capacities at 90–150 mg/L but experienced reduced breakthrough efficiency at the highest loading. This behavior reflects a typical trade-off in fixed-bed systems, where high inflow concentrations improve total adsorption but compromise operational longevity (Baur et al., 2016).

Overall, increasing the initial phenolic concentration enhanced total adsorption capacity due to improved mass transfer, but also reduced breakthrough time, indicating faster column saturation. Among the tested concentrations, 50 mg/L showed the longest breakthrough time (3.06 minutes), ensuring better contact time and more stable column operation. Although its adsorption capacity was lower, the extended breakthrough behavior makes it more suitable for continuous applications. Thus, 50 mg/L was selected as the optimal concentration condition for subsequent studies.

4.4.3 Effect of Mass of Adsorbent

Figure 4.11 presents the breakthrough curves for different adsorbent masses of 0.50 g to 1.50 g using 3D-N/rGO with 10% urea loading in a continuous fixed-bed column. The curves show Ci/Co with time, allowing the assessment of how adsorbent dosage influences the column's adsorption performance. This comparison highlights the impact of available surface area and active sites on breakthrough behavior.

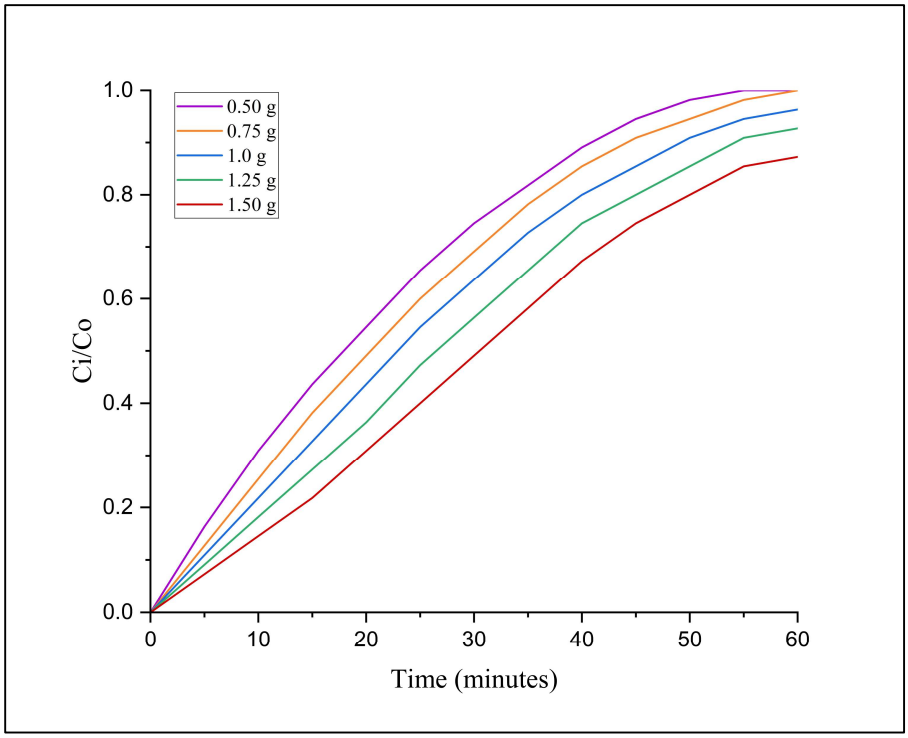


Figure 4.11 Breakthrough Curve at Different Mass of Adsorbent

Table 4.7
Effect of Mass adsorbent on Adsorption Capacity of 3D-N/rGO Adsorbents

Mass of Adsorbent (g)	Breakthrough Time (minutes)	Adsorption Capacity (mg/g)	Total Adsorption Capacity (mg/g)
0.5	3.06	1.2771	87.7273
0.75	3.93	1.3693	66.3636
1.0	4.58	0.9544	56.5909
1.25	5.50	0.9174	51.6364
1.50	6.88	0.9562	48.6364

As shown in Figure 4.11 and Table 4.7, increasing the mass of adsorbent led to a noticeable delay in the breakthrough time, from 3.06 minutes at 0.5 g to 6.88 minutes at 1.5 g. This trend can be attributed to the larger number of active sites and surface area available for adsorption when more adsorbent is packed into the column. With greater adsorbent dosage, the phenolic molecules had a longer contact time with the material and more opportunities for interaction and attachment to the adsorbent surface, thus prolonging the column's effective operating time before saturation (Issabayeva et al., 2018).

Despite the prolonged breakthrough time with higher dosages, the adsorption capacity per gram of adsorbent showed a declining trend beyond 0.75 g. The highest adsorption capacity was observed at 0.75 g, with a value of 1.3693 mg/g. A further increase in adsorbent mass to 1.0, 1.25, and 1.5 g resulted in lower capacities of 0.9544, 0.9174, and 0.9562 mg/g, respectively. This reduction in adsorption capacity per unit mass is commonly associated with the overlapping or aggregation of active sites in higher dosages, which leads to decreased effective surface area utilization (Issabayeva et al., 2018). Additionally, an increased bed height may reduce the driving force for mass transfer, limiting the rate of adsorption due to intraparticle diffusion resistance.

Moreover, the total adsorption capacity (mg/g) followed a similar decreasing trend with increased mass. The highest total adsorption capacity was recorded at 0.5 g (87.7273 mg/g), while 1.50 g exhibited the lowest value (48.6364 mg/g), even though more adsorbent was available. This observation indicates that beyond a certain threshold, increasing the mass of 3D-N/rGO does not proportionally enhance the overall

adsorption performance and may in fact, hinder it due to internal mass transfer limitations and underutilized binding sites (Bezza et al., 2025).

These findings supported with Foo and Hameed (2012) (Foo et al., 2010), who reported that although higher adsorbent dosages increase the number of available active sites and extend breakthrough time, they often result in lower adsorption capacity per gram due to overlapping or aggregation of adsorbent particles. Similarly, Wang et al. (2013) (H. Wang et al., 2013) observed a reduction in adsorption efficiency beyond the optimal dosage in fixed-bed columns, which they attributed to internal mass transfer limitations and reduced accessibility of adsorption sites. Balasubramanian et al. (2025) (Balasubramanian et al., 2025) also emphasized that overpacking the column may hinder solute diffusion into deeper layers, leading to underutilization of adsorbent potential. These studies reinforce the conclusion that while increasing adsorbent mass improves operational time, it may not linearly translate to enhanced efficiency per unit mass.

Overall, 0.50 g was selected as the optimal adsorbent mass due to its superior total adsorption capacity (87.7273 mg/g) and effective utilization of active sites. Although a slightly higher adsorption capacity per gram was observed at 0.75 g, the 0.50 g dosage provided better overall uptake and minimized internal diffusion resistance commonly associated with higher dosages. Additionally, it ensured a more compact and efficient bed design for continuous operation. Therefore, 0.50 g was considered the most suitable adsorbent mass for subsequent fixed-bed adsorption studies.

4.5 Adsorption Mechanism Insight

4.5.1 Adsorption Kinetics

Kinetic studies are crucial for understanding the adsorption rate and mechanism, as well as identifying the potential rate-controlling steps such as film diffusion, surface interaction, or intraparticle diffusion. In this study, the adsorption kinetics of phenolic compounds onto 3D nitrogen-doped reduced graphene oxide (3D-N/rGO) were investigated under fixed-bed conditions. Three key parameters were varied to evaluate their influence on adsorption rate which were temperature, initial phenolic concentration, and adsorbent mass. The experimental data were analyzed using pseudo-first-order and pseudo-second-order kinetic models to determine the best-fitting model

and to gain insights into the adsorption mechanism and rate behavior under each condition.

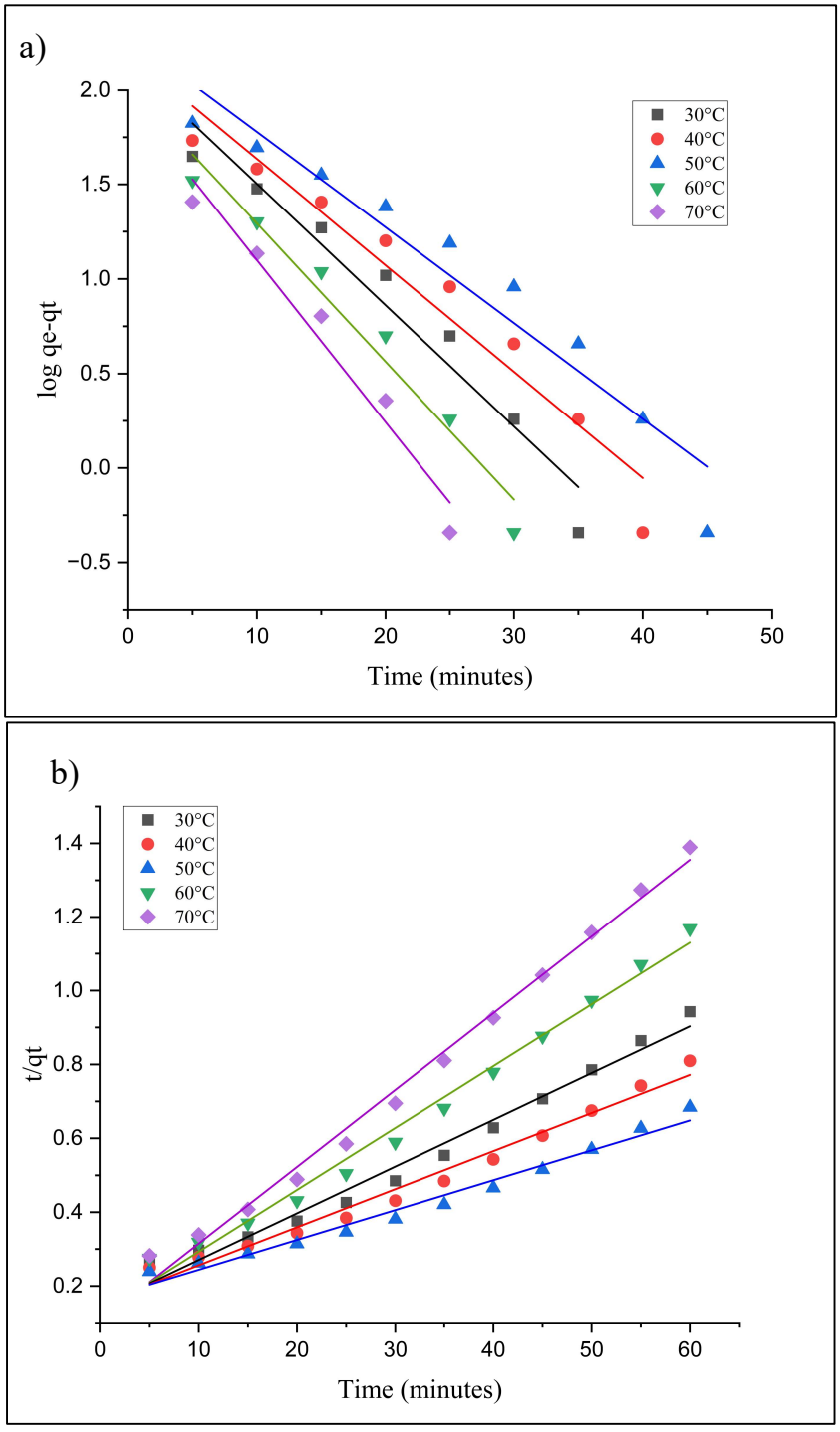


Figure 4.12 Kinetic Study at Different Temperature; a) Pseudo-First-Order and b) Pseudo-Second-Order

Table 4.8
Pseudo-First-Order and Pseudo-Second-Order Parameters at Different Temperature

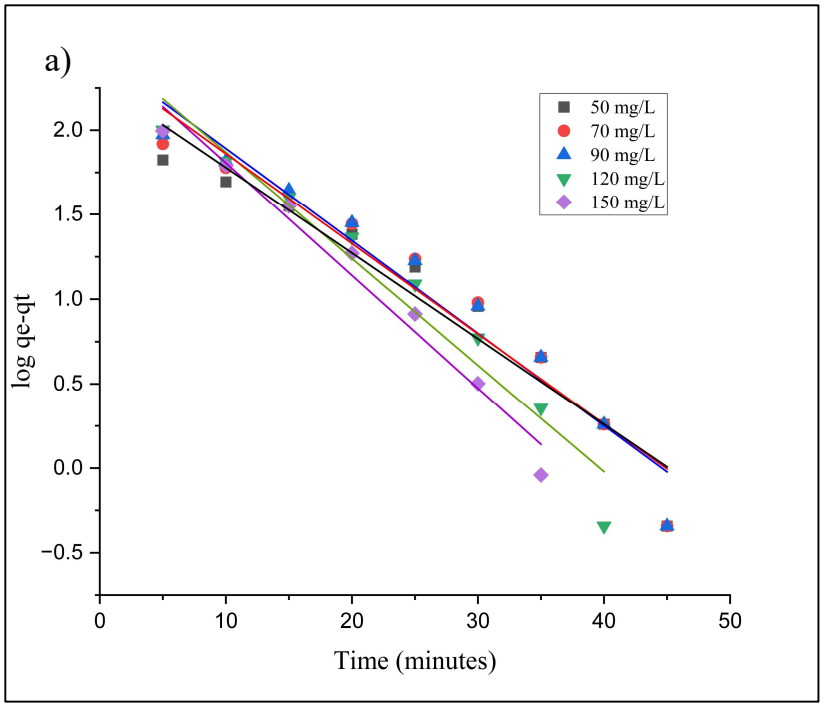
Temperature (°C)	Pseudo-first-order			Pseudo-second-order		
	qe (mg/g)	K_1 (min^{-1})	R^2	qe (mg/g)	K_2 (g mg^{-1} min^{-1})	R^2
30	139.4762	0.1476	0.9508	78.7402	0.001119	0.9818
40	157.6522	0.1297	0.9458	97.0874	0.000693	0.9796
50	192.5750	0.1165	0.9341	123.4568	0.000402	0.9769
60	105.6574	0.1681	0.9653	59.8802	0.002220	0.9879
70	89.9498	0.1969	0.9625	48.0769	0.004055	0.9920

The adsorption kinetics of phenolic compounds onto 3D-N/rGO were evaluated at various temperatures (30–70 °C) using pseudo-first-order and pseudo-second-order models to determine the rate and mechanism of adsorption. The linearized plots and fitting parameters are presented in Figure 4.12 and Table 4.8. From the correlation coefficients (R^2), it is evident that the pseudo-second-order model provides a better fit to the experimental data across all temperatures, with R^2 values ranging from 0.9769 to 0.9920, compared to 0.9341 to 0.9653 for the pseudo-first-order model. This indicates that the adsorption process is likely controlled by chemisorption, involving valence forces through electron sharing or exchange between the phenolic molecules and the nitrogen-doped adsorbent surface (Dehmani et al., 2022).

The calculated equilibrium adsorption capacities (qe) derived from the pseudo-second-order model increased with temperature, rising from 78.74 mg/g at 30 °C to a peak of 123.46 mg/g at 50 °C. This increase indicates that higher temperatures enhance the interaction between phenolic molecules and the adsorbent surface, likely by increasing molecular motion and reducing solution viscosity, which facilitates better diffusion and access to active sites . However, a slight decline in qe was observed at 60 °C (59.88 mg/g) and 70 °C (48.08 mg/g), which a decrease in adsorption efficiency at higher temperatures. This could be due to the desorption of loosely bound phenolic molecules or the disruption of specific adsorption interactions at elevated thermal conditions (Rocchetti et al., 2022).

The rate constants (k_2) from the pseudo-second-order model increased slightly with temperature up to 60 °C, indicating that the adsorption rate is enhanced with

temperature due to increased molecular motion and reduced viscosity, which facilitates the diffusion of phenolic compounds toward active sites. However, a slight decline in both qe and k_2 was observed at 70 °C, possibly due to partial desorption or weakening of interactions at excessively high temperatures.



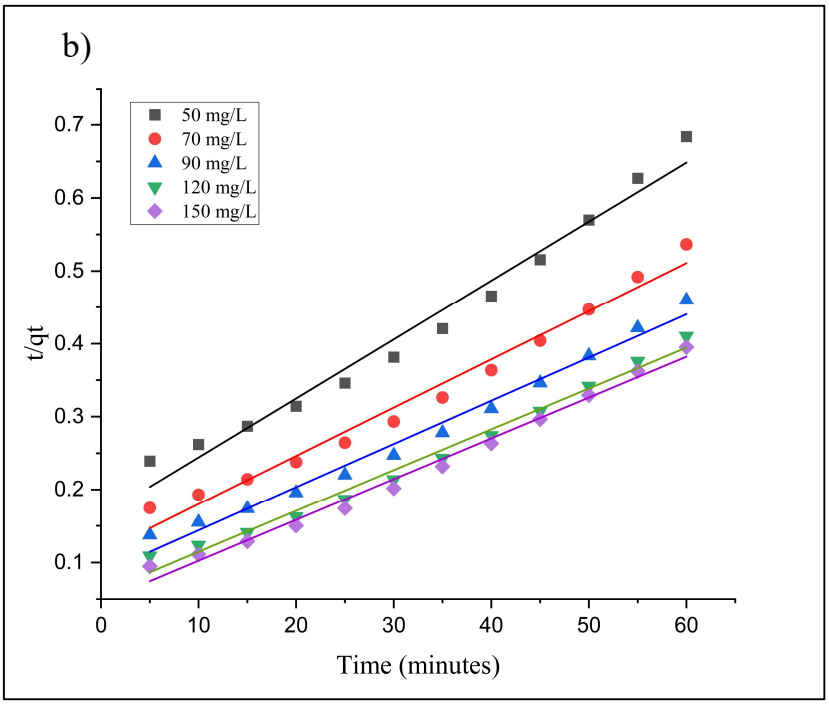


Figure 4.13 Kinetic Study at Different Concentration; a) Pseudo-First-Order and b) Pseudo-Second-Order

Table 4.9
Pseudo-First-Order and Pseudo-Second-Order Parameters at Different Concentration

Concentration (mg/L)	Pseudo-first-order			Pseudo-second-order		
	qe (mg/g)	K_1 (min^{-1})	R^2	qe (mg/g)	K_2 (g mg^{-1} min^{-1})	R^2
50	192.5750	0.1165	0.9341	123.4568	0.000402	0.9769
70	248.0847	0.1227	0.9426	151.5152	0.000383	0.9806
90	274.7894	0.1260	0.9525	169.4915	0.000410	0.9845
120	316.8108	0.1451	0.951	178.5714	0.000533	0.9867
150	296.8247	0.1534	0.9722	178.5714	0.000674	0.9888

The influence of initial phenolic concentration (50–150 mg/L) on the adsorption kinetics of phenolic compounds onto 3D-N/rGO was evaluated using pseudo-first-order and pseudo-second-order models. The linearized plots and model parameters are summarized in Figure 4.13 and Table 4.9 respectively. The results show that the pseudo-second-order model consistently provides a better fit to the experimental data across all concentrations, with high correlation coefficients ($R^2 = 0.9769–0.9888$). In contrast, the R^2 values for the pseudo-first-order model were slightly lower, ranging from 0.9426 to

0.9722. This confirms that the adsorption process is primarily governed by a chemisorption mechanism, involving valence forces and electron exchange between the phenolic compounds and nitrogen-doped surface of the adsorbent.

As the initial phenolic concentration increased from 50 mg/L to 150 mg/L, the equilibrium adsorption capacity (qe) calculated by both models also increased. In the pseudo-second-order model, qe increased from 123.46 mg/g to 178.57 mg/g, indicating greater adsorption due to a stronger concentration gradient and increased driving force for mass transfer. This trend is consistent with typical adsorption behavior, where higher concentrations enhance the likelihood of collision and binding between adsorbate molecules and active sites on the adsorbent surface (Hira et al., 2023). The rate constant k_2 showed some variation with increasing concentration, generally decreasing from 0.000402 to 0.000337, then increasing to 0.000674 g mg^{-1} min^{-1} at 150 mg/L. This may be attributed to the increased availability of phenolic molecules enhancing initial adsorption rates, followed by a potential saturation or crowding effect at the adsorbent surface at intermediate concentrations (Yang et al., 2025).

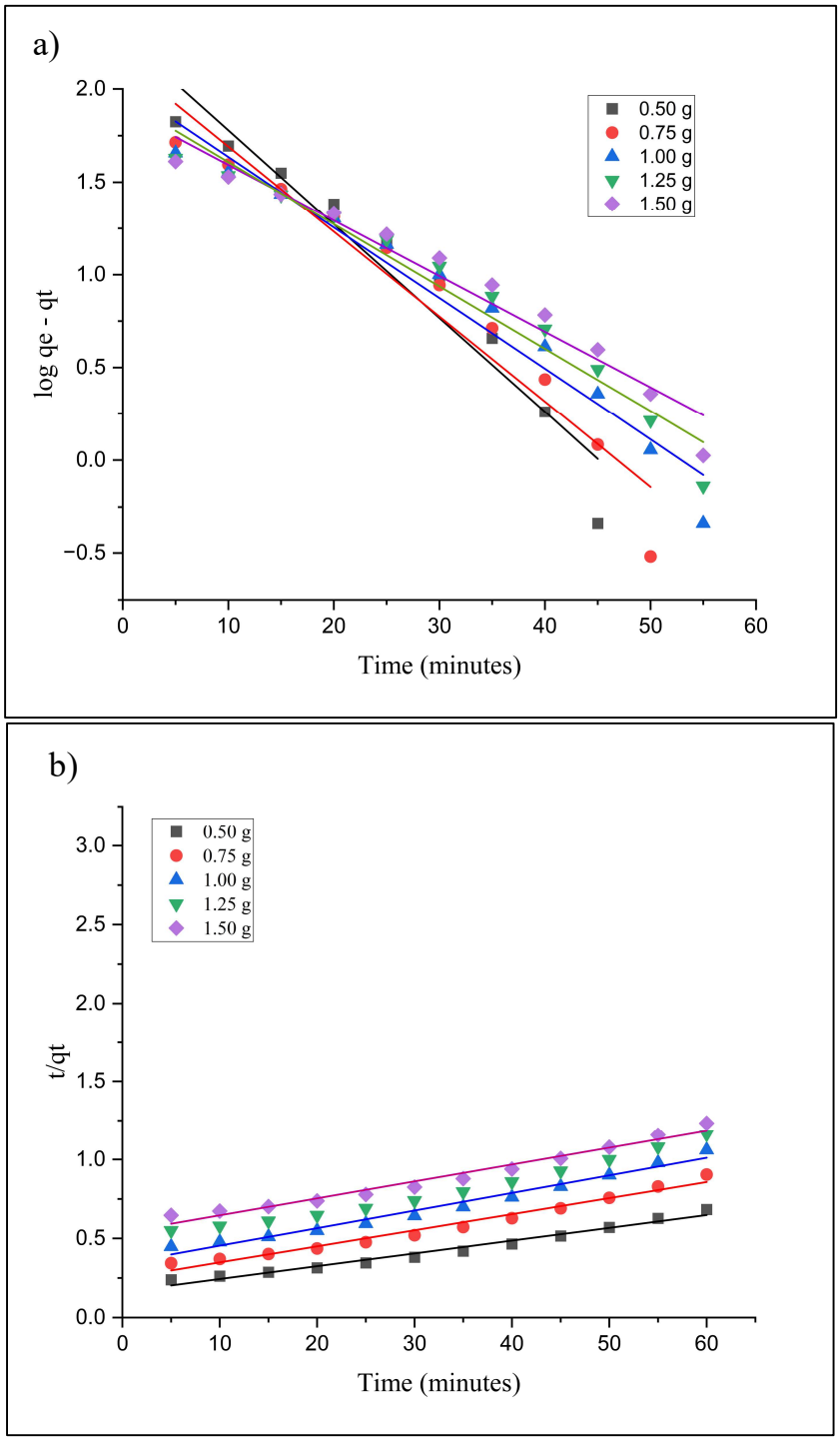


Figure 4.14 Kinetic Study at Different Mass of Adsorbent; a) Pseudo-First-Order and b) Pseudo-Second-Order

Table 4.10
Pseudo-First-Order and Pseudo-Second-Order Parameters at Different Mass of Adsorbent

Mass of adsorbent (g)	Pseudo-first-order			Pseudo-second-order		
	qe (mg/g)	K_1 (min^{-1})	R^2	qe (mg/g)	K_2 (g mg^{-1} min^{-1})	R^2
0.50	192.5750	0.1165	0.9341	123.4568	0.000402022	0.9769
0.75	141.1562	0.1057	0.9373	98.0392	0.000420704	0.9766
1.00	104.0399	0.0877	0.9587	90.0901	0.000359003	0.9775
1.25	88.0238	0.0774	0.9588	90.0900	0.00027907	0.9745
1.50	78.2708	0.0691	0.9585	93.4579	0.000212019	0.9721

The effect of adsorbent mass (0.50–1.50 g) on the adsorption kinetics of phenolic compounds onto 3D-N/rGO was investigated using pseudo-first-order and pseudo-second-order models. The kinetic plots and model parameters are presented in Figure 4.14 and Table 4.10. Across all adsorbent dosages, the pseudo-second-order model yielded higher correlation coefficients (R^2 = 0.9721–0.9775) compared to the pseudo-first-order model (R^2 = 0.9341–0.9588), indicating that chemisorption is the dominant mechanism. This supports previous observations from the temperature and concentration studies, reinforcing the idea that the adsorption process involves chemical bonding interactions between the phenolic compounds and the functional groups on the 3D-N/rGO surface.

As the adsorbent mass increased from 0.50 g to 1.50 g, the calculated adsorption capacity per unit mass (qe) decreased significantly for both models. For instance, the pseudo-second-order model showed a drop from 123.46 mg/g at 0.50 g to 93.46 mg/g at 1.50 g. This decline shows that as increasing the adsorbent dosage increases the total number of active sites but reduces the available phenolic molecules per gram of adsorbent, leading to lower utilization efficiency per unit mass. This trend is typical of fixed-bed systems operating under excess adsorbent conditions (Darla et al., 2024).

The pseudo-second-order rate constant (k_2) decreased with increasing adsorbent mass, from 0.000420022 g mg^{-1} min^{-1} at 0.50 g to 0.000121019 g mg^{-1} min^{-1} at 1.50 g. The declining k_2 values at higher dosages suggest that despite the availability of more adsorption sites, the per-site adsorption rate slows due to reduced driving force and possible adsorbent aggregation or channelling effects in the packed bed.

Soudagar et al. (2022) (Soudagar et al., 2022) demonstrated that the adsorption of methylene blue onto nano graphene oxide followed the pseudo-second-order kinetic model with a high correlation coefficient, $R^2 = 0.999$. This indicate that the process was governed by chemisorption. The result also aligns with the findings of Kyzas et al. (2014) (Kyzas et al., 2014), who also observed pseudo-second-order kinetics during the adsorption of pollutants using graphene-based materials, suggesting that chemical interactions, such as π–π stacking and surface functional group binding play a crucial role.

4.5.2 Adsorption Thermodynamic

Thermodynamic analysis provides crucial insights into the nature, spontaneity, and energy changes associated with the adsorption process. In this study, thermodynamic parameters for the adsorption of phenolic compounds onto 3D nitrogen-doped reduced graphene oxide (3D-N/rGO) were evaluated using the Van't Hoff equation. The linear relationship between ln qe/Ce vs 1/T shown in Figure 4.15, confirms the temperature dependence of the adsorption process, with a strong correlation ($R^2 = 0.9976$), indicating excellent model fit.

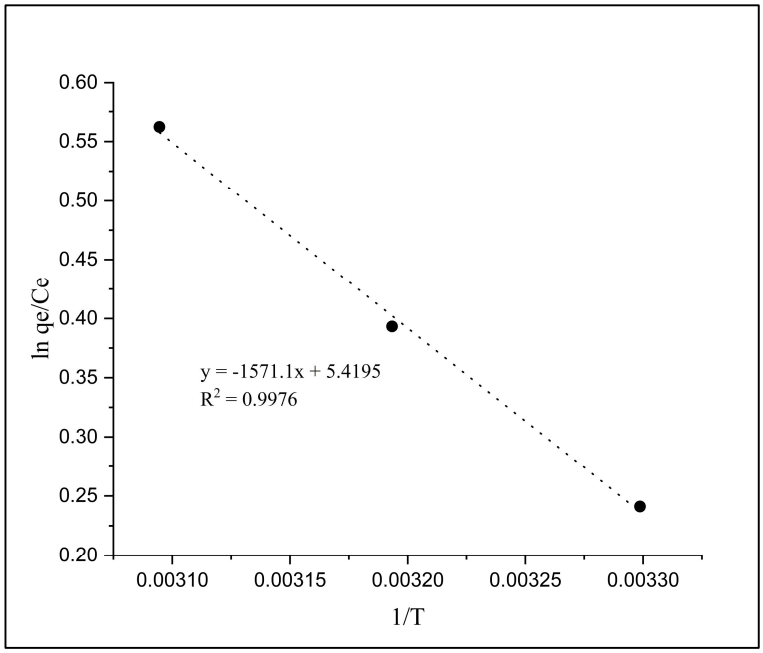


Figure 4.15 Van't Hoff Equation

Table 4.11
Thermodynamic Properties of 3D-N/rGO Adsorbent

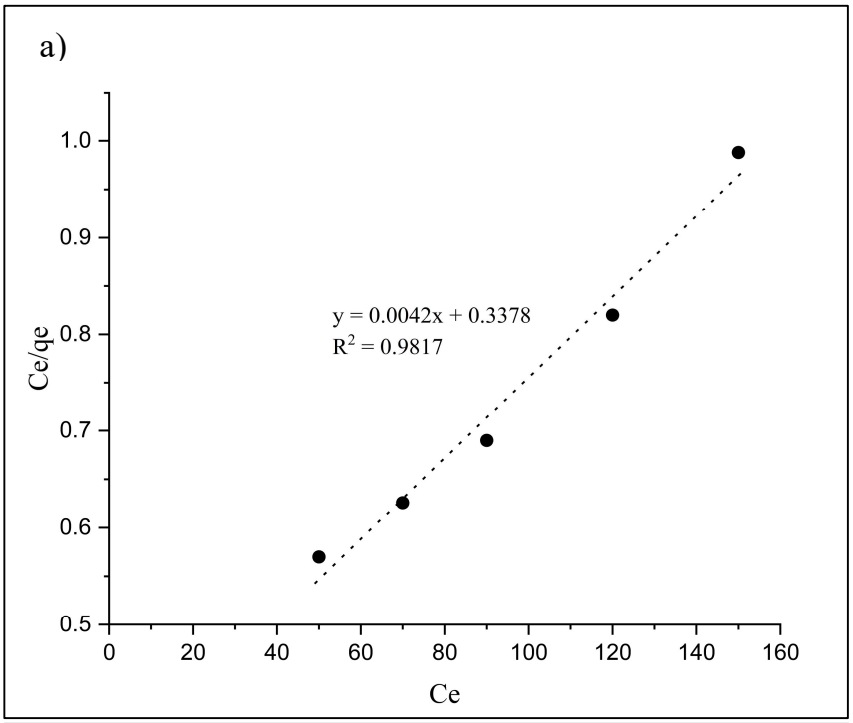
Temperature (℃)	**qe (mg/g)**	**Ce (mg/L)**	**ΔH^o (kJ/mol)**	**ΔS^o (J/mol.K)**	**ΔG^o (kJ/mol)**
30	63.6364				-0.5971
40	74.0909				-1.0477
50	87.7273	50	13.0621	45.0577	-1.4983
60	51.3636				-1.9489
70	43.1818				-2.3994

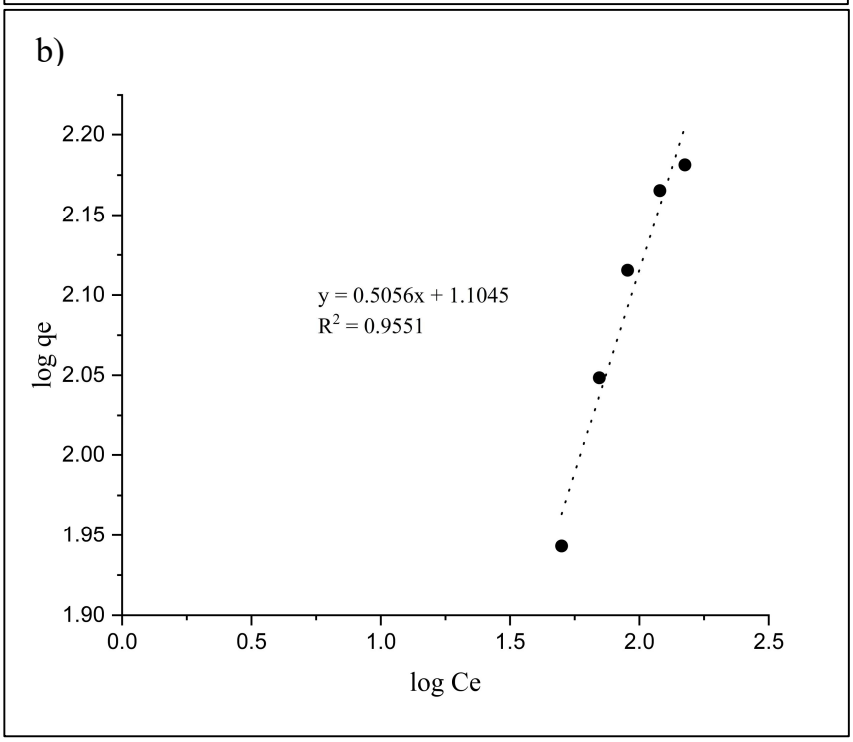
From the slope and intercept of the Van't Hoff plot, the standard enthalpy change (ΔH°) and entropy change (ΔS°) were calculated as +13.06 kJ/mol and +45.06 J/mol·K respectively. The positive ΔH° value indicates that the adsorption of phenolic compounds onto 3D-N/rGO is an endothermic process, meaning that increased temperature enhances the adsorption capacity consistent with the experimental trend where qe increased from 63.64 mg/g at 30 °C to 87.73 mg/g at 50 °C. Furthermore, the Gibbs free energy change (ΔG°) values were negative at all temperatures studied, ranging from –0.5971 to –2.3994 kJ/mol. The increasing negativity of ΔG° with temperature confirms that the adsorption process is spontaneous and becomes more thermodynamically favorable at higher temperatures.

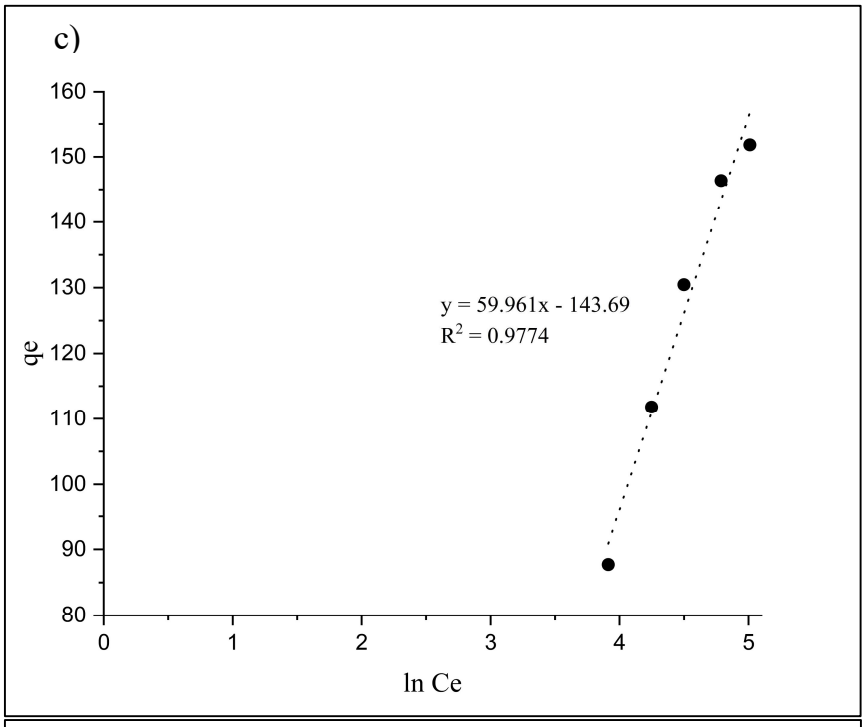
Kyzas et.al (2014) (Kyzas et al., 2014) also demonstrated that the adsorption of phenolic compounds onto graphene oxide-based materials is an endothermic process, reporting positive enthalpy changes that indicated improved adsorption at elevated temperatures. Similarly, Thangavel et al. (2014) (Thangavel, 2014) found that the adsorption capacity of graphene oxide increased with temperature, especially for materials with a higher degree of oxidation, confirming the endothermic behavior of the process. These findings align with the current study, in which a positive enthalpy change and an increase in adsorption capacity were recorded.

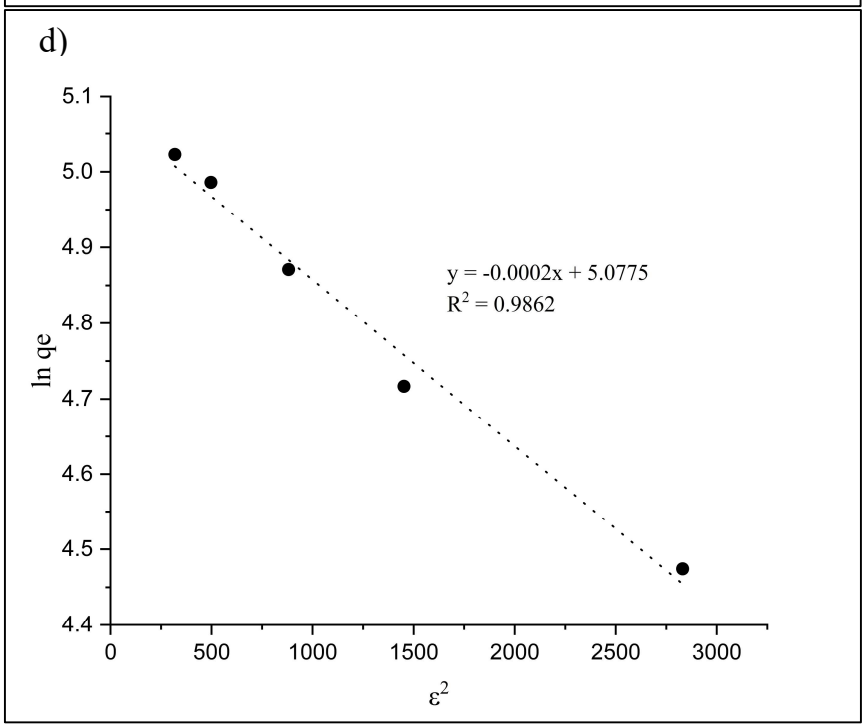
4.5.3 Adsorption Isotherm

Adsorption isotherms are essential in understanding the interaction between adsorbate molecules and the surface of adsorbents, particularly at equilibrium. In this study, isotherm modeling was performed to investigate the equilibrium adsorption behavior of phenolic compounds derived from palm kernel cake (PKC) onto 3D nitrogen-doped reduced graphene oxide (3D-N/rGO) in a fixed-bed column system. This evaluation reveals the nature of adsorption whether it occurs as monolayer or multilayer, and whether the adsorbent surface is homogeneous or heterogeneous. The isotherm analysis was conducted at different initial phenolic concentrations which are 50 , 70, 90, 120 and 150 mg/L. The experimental data were fitted to five isotherm models which were Langmuir, Freundlich, Temkin, Dubinin–Radushkevich (D-R), and Redlich–Peterson, using linear regression analysis as shown in Figure 4.16.


a)
Ce/qe
Ce
y = 0.0042x + 0.3378
R2 = 0.9817
1.0
0.9
0.8
0.7
0.6
0.5
0
20
40
60
80
100
120
140
160


b)
log qe
log Ce
y = 0.5056x + 1.1045
R2 = 0.9551
2.20
2.15
2.10
2.05
2.00
1.95
1.90
0.0
0.5
1.0
1.5
2.0
2.5


c)
160
150
140
130
120
110
100
90
80
qe
0
1
2
3
4
5
ln Ce
y = 59.961x - 143.69
R2 = 0.9774


d)
5.1
5.0
4.9
4.8
4.7
4.6
4.5
4.4
ln qe
0
500
1000
1500
2000
2500
3000
ε2
y = -0.0002x + 5.0775
R2 = 0.9862

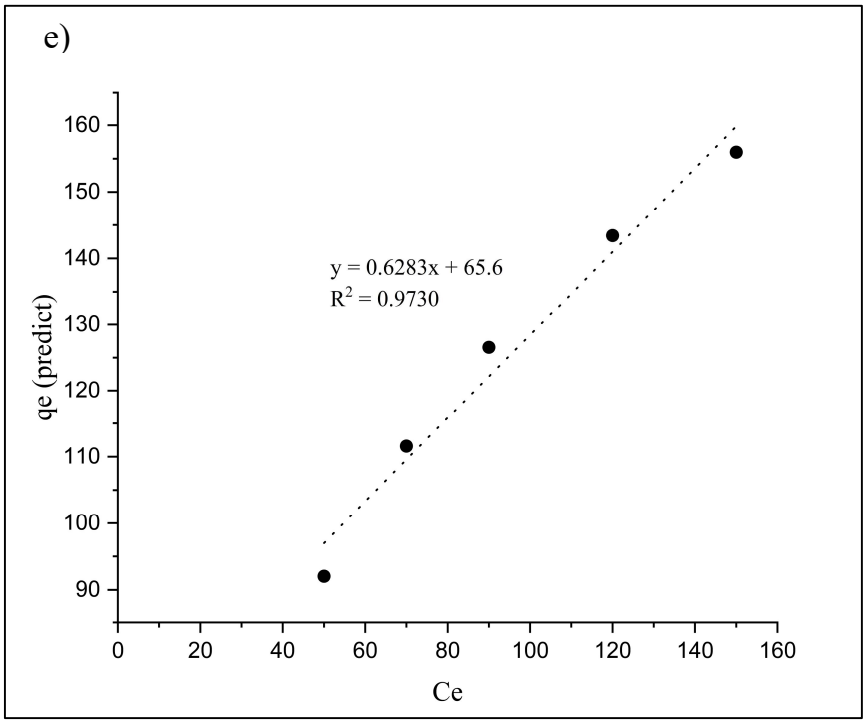


Figure 4.16 Isotherm Model; a) Langmuir, b) Freundlich, c) Temkin, d) Dubinin-Radushkevic, and e) Redlich-Peterson

Table 4.12
Summary of Isotherm Model

Isotherm Model	Linearization Method	R^2
Langmuir	$\frac{C_e}{q_e} = \frac{1}{Q_m K_L} + \frac{1}{Q_m} C_e$	0.9817
Freundlich	$\log q_e = \log K_F + \frac{1}{n} \log C_e$	0.9551
Temkin	$q_e = \mathrm{B}\ \ln K_T - \mathrm{B}\ \ln C_e$	0.9774
Dubinin-Radushkevich	$\ln q_e = \ln q_m - \beta \varepsilon^2$	0.9862
Redlich-Peterson	$\ln\left(\frac{K_R C_e}{q_e} - 1\right) = \beta \ln C_e$	0.9730

Among all the isotherm models investigated, the D-R model produced the highest correlation coefficient ($R^2 = 0.9862$), indicating the best statistical fit with the experimental data. This was followed by the Langmuir model ($R^2 = 0.9817$), Temkin ($R^2 = 0.9774$), and Redlich–Peterson ($R^2 = 0.9730$). The Freundlich model showed the lowest correlation ($R^2 = 0.9551$), suggesting it was the least representative of the adsorption behavior observed.

The excellent fit of the D-R model suggests a chemisorption-dominated mechanism, as further supported by the calculated mean adsorption energy

(E = 50 kJ/mol), derived from the model's slope (β = 0.0002 mol²/kJ²). This value far exceeds the typical threshold for physisorption (<8 kJ/mol), indicating strong chemical interactions between the phenolic compounds and the functionalized surface of 3D-N/rGO. These interactions likely involve π–π stacking, hydrogen bonding, and charge transfer facilitated by nitrogen-containing groups introduced through urea doping (Yao et al., 2023).

Despite the slightly lower R^2, the Langmuir model remains highly relevant, as it provides valuable insight into the nature of the adsorption process. Its strong fit ($R^2 = 0.9817$) indicates monolayer adsorption on a homogeneous surface with finite and energetically equivalent sites. This is consistent with the structural characteristics of 3D-N/rGO, which offers a uniform distribution of active sites and enhanced accessibility due to its porous framework.

On the other hand, the relatively weak fit of the Freundlich model suggests that the adsorption process does not predominantly involve multilayer formation on a heterogeneous surface. However, the moderate correlations with the Redlich–Peterson and Temkin models imply that some degree of surface heterogeneity or adsorbate–adsorbate interaction may still be present in the system (Amrutha et al., 2023).

The finding that the adsorption of phenolic compounds onto 3D-N/rGO is primarily governed by chemisorption as evidenced by the strong fit to the Dubinin–Radushkevich (D–R) isotherm model ($R^2 = 0.9862$) is supported by Bahadi et al. (2024) (Bahadi et al., 2024), who reported that nitrogen doping and thermal treatment enhanced phenolic adsorption due to increased surface aromaticity and stronger functional group interactions. This finding is further supported by Aliakbarian et al. (2015) (Aliakbarian et al., 2015), who observed that phenolic compounds adhered predominantly through monolayer adsorption on homogeneous surfaces, which aligns with the strong agreement of the Langmuir model ($R^2 = 0.9817$) in the present study.

4.5.4 Proposed Adsorption Mechanism

The adsorption kinetics results revealed that the pseudo-second-order model provided the best fit across all studied conditions, with higher correlation coefficients compared to the pseudo-first-order model. This indicates that the adsorption of phenolic compounds onto 3D-N/rGO is predominantly governed by chemisorption, involving

valence forces through the sharing or exchange of electrons between adsorbate molecules and the functional groups on the adsorbent surface.

Thermodynamic analysis further supported this observation, as the positive enthalpy change ($\Delta H°$) confirmed the endothermic nature of the process, while the positive entropy change ($\Delta S°$) indicated increased randomness at the solid–liquid interface during adsorption. Additionally, the calculated Gibbs free energy ($\Delta G°$) values were negative at all temperatures studied, suggesting that the adsorption process is spontaneous and thermodynamically favorable.

Isotherm modelling showed that among the models tested, the Dubinin–Radushkevich (D–R) model provided the best fit ($R^2 = 0.9862$), followed closely by the Langmuir ($R^2 = 0.9817$), Temkin ($R^2 = 0.9774$), and Redlich–Peterson ($R^2 = 0.9730$) models, whereas the Freundlich model had the lowest correlation ($R^2 = 0.9551$). The D–R model's calculated mean adsorption energy (E = 50 kJ/mol) exceeded the typical physisorption threshold (< 8 kJ/mol), confirming that the mechanism is chemisorption-dominated. This strong interaction is likely attributed to π–π stacking between the aromatic rings of phenolic compounds and the conjugated graphene structure, hydrogen bonding with oxygenated functional groups, and electrostatic attraction involving nitrogen-doped sites. These synergistic effects contribute to the enhanced adsorption performance of 3D-N/rGO in the purification of phenolic compounds.

CHAPTER 5
CONCLUSION

5.1 Conclusions

In conclusion, this study successfully achieved the three research objectives outlined in Chapter 1. Objective 1 was accomplished through the synthesis and comprehensive characterization of three-dimensional nitrogen-doped reduced graphene oxide (3D-N/rGO). Structural and chemical analyses using FTIR, BET, TGA, XPS, and HRTEM confirmed successful nitrogen incorporation and the formation of a stable three-dimensional porous framework. The presence of pyridinic and graphitic nitrogen species verified via XPS demonstrated effective surface modification, establishing additional active sites that enhanced selective interaction with aromatic phenolic compounds.

Objective 2 was fulfilled through systematic evaluation of key adsorption parameters in both batch and fixed-bed systems. Adsorption temperature (30–60 °C), initial phenolic concentration (50–150 mg/L), and adsorbent mass (0.5–1.5 g) were investigated to determine their influence on adsorption capacity, breakthrough behavior, and overall efficiency. The optimum condition of 50 °C, 50 mg/L, and 0.50 g adsorbent achieved a maximum adsorption capacity of 87.73 mg/g. This condition reflects a balance between enhanced molecular mobility at moderate temperature, sufficient driving force for mass transfer, and effective utilization of active sites without premature saturation. Compared with literature benchmarks for graphene-based materials, the performance demonstrates competitive adsorption capacity while offering improved selectivity for phenolic recovery from complex biomass extracts.

Objective 3 was achieved through mechanistic evaluation using isotherm, kinetic, and thermodynamic models. The Langmuir model provided the best fit (R^2 = 0.9962), indicating monolayer adsorption on energetically uniform sites, while the pseudo-second-order kinetic model (R^2 = 0.9920) suggested chemisorption involvement. Thermodynamic parameters confirmed that the adsorption process was spontaneous ($\Delta G° < 0$), endothermic ($\Delta H°$ = +18.49 kJ/mol), and entropy-driven ($\Delta S°$ = +0.072 kJ/mol·K), supporting the feasibility and temperature sensitivity of the system.

The novelty of this work lies in demonstrating the synergistic role of nitrogen doping and three-dimensional structuring in enhancing adsorption selectivity rather than relying solely on high surface area. Although the BET surface area decreased with increasing nitrogen content, the improved electronic properties and functional active sites significantly enhanced phenolic affinity, highlighting that surface chemistry plays a more critical role than surface area alone in selective purification.

Despite these promising findings, several limitations should be acknowledged. The study was conducted at laboratory scale using a single-solute model system, with limited long-term regeneration and stability evaluation. Scale-up considerations, cost analysis, and multi-component competitive adsorption in real industrial streams require further investigation.

Overall, this research establishes 3D-N/rGO as a selective and efficient adsorbent platform for phenolic purification and contributes new understanding on the structure–selectivity relationship in nitrogen-doped graphene systems for biomass valorization.

5.2 Recommendations

Based on the findings and limitations of this study, the following recommendations are proposed to guide future research and enhance the practical applicability of 3D-N/rGO for phenolic compound purification:

i) Beyond the nitrogen-doped system evaluated in this study, future research may investigate alternative dopants or composite materials, such as metal oxides or dual-doping strategies, to further enhance phenolic selectivity and adsorption capacity.
ii) Although 3D-N/rGO demonstrated effective adsorption performance for phenolic recovery, the regeneration and reusability of the adsorbent were not evaluated in this study. Therefore, future work should focus on investigating multiple adsorption–desorption cycles to assess the long-term stability, regeneration efficiency, and economic feasibility of 3D-N/rGO, particularly under continuous fixed-bed operation.
iii) In this study, the synthesis of 3D-N/rGO and the optimization of adsorption parameters were conducted at laboratory scale. To facilitate

practical implementation, future research should explore scale-up studies, including larger fixed-bed columns and continuous-flow systems, to evaluate process robustness, pressure drop behaviour, and adsorption performance under industrially relevant conditions.

iv) While this study focused on key adsorption parameters such as temperature, phenolic concentration, and adsorbent mass, additional operating variables such as flow rate, particle size distribution, and bed height were not investigated. Future studies should examine the influence of these parameters to further optimize breakthrough behaviour, enhance column efficiency, and improve process control.

v) The adsorption experiments in this study were primarily conducted using phenolic-rich extracts under controlled conditions. To better reflect real processing environments, future work should consider competitive adsorption studies involving complex plant extracts or multicomponent systems. This would allow evaluation of the selectivity of 3D-N/rGO towards phenolic compounds in the presence of co-existing substances such as sugars, proteins, and other antioxidants.

REFERENCES

Aagaard, N., Azcárate, J., & Microanalysis, E. Z.-M. and. (2020). HRTEM Characterization and Simulation of Ag Nanoplates. *Cambridge.Org*. https://www.cambridge.org/core/journals/microscopy-and-microanalysis/article/hrtem-characterization-and-simulation-of-ag-nanoplates/4C0455AC37A410FE2D2A9099E9D0FAC1

Abdelhamid, H. N., & Hussein, K. H. (2021). Graphene oxide as a carrier for drug delivery of methotrexate. *Biointerface Research in Applied Chemistry*, *11*(6), 14726–14735. https://doi.org/10.33263/BRIAC116.1472614735

Abdullah, N., & Sulaiman, F. (2013a). The oil palm wastes in Malaysia. *Biomass Now-Sustainable Growth and Use, 1(3), 75-93*.

Abdullah, N., & Sulaiman, F. (2013b). The oil palm wastes in Malaysia. *Biomass Now-Sustainable Growth and Use, 1(3), 75-93*.

Al Mamari, H. H. (n.d.). *Phenolic Compounds: Classification, Chemistry, and Updated Techniques of Analysis and Synthesis*. Retrieved www.intechopen.com

Al-Asheh, S., Banat, F., & Abu-Aitah, L. (2003). Adsorption of phenol using different types of activated bentonites. *Separation and Purification Technology*, *33*(1), 1–10. https://doi.org/10.1016/S1383-5866(02)00180-6

Albayrak, S., Atasagun, B., & Aksoy, A. (2017a). Comparison of phenolic components and biological activities of two Centaurea sp. obtained by three extraction techniques. *Asian Pacific Journal of Tropical Medicine*, *10*(6), 599–606. https://doi.org/10.1016/j.apjtm.2017.06.010

Albayrak, S., Atasagun, B., & Aksoy, A. (2017b). Comparison of phenolic components and biological activities of two Centaurea sp. obtained by three extraction techniques. *Asian Pacific Journal of Tropical Medicine*, *10*(6), 599–606. https://doi.org/10.1016/j.apjtm.2017.06.010

Albuquerque, B. R., Heleno, S. A. 8., Oliveira, M. B. P. P., Barros, L., & Ferreira, I. C. F. R. (2021). Phenolic compounds: Current industrial applications, limitations and future challenges. In *Food and Function* (Vol. 12, Number 1, pp. 14–29). Royal Society of Chemistry. https://doi.org/10.1039/d0fo02324h

Ali, A., Siddique, M., Chen, W., Han, Z., … R. K.-I. J. of, & 2022, undefined. (2022). Promising low-cost adsorbent from waste green tea leaves for phenol removal in aqueous solution. *Mdpi.Com*. https://www.mdpi.com/1660-4601/19/11/6396

Aliakbarian, B., Casazza, A. A., & Perego, P. (2015). Kinetic and isotherm modelling of the adsorption of phenolic compounds from olive mill wastewater onto activated carbon. *Food Technology and Biotechnology*, *53*(2), 207–214.

Amrutha, Jeppu, G., Girish, C. R., Prabhu, B., & Mayer, K. (2023). Multi-component adsorption isotherms: review and modeling studies. *Springer*, *10*, 38. https://doi.org/10.1007/S40710-023-00631-0

Anegbe, B., Ifijen, I. H., Maliki, M., Uwidia, I. E., & Aigbodion, A. I. (2024). Research progress in graphene-based adsorbents for wastewater treatment: Preparation, adsorption properties and mechanisms for inorganic and organic. *Mdpi.Com*, *36*(1). https://doi.org/10.1186/s12302-023-00814-4

Aparamarta, H. W., Gunawan, S., Ihsanpuro, S. I., Safawi, I., Bhuana, D. S., Mochtar, A. F., & Yusril Izhar Noer, M. (2022). Optimization and kinetic study of biodiesel production from nyamplung oil with microwave-assisted extraction (MAE) technique. *Heliyon*, *8*(8). https://doi.org/10.1016/j.heliyon.2022.e10254

Arruda, C., Ribeiro, V., Almeida, M., … J. M.-… of P. and, & 2020, undefined. (2020). Effect of light, oxygen and temperature on the stability of artepillin C and p-coumaric acid from Brazilian green propolis. *Elsevier*. https://www.sciencedirect.com/science/article/pii/S0731708519309501

Arsalani, N., Nasiri, R., & Design, M. Z.-C. E. R. and. (2018). Synthesis of magnetic 3D graphene decorated with CaCO3 for anionic azo dye removal from aqueous solution: kinetic and RSM modeling approach. *Elsevier*. https://www.sciencedirect.com/science/article/pii/S0263876218303198

Awoh, E. T., Kiplagat, J., Kimutai, S. K., & Mecha, A. C. (2023). Current trends in palm oil waste management: A comparative review of Cameroon and Malaysia. In *Heliyon* (Vol. 9, Number 11). Elsevier Ltd. https://doi.org/10.1016/j.heliyon.2023.e21410

Ayoob, H. W., Ridha, A. M., Jassim, A. A., Taieh, N. K., Homod, R. Z., & Mohammed, H. I. (2024). Enhanced adsorption of phenol using graphene oxide-bentonite nanocomposites: Synthesis, characterisation, and optimisation. *Journal of Molecular Liquids*, *395*, 123833. https://doi.org/10.1016/J.MOLLIQ.2023.123833

Azizi, M. N., Loh, T. C., Foo, H. L., & Chung, E. L. T. (2021). Is palm kernel cake a suitable alternative feed ingredient for poultry? In *Animals* (Vol. 11, Number 2, pp. 1–15). MDPI AG. https://doi.org/10.3390/ani11020338

Babu, B. V., & Gupta, S. (2005). Modeling And Simulation Of Fixed Bed Adsorption Column: Effect Of Velocity Variation. *I-Manager's Journal on Future Engineering and Technology*, *1*(1), 60–66. https://doi.org/10.26634/jfet.1.1.966

Bahadi, S. A., Iddrisu, M., Al-Sakkaf, M. K., Elgzoly, M. A. A., Al-Amrani, W. A., Ahmed, U., Zahid, U., Drmosh, Q. A., & Onaizi, S. A. (2024). Chemically versus thermally reduced graphene oxide: effects of reduction methods and reducing agents on the adsorption of phenolic compounds from wastewater. *Emergent Materials*, *7*(2), 533–545. https://doi.org/10.1007/s42247-023-00514-y

Bakewell-Stone, P. (2023). *Elaeis guineensis (African oil palm)*. https://cabidigitallibrary.org

Balasubramanian, S., Kapoor, A., Nakkeran, E., Murugasen, K., NaveenKumar, R., Harini, S. B., Venkatesan, D., & Bhatlu, M. L. D. (2025). Review on process intensification for adsorptive wastewater treatment: focus on bed geometries. *Springer*, *31*(4). https://doi.org/10.1007/S10450-025-00622-7

Baur, D., Angarita, M., Müller-Späth, T., Steinebach, F., & Morbidelli, M. (2016). Comparison of batch and continuous multi-column protein A capture processes by optimal design. *Wiley Online Library*, *11*(7), 920–931. https://doi.org/10.1002/BIOT.201500481

Bazargan, A., Kostić, M. D., Stamenković, O. S., Veljković, V. B., & McKay, G. (2015). A calcium oxide-based catalyst derived from palm kernel shell gasification residues for biodiesel production. *Fuel*, *150*, 519–525. https://doi.org/10.1016/j.fuel.2015.02.046

Bellier, N., Baipaywad, P., Ryu, N., Lee, J. Y., & Park, H. (2022). Recent biomedical advancements in graphene oxide- and reduced graphene oxide-based nanocomposite nanocarriers. In *Biomaterials Research* (Vol. 26, Number 1). BioMed Central Ltd. https://doi.org/10.1186/s40824-022-00313-2

Bezza, F. A., Iwarere, S. A., Tichapondwa, S. M., Brink, H. G., Daramola, M. O., & Chirwa, E. M. N. (2025). Synthesis and Evaluation of 3D Nitrogen Doped Reduced Graphene Oxide (3D N@ rGO) Macrostructure for Boosted Solar Driven Interfacial Desalination of Saline. *Wiley Online Library*, *9*(4). https://doi.org/10.1002/GCH2.202400080

Borenstein, S. A., Trolles-Cavalcante, S. Y. T., Dutta, A., Sofer, Z., & Borenstein, A. (2021). The effectiveness of Soxhlet extraction as a simple method for GO rinsing

as a precursor of high-quality graphene. *Pubs.Rsc.Org*. https://doi.org/10.1039/d1na00382h

Bradley, N. (2007). *Thesis Proposal: THE RESPONSE SURFACE METHODOLOGY*.

Cao, D., Bu, F., Cheng, X., Zhao, C., Yin, Y., & Liu, P. (2024). Purification of phenolics from Plantago depressa by macroporous resin: Adsorption/desorption characteristics, chromatographic process development and UPLC-TQ-MS/MS quantitative analysis. *LWT*, *203*. https://doi.org/10.1016/j.lwt.2024.116405

Carpentieri, S., Soltanipour, F., Ferrari, G., Pataro, G., & Donsì, F. (2021). Emerging green techniques for the extraction of antioxidants from agri-food by-products as promising ingredients for the food industry. In *Antioxidants* (Vol. 10, Number 9). MDPI. https://doi.org/10.3390/antiox10091417

Cegledi, E. (2023). *Optimization of extraction and encapsulation techniques of bioactive molecules from nettle (Urtica dioica L.)*. https://urn.nsk.hr/urn:nbn:hr:159:894962

Chaves, J. O., de Souza, M. C., da Silva, L. C., Lachos-Perez, D., Torres-Mayanga, P. C., Machado, A. P. da F., Forster-Carneiro, T., Vázquez-Espinosa, M., González-de-Peredo, A. V., Barbero, G. F., & Rostagno, M. A. (2020). Extraction of flavonoids from natural sources using modern techniques. *Frontiersin.Org*, *8*, 507887. https://doi.org/10.3389/FCHEM.2020.507887/FULL

Chen, J., Yang, J., Ma, L., Li, J., Shahzad, N., reports, C. K.-S., & 2020, undefined. (2020). Structure-antioxidant activity relationship of methoxy, phenolic hydroxyl, and carboxylic acid groups of phenolic acids. *Nature.Com*, *10*, 2611. https://doi.org/10.1038/s41598-020-59451-z

Cheng, X. L., Wan, J. Y., Li, P., & Qi, L. W. (2011). Ultrasonic/microwave assisted extraction and diagnostic ion filtering strategy by liquid chromatography–quadrupole time-of-flight mass spectrometry for rapid characterization of flavonoids in Spatholobus suberectus. *Journal of Chromatography A, 1218(34), 5774-5786*.

Chi, C., Liu, Z., Wang, G., Qi, B., Qiu, Z., Yan, Y., Huangfu, C., Lu, X., Yang, X., Gong, M., Cao, K., Wei, T., & Fan, Z. (2023). Graphene Oxide Block Derived Edge-Nitrogen Doped Quasi-Graphite for High K+ Intercalation Capacity and Excellent Rate Performance. *Wiley Online Library*, *13*(46). https://doi.org/10.1002/AENM.202302055

Cotas, J., Leandro, A., Monteiro, P., drugs, D. P.-M., & 2020, undefined. (2020). Seaweed phenolics: From extraction to applications. *Mdpi.Com*. https://www.mdpi.com/1660-3397/18/8/384

Dada, A. O., Olalekan, A. P., Olatunya, A. M., & Dada. (2012). Langmuir, Freundlich, Temkin and Dubinin-Radushkevich Isotherms Studies of Equilibrium Sorption of Zn 2+ Unto Phosphoric Acid Modified Rice Husk. In *IOSR Journal of Applied Chemistry (IOSR-JAC* (Vol. 3, Number 1). www.iosrjournals.org

Dakhil, I. H., & Habib Dakhil, I. (2013). Removal of Phenol from Industrial Wastewater Using Sawdust. In *Research Inventy: International Journal Of Engineering And Science* (Vol. 3, Number 1). https://www.researchgate.net/publication/297209123

Dargahi, A., Samarghandi, M. R., Shabanloo, A., Mahmoudi, M. M., & Nasab, H. Z. (2023). modeling of phenolic compounds adsorption onto low-cost adsorbent prepared from aloe vera leaves wastes using CCD-RSM optimization: effect of parameters …. *Springer*, *13*(9), 7859–7873. https://doi.org/10.1007/S13399-021-01601-Y

Darla, U., Lataye, D., Kumar, A., Reports, B. P.-S., & 2023, undefined. (2023). Adsorption of phenol using adsorbent derived from Saccharum officinarum biomass: optimization, isotherms, kinetics, and thermodynamic study. *Nature.Com*, *13*, 18356. https://doi.org/10.1038/s41598-023-42461-y

Darla, U., Lataye, D., Kumar, A., Reports, B. P.-S., & 2023, undefined. (2024). Adsorption of phenol using adsorbent derived from Saccharum officinarum biomass: optimization, isotherms, kinetics, and thermodynamic study. *Nature.Com*, *31*(60), 67442–67460. https://doi.org/10.1007/s11356-024-32971-1

de Andrade Lima, M., Charalampopoulos, D., & Chatzifragkou, A. (2018). Purification of supercritical-fluid carotenoid-rich extracts by hydrophobic interaction chromatography. *Separation and Purification Technology*, *203*, 1–10. https://doi.org/10.1016/j.seppur.2018.04.018

De La Luz-Asunción, M., Sánchez-Mendieta, V., Martínez-Hernández, A. L., Castaño, V. M., & Velasco-Santos, C. (2015). Adsorption of phenol from aqueous solutions by carbon nanomaterials of one and two dimensions: Kinetic and equilibrium studies. *Journal of Nanomaterials*, *2015*. https://doi.org/10.1155/2015/405036

Dehmani, Y., Dridi, D., … T. L.-J. of water process, & 2022, undefined. (2022). Review of phenol adsorption on transition metal oxides and other adsorbents. *Elsevier*. https://www.sciencedirect.com/science/article/pii/S2214714422004093

Destandau, E., & Michel, T. (2022). *Microwave-assisted extraction*. https://doi.org/10.1039/9781849737579-FP001

Ding, Z., Hu, X., Morales, V. L., & Gao, B. (2014). Filtration and transport of heavy metals in graphene oxide enabled sand columns. *Chemical Engineering Journal*, *257*, 248–252. https://doi.org/10.1016/j.cej.2014.07.034

Djenar, N. S., Mulyono, E. W. S., & Saputra, T. R. (2020). The effect of microwave power variations on phytochemical characteristic of pandan leaves (Pandanus Amaryllifolius) using the Microwave-Assisted Extraction (MAE). *Journal of Physics: Conference Series*, *1450*(1). https://doi.org/10.1088/1742-6596/1450/1/012007

Doughari, J. H. (2012). *Phytochemicals: Extraction Methods, Basic Structures and Mode of Action as Potential Chemotherapeutic Agents*. www.intechopen.com

Doulabi, M., Golmakani, M. T., & Ansari, S. (2020). Evaluation and optimization of microwave-assisted extraction of bioactive compounds from eggplant peel by-product. *Wiley Online Library*, *44*(11). https://doi.org/10.1111/JFPP.14853

Dunham, A., biology, P. B.-M. systems, & 2021, undefined. (2021). Exploring amino acid functions in a deep mutational landscape. *Embopress.Org*, *17*(7). https://doi.org/10.15252/msb.202110305

El-Shazly, M. A. M., Hamed, A. A., Kabary, H. A., & Ghareeb, M. A. (2022). LC-MS/MS profiling, antibiofilm, antimicrobial and bacterial growth kinetic studies of Pluchea dioscoridis extracts. *Acta Chromatographica*, *34*(3), 338–350. https://doi.org/10.1556/1326.2021.00956

Ercoli, S., Cartes, J., Cornejo, P., LWT, G. T.-, & 2021, undefined. (2021). Stability of phenolic compounds, antioxidant activity and colour parameters of a coloured extract obtained from coloured-flesh potatoes. *Elsevier*. https://www.sciencedirect.com/science/article/pii/S0023643820313591

Fabian, F. M. (2012). *Application of Response Surface Methodology and Central Application of Response Surface Methodology and Central Composite Design for 5P12-RANTES Expression in the Composite Design for 5P12-RANTES Expression in the Pichia Pichia pastoris pastoris System System*. https://digitalcommons.unl.edu/chemengtheseshttps://digitalcommons.unl.edu/chemengtheses/16

Farooq, S., Abdullah, Zhang, H., & Weiss, J. (2021). A comprehensive review on polarity, partitioning, and interactions of phenolic antioxidants at oil–water

interface of food emulsions. *Wiley Online Library*, *20*(5), 4250–4277. https://doi.org/10.1111/1541-4337.12792

Feng, W., Avvaru, V. S., Maça, R. R., Hinder, S. J., Rodríguez, M. C., & Etacheri, V. (2021). Realization of High Energy Density Sodium-Ion Hybrid Capacitors through Interface Engineering of Pseudocapacitive 3D-CoO-NrGO Hybrid Anodes. *ACS Applied Materials and Interfaces*, *13*(24), 27999–28009. https://doi.org/10.1021/acsami.1c01207

Foo, K., journal, B. H.-C. engineering, & 2010, undefined. (2010). Insights into the modeling of adsorption isotherm systems. *ElsevierKY Foo, BH HameedChemical Engineering Journal, 2010•Elsevier*, *156*(1), 2–10. https://doi.org/10.1016/J.CEJ.2009.09.013

Galal, A., Hassan, H., Atta, N., & reports, A. A.-M.-S. (2019). Synthesis, structural and morphological characterizations of nano-Ru-based perovskites/RGO composites. *Nature.Com*. https://doi.org/10.1038/s41598-019-43726-1

Gallo, M., Ferracane, R., Graziani, G., Ritieni, A., & Fogliano, V. (2010). Microwave assisted extraction of phenolic compounds from four different spices. *Molecules*, *15*(9), 6365–6374. https://doi.org/10.3390/molecules15096365

Gao, M., Song, B. Z., & Liu, C. Z. (2006). Dynamic microwave-assisted extraction of flavonoids from Saussurea medusa Maxim cultured cells. *Biochemical Engineering Journal, 32(2), 79-83.*

Ge, X., Wu, Z., Manzoli, M., Wu, Z., & Cravotto, G. (2020). Feasibility and the Mechanism of Desorption of Phenolic Compounds from Activated Carbons. *Industrial and Engineering Chemistry Research*, *59*(26), 12223–12231. https://doi.org/10.1021/acs.iecr.0c01402

Ghaffar, N., Botany, A. P.-N. Z. J. of, & 2025, undefined. (2025). Solvent polarity effects on extraction yield, phenolic content, and antioxidant properties of Malvaceae family seeds: a comparative study. *Taylor & Francis*, *63*(4), 627–637. https://doi.org/10.1080/0028825X.2024.2392705

Gopal, K., Raaov, M., Suah, F., … N. S.-M., & 2020, undefined. (2020). dispersive solid phase extraction based magnetic silicone surfactant activated charcoal adsorbent for extraction of phenolic compounds from industrial wastewater. *Elsevier*. https://www.sciencedirect.com/science/article/pii/S0026265X20309036

Gras, S., Waddington, L., Folding, K. G.-P., Misfolding, undefined, and, undefined, & 2011, undefined. (2011). Transmission electron microscopy of amyloid fibrils. *Springer*, *752*, 197–214. https://doi.org/10.1007/978-1-60327-223-0_13

Gutiérrez-Gamboa, G., Garde-Cerdán, T., Martínez-Lapuente, L., Costa, B. S. D., Rubio-Bretón, P., & & Pérez-Álvarez, E. P. (2020). Phenolic composition of Tempranillo Blanco (Vitis vinifera L.) grapes and wines after biostimulation via a foliar seaweed application. *Journal of the Science of Food and Agriculture, 100(2), 825-835*.

Hashim, M. R., Mohamad, Z., Ngadi, N., Jusoh, Y. M. M., Zakaria, Z. Y., & Jusoh, M. (2020). Microwave-assisted extraction and phytochemical analysis of peperomia pellucida for treatment of dengue. *Chemical Engineering Transactions*, *78*, 409–414. https://doi.org/10.3303/CET2078069

Haydari, I., Aziz, K., Kaya, S., Daştan, T., Ouazzani, N., Mandi, L., & Aziz, F. (2023). Green synthesis of reduced graphene oxide and their use on column adsorption of phenol from olive mill wastewater. *Process Safety and Environmental Protection*, *170*, 1079–1091. https://doi.org/10.1016/j.psep.2022.12.086

He, L., Zhang, X., Xu, H., Yuan, F., Knez, Ž., & Gao, Y. (2012). Subcritical water extraction of phenolic compounds from pomegranate (Punica granatum L.) seed residues and investigation into their antioxidant activities with HPLC–ABTS+ assay. *Food and Bioproducts Processing, 90(2), 215-223.*

Hira, N., Lock, S., Shoparwe, N., Lock, I., Sustainability, L. L.-, & 2023, undefined. (2023). Review of adsorption studies for contaminant removal from wastewater using molecular simulation. *Mdpi.Com*. https://www.mdpi.com/2071-1050/15/2/1510

Hossain, M., Lee, G., Technology, S. J.-S. and P., & 2024, undefined. (2024). Exploring the versatile production techniques and applications of nitrogen-doped activated carbon. *Researchgate.Net*. https://www.researchgate.net/profile/Reza-Joia/publication/381370913_Exploring_the_versatile_production_techniques_and_applications_of_nitrogen-doped_activated_carbon/links/666a959ade777205a32a8f27/Exploring-the-versatile-production-techniques-and-applications-of-nitrogen-doped-activated-carbon.pdf

Hou, Y., Wen, Z., Cui, S., Feng, X., & Chen, J. (2016). Strongly Coupled Ternary Hybrid Aerogels of N-deficient Porous Graphitic-C3N4 Nanosheets/N-Doped

Graphene/NiFe-Layered Double Hydroxide for Solar-Driven Photoelectrochemical Water Oxidation. *Nano Letters*, *16*(4), 2268–2277. https://doi.org/10.1021/acs.nanolett.5b04496

Issabayeva, G., Hang, S. Y., Wong, M. C., & Aroua, M. K. (2018). A review on the adsorption of phenols from wastewater onto diverse groups of adsorbents. *Degruyterbrill.Com*, *34*(6), 855–873. https://doi.org/10.1515/REVCE-2017-0007/HTML

Jalani, N. F., & Zainal, N. H. (2024). Sustainable Biorefinery Concept with Valorization and Utilization of Oil Palm Biomass for Value-Added Products. *Palm Oil Industry*, 59–77. https://doi.org/10.1007/978-981-97-8277-2_5

James, D., research, J. T.-A. of chemical, & 2013, undefined. (2013). Graphene: powder, flakes, ribbons, and sheets. *ACS Publications*, *46*(10), 2307–2318. https://doi.org/10.1021/AR300127R

Jing, L., Li, P., Li, Z., Ma, D., Reviews, J. H.-C. S., & 2025, undefined. (2025). Influence of π–π interactions on organic photocatalytic materials and their performance. *Pubs.Rsc.Org*, *54*, 2054. https://doi.org/10.1039/d4cs00029c

Jovanović, A., Vajić, U., Mijin, D., … G. Z.-J. of A., & 2022, undefined. (2022). Polyphenol extraction in microwave reactor using by-product of Thymus serpyllum L. and biological potential of the extract. *Elsevier*. https://www.sciencedirect.com/science/article/pii/S2214786122000493

Kalaskar, M., Yele, S. U., Ayyanar, M., Gurav, N., Beldar, V., & Surana, S. J. (2025). Methods of Extraction. *Wiley Online Library*, 121–142. https://doi.org/10.1002/9781394203680.CH07

Kalia, K., Sharma, K., Singh, H. P., & Singh, B. (2008). Effects of extraction methods on phenolic contents and antioxidant activity in aerial parts of Potentilla atrosanguinea Lodd. and quantification of its phenolic constituents by RP-HPLC. *Journal of Agricultural and Food Chemistry, 56(21), 10129-10134.*

Kaniyoor, A., Baby, T. T., Arockiadoss, T., Rajalakshmi, N., & Ramaprabhu, S. (2011). Wrinkled graphenes: a study on the effects of synthesis parameters on exfoliation-reduction of graphite oxide. *ACS Publications*, *115*(36), 17660–17669. https://doi.org/10.1021/JP204039K

Karunarathne, H. D. S. S., & Amarasinghe, B. M. W. P. K. (2013). Fixed bed adsorption column studies for the removal of aqueous phenol from activated carbon prepared

from sugarcane bagasse. *Energy Procedia*, *34*, 83–90. https://doi.org/10.1016/j.egypro.2013.06.736

Kaveh, R., Mortazavi, M., Alijani, H., Abdouss, M., Dehkalani, A. S., & Mazinani, S. (2024). Ternary nanohybrid of biochar/ NiFe2O4 /Ag3PO4 for simultaneous adsorption of Hg(II) and photodegradation of methylene blue; modeling, kinetic and isotherm studies. *Journal of Solid State Chemistry*, *331*, 124503. https://doi.org/10.1016/j.jssc.2023.124503

Khoddami, A., Wilkes, M. A., & Roberts, T. H. (2013). Techniques for analysis of plant phenolic compounds. In *Molecules* (Vol. 18, Number 2, pp. 2328–2375). https://doi.org/10.3390/molecules18022328

Khojasteh, H., Salavati-Niasari, M., Safajou, H., & Safardoust-Hojaghan, H. (2018). *Facile reduction of graphene using urea in solid phase and surface modification by N-doped graphene quantum dots for adsorption of organic dyes*.

Kim, G., Lee, J., Liu, T., & Grey, C. P. (2021). Characterizing Nitrogen Sites in Nitrogen-Doped Reduced Graphene Oxide: A Combined Solid-State 15N NMR, XPS, and DFT Approach. *ACS Publications*, *125*(19), 10558–10564. https://doi.org/10.1021/acs.jpcc.1c02669

Knaebel, K. S. (2016). *ADSORBENT SELECTION*.

Komaikul, J., Kitisripanya, T., Likhitwitayawuid, K., Sritularak, B., Tanaka, H., & Putalun, W. (2019). Improvement of stilbenoid production by 2-hydroxypropyl-β-cyclodextrin in white mulberry (Morus alba L.) callus cultures. *Natural Product Research, 33(19), 2762-2769.*

Kong, H., Chen, Y., Yang, G., Liu, B., & Guo, L. (2022). Two-dimensional material-based functional aerogels for treating hazards in the environment: synthesis, functional tailoring, applications, and sustainability analysis. *Pubs.Rsc.Org*. https://pubs.rsc.org/en/content/articlehtml/2022/nh/d1nh00633a

Kua, S. F., Ibrahim, J., Ooi, C. K. W., Nan, K. I., Hashim, N., & Mohd Yusof, H. (2015). Optimisation of phenolic extraction and quantification of phenolics in palm kernel cake. *Renewable Bioresources*, *3*(1), 2. https://doi.org/10.7243/2052-6237-3-2

Kumar, S., Abedin, Md. M., Singh, A. K., & Das, S. (2020). Role of Phenolic Compounds in Plant-Defensive Mechanisms. In *Plant Phenolics in Sustainable Agriculture* (pp. 517–532). Springer Singapore. https://doi.org/10.1007/978-981-15-4890-1_22

Kumar, S., Mary, D., Josephine, G., & Advances, M. A.-H. (2024). Graphene/GO/rGO based nanocomposites: Emerging energy and environmental application–review. *Elsevier*. https://www.sciencedirect.com/science/article/pii/S2773207X24000290

Kyzas, G. Z., Deliyanni, E. A., & Matis, K. A. (2014). Graphene oxide and its application as an adsorbent for wastewater treatment. *Wiley Online Library*, *89*(2), 196–205. https://doi.org/10.1002/JCTB.4220

Lama-Muñoz, A., Foods, M. C.-, & 2022, undefined. (2022). Extraction systems and analytical techniques for food phenolic compounds: a review. *Mdpi.Com*. https://www.mdpi.com/2304-8158/11/22/3671

Lattanzio, V. (2013). Phenolic compounds: Introduction. In *Natural Products: Phytochemistry, Botany and Metabolism of Alkaloids, Phenolics and Terpenes* (pp. 1543–1580). Springer Berlin Heidelberg. https://doi.org/10.1007/978-3-642-22144-6_57

Lee, S. Y., Khoiroh, I., Vo, D. V. N., Senthil Kumar, P., & Show, P. L. (2021). Techniques of lipid extraction from microalgae for biofuel production: a review. *Springer*, *19*(1), 231–251. https://doi.org/10.1007/S10311-020-01088-5

Li, S., Duan, Q., Li, T., Gao, X., Yang, X., Bao, L., & Li, Y. (2023). A simple one-pot method for growing metal (Co, Ni, Cu) oxide naoparticles on N-doped reduced graphene oxide and their application in lithium-ion storage. *Springer*, *108*(2), 477–489. https://doi.org/10.1007/S10971-023-06208-5

Li, Y., Du, Q., Liu, T., Sun, J., Jiao, Y., Xia, Y., Xia, L., Wang, Z., Zhang, W., Wang, K., Zhu, H., & Wu, D. (2012). Equilibrium, kinetic and thermodynamic studies on the adsorption of phenol onto graphene. *Materials Research Bulletin*, *47*(8), 1898–1904. https://doi.org/10.1016/j.materresbull.2012.04.021

life, U. K.-I., & 2019, undefined. (2018). The story of PKC: A discovery marked by unexpected twists and turns. *Wiley Online Library*, *71*(6), 697–705. https://doi.org/10.1002/iub.1963

Lippa, K. A., Aristizabal-Henao, J. J., Beger, R. D., Bowden, J. A., Broeckling, C., Beecher, C., Clay Davis, W., Dunn, W. B., Flores, R., Goodacre, R., Gouveia, G. J., Harms, A. C., Hartung, T., Jones, C. M., Lewis, M. R., Ntai, I., Percy, A. J., Raftery, D., Schock, T. B., … Ubhi, B. K. (2022). Reference materials for MS-based untargeted metabolomics and lipidomics: a review by the metabolomics quality assurance and quality control consortium (mQACC). *Springer*, *18*(4), 24. https://doi.org/10.1007/S11306-021-01848-6

Liu, H., Journal, H. Q.-C. E., & 2020, undefined. (2020). Recent advances of 3D graphene-based adsorbents for sample preparation of water pollutants: A review. *Elsevier*. https://www.sciencedirect.com/science/article/pii/S1385894720306823

Lu, J., Zhang, H., Yuan, M., Di, X., Ni, L., Luo, Y., Carbon, Y. C.-, & 2023, undefined. (2023). In-situ flowering of RGO with 3D distribution: Towards super-broadband microwave absorption and ultralight synergy in aramid honeycomb. *Elsevier*. https://www.sciencedirect.com/science/article/pii/S0008622323003640

Luisa, S., De Luna, R., Ramírez-Garza, R. E., & Serna Saldívar, S. O. (2021). Solvent Extraction of Jatropha Oil for Biodiesel Production: Effects of Solvent-to-Solid Ratio, Particle Size, Type of Solvent, Extraction Time, and Temperature on Oil. *Wiley Online Library*, *2021*, 1–8. https://doi.org/10.1155/2021/9221168

Malik, M., Sarker, A., & … S. R.-M. T. (2021). Performance enhancement of graphene/GO/rGO based supercapacitors: A comparative review. *Elsevier*. https://www.sciencedirect.com/science/article/pii/S2352492821006772

Mamman, S., Abdullahi, S., … A. B.-D. and W., & 2024, undefined. (2024). Influence of adsorption parameters on phenolic compounds removal from aqueous solutions: A mini review. *Elsevier*. https://www.sciencedirect.com/science/article/pii/S1944398624021234

Masoumi, B., Tabibiazar, M., Golchinfar, Z., Mohammadifar, M., & Hamishehkar, H. (2024). A review of protein-phenolic acid interaction: Reaction mechanisms and applications. *Taylor & Francis*, *64*(11), 3539–3555. https://doi.org/10.1080/10408398.2022.2132376

Mohamed Yunus, S. N., Abas, F., Jaafar, A. H., Azizan, A., Zolkeflee, N. K. Z., & Abd Ghafar, S. Z. (2021). Antioxidant and α-glucosidase inhibitory activities of eight neglected fruit extracts and UHPLC-MS/MS profile of the active extracts: SN Mohamed Yunus et al. *Springer*, *30*(2), 195–208. https://doi.org/10.1007/s10068-020-00856-x

Mourão, P. A. M., Carrott, P. J. M., & Ribeiro Carrott, M. M. L. (2006). Application of different equations to adsorption isotherms of phenolic compounds on activated carbons prepared from cork. *Carbon*, *44*(12), 2422–2429. https://doi.org/10.1016/j.carbon.2006.05.015

Nam, S. N., Jun, B. M., Park, C. M., Jang, M., Cho, K. S., Lee, J. Y., Park, C., Snyder, S. A., Son, A., & Yoon, Y. (2024). Research progress in graphene-based adsorbents for wastewater treatment: Preparation, adsorption properties and

mechanisms for inorganic and organic. *Mdpi.Com*, *53*(3), 231–249. https://doi.org/10.1080/15422119.2023.2242350

Nikolaeva, L., Materials, N. A.-I. C. S., & 2021, undefined. (2021). Adsorption purification of phenol-containing wastewater from oil refineries. *Iopscience.Iop.Org*. https://doi.org/10.1088/1757-899X/1089/1/012022/META

Nor, M., Norrrahim, F., Abdillah, M., Farid, A., Abubakar, B., Lawal, A., Arisyah, T., Yasim-Anuar, T., Mohd, B., Samsudin, H., & Zulkifli, A. A. (2022). Emerging technologies for value-added use of oil palm biomass. *Pubs.Rsc.Org*. https://doi.org/10.1039/d2va00029f

Oskoueian, E., Abdullah, N., Zulkifli, I., Ebrahimi, M., Karimi, E., Goh, Y. M., & Shakeri, M. (2015). Cytoprotective effect of palm kernel cake phenolics against aflatoxin B1-induced cell damage and its underlying mechanism of action. *BMC Complementary and Alternative Medicine, 15(1), 1-12*.

Osorio-Tobón, J. F. (2020). Recent advances and comparisons of conventional and alternative extraction techniques of phenolic compounds. *Journal of Food Science and Technology, 57, 4299-4315*.

Oufighou, A., Brahmi, F., Achat, S., Slimani, S., Arroul, Y., Kadi, A., Saadi, S., Guemghar-Haddadi, H., Madani, K., & Boulekbache-Makhlouf, L. (2024). Microwave-assisted extraction of total phenolics from pumpkin (Cucurbita pepo L.) pulp and peel: optimization process, antioxidant and antimicrobial properties. *Journal of Food Measurement and Characterization*, *18*(5), 3199–3214. https://doi.org/10.1007/s11694-024-02396-y

Oufighou, A., Brahmi, F., Achat, S., Yekene, S., Processes, S. S.-, & 2025, undefined. (2025). Optimization of Microwave-Assisted Extraction of Phenolic Compounds from Opuntia ficus-indica Cladodes. *Mdpi.Com*. https://www.mdpi.com/2227-9717/13/3/724

Padma, A., Venkateswara Reddy, B., Meghana, P., Venkatalakshmi, M., Saikalyan, M., & Naveen, M. (2019). *Review on Analytical Methods For The Quantification of Inorganic Elements and Inorganic Impurities*.

Pandey, R., Singhal, N., Kumar, P., Choudhary, K., & Kumar, S. (2022). Gold nanoparticles and graphene oxide based low cost glucose sensing technique. *Optical and Quantum Electronics*, *54*. https://doi.org/10.1007/s11082-022-03844-z

Panzella, L., Moccia, F., Nasti, R., Marzorati, S., Verotta, L., & Napolitano, A. (2020). Bioactive Phenolic Compounds From Agri-Food Wastes: An Update on Green and Sustainable Extraction Methodologies. In *Frontiers in Nutrition* (Vol. 7). Frontiers Media S.A. https://doi.org/10.3389/fnut.2020.00060

Papaoikonomou, L., Labanaris, K., Kaderides, K., & Goula, A. M. (2021). Adsorption–desorption of phenolic compounds from olive mill wastewater using a novel low-cost biosorbent. *Springer*, *28*(19), 24230–24244. https://doi.org/10.1007/s11356-019-07277-2

Patel, H. (2019). Fixed-bed column adsorption study: a comprehensive review. In *Applied Water Science* (Vol. 9, Number 3). Springer Verlag. https://doi.org/10.1007/s13201-019-0927-7

Petcharat, T., Sae-leaw, T., Benjakul, S., Quan, T. H., Indriani, S., Phimolsiripol, Y., & Karnjanapratum, S. (2024). Extraction of Kratom (Mitragyna speciosa) leaf compounds by enzymatic hydrolysis-assisted process: Yield, characteristics and its in vitro cytotoxicity in cell lines. *Process Biochemistry*, *142*, 212–222. https://doi.org/10.1016/J.PROCBIO.2024.04.033

Pistelli, L., Tonelli, M., Pellegrini, E., Cotrozzi, L., Pucciariello, C., Trivellini, A., & Nali, C. (2019). Accumulation of rosmarinic acid and behaviour of ROS processing systems in Melissa officinalis L. under heat stress. *Industrial Crops and Products, 138, 111469.*

Razuan, R., Finney, K. N., Chen, Q., Sharifi, V. N., & Swithenbank, J. (2011). Pelletised fuel production from palm kernel cake. *Fuel Processing Technology*, *92*(3), 609–615. https://doi.org/10.1016/j.fuproc.2010.11.018

Ricci, A., Cataldi, A., Zara, S., & Gallorini, M. (2022). Graphene-Oxide-Enriched Biomaterials: A Focus on Osteo and Chondroinductive Properties and Immunomodulation. In *Materials* (Vol. 15, Number 6). MDPI. https://doi.org/10.3390/ma15062229

Rocchetti, G., Gregorio, R. P., Lorenzo, J. M., Barba, F. J., Oliveira, P. G., Prieto, M. A., Simal-Gandara, J., Mosele, J. I., Motilva, M. J., Tomas, M., Patrone, V., Capanoglu, E., & Lucini, L. (2022). Functional implications of bound phenolic compounds and phenolics–food interaction: A review. *Wiley Online Library*, *21*(2), 811–842. https://doi.org/10.1111/1541-4337.12921

Rosli, E. N., Mohamad Nor, N., & Mat Yaman, S. H. (2025). Solvent selection for efficient phenolic extraction from palm kernel cake using microwave-assisted

techniques. *Malaysian Journal of Chemical Engineering and Technology*, *8*(1), 15–25. https://doi.org/10.24191/mjcet.v8i1.4580

Rosli, E. N., Mohd Ariff, M. A., Mohamad Nor, N., Osman, M. S., Ismail, N. F., & Mat Yaman, S. H. (2025). Kinetics modeling for the extraction of phenolic compound from palm kernel cake using microwave-assisted method. *Materials Research Proceedings*, *53*, 173–185. https://doi.org/10.21741/9781644903575-17

Sada Khan, A., Taleb Ibrahim, ab H., Abdel Jabbar, N., Khamis, M. I., Nancarrow, P., & Sabri Mjalli, F. (2021). Ionic liquids and deep eutectic solvents for the recovery of phenolic compounds: effect of ionic liquids structure and process parameters. *Pubs.Rsc.Org*. https://doi.org/10.1039/d0ra10560k

Saifuddin, N. M., Uskenbayeva, S., & Ong, M. Y. (2018). *On increase of the efficiency of extracting phenolic compounds from palm oil mill effluent Development of Bio-Hydrogen Production From Algae : A Review View project adsorption and waste water treatment View project References 3*. https://www.researchgate.net/publication/322674594

Saifuddin, N., Saltanat, A., & Refal, H. (2014). Enhancing the Removal of Phenolic Compounds from Palm Oil Mill Effluent by Enzymatic Pre-treatment and Microwave-Assisted Extraction. *Chemical Science Transactions*. https://doi.org/10.7598/cst2014.797

Saputera, W. H., Putrie, A. S., Esmailpour, A. A., Sasongko, D., Suendo, V., & Mukti, R. R. (2021). Technology Advances in Phenol Removals: Current Progress and Future Perspectives. *Catalysts 2021, Vol. 11, Page 998*, *11*(8), 998. https://doi.org/10.3390/catal11080998

Saw, H. Y., Janaun, J., Kumaresan, S., & Chu, C. M. (2012). Characterization of the physical properties of palm kernel cake. *International Journal of Food Properties*, *15*(3), 536–548. https://doi.org/10.1080/10942912.2010.492543

Shakil, N., & … N. A.-… M. and. (2023). Solid Waste Management in Malaysia: An overview. *Ojs.Amhinternational.Com*. https://ojs.amhinternational.com/index.php/imbr/article/view/3410

Shakoor, R., Hussain, N., Younas, S., & Bilal, M. (2023). Polyphenols: natural preservatives with promising applications in food, cosmetics and pharma industries; problems and toxicity associated with synthetic preservatives. *Mdpi.Com*, *63*(3–4), 276–291. https://doi.org/10.1002/jobm.202200401

Sharifi-Rad, J., Song, S., Ali, A., Subbiah, V., Taheri, Y., & Suleria, H. A. R. (2021). LC-ESI-QTOF-MS/MS characterization of phenolic compounds from Pyracantha coccinea M.Roem. and their antioxidant capacity. *Cellular and Molecular Biology*, *67*(1), 201–211. https://doi.org/10.14715/cmb/2021.67.1.29

Sharmila, Alimon, Azhar, & Samsudin. (2014). Malaysian Society of Animal Production 1 Improving Nutritional Values of Palm Kernel Cake (PKC) as Poultry Feeds: A Review. In *J. Anim. Sci* (Vol. 17, Number 1). http://www.etawau.com/OilPalm/Elaeis_guineensis.htm

Shi, L., Zhao, W., Yang, Z., Subbiah, V., & Suleria, H. A. R. (2022a). Extraction and characterization of phenolic compounds and their potential antioxidant activities. In *Environmental Science and Pollution Research* (Vol. 29, Number 54, pp. 81112–81129). Springer Science and Business Media Deutschland GmbH. https://doi.org/10.1007/s11356-022-23337-6

Shi, L., Zhao, W., Yang, Z., Subbiah, V., & Suleria, H. A. R. (2022b). Extraction and characterization of phenolic compounds and their potential antioxidant activities. In *Environmental Science and Pollution Research* (Vol. 29, Number 54, pp. 81112–81129). Springer Science and Business Media Deutschland GmbH. https://doi.org/10.1007/s11356-022-23337-6

Sik, B., Székelyhidi, R., Lakatos, E., Kapcsándi, V., & Ajtony, Z. (2022). Analytical procedures for determination of phenolics active herbal ingredients in fortified functional foods: an overview. In *European Food Research and Technology* (Vol. 248, Number 2, pp. 329–344). Springer Science and Business Media Deutschland GmbH. https://doi.org/10.1007/s00217-021-03908-6

Singh, R. K., Martins, V., Soares, B., Castro, I., & Falco, V. (2020). Chitosan application in vineyards (Vitis vinifera L. cv. Tinto Cão) induces accumulation of anthocyanins and other phenolics in berries, mediated by modifications in the transcription of secondary metabolism genes. *International Journal of Molecular Sciences, 21(1), 306*.

Singh, R. P., Ibrahim, M. H., Esa, N., & Iliyana, M. S. (2010). Composting of waste from palm oil mill: A sustainable waste management practice. In *Reviews in Environmental Science and Biotechnology* (Vol. 9, Number 4, pp. 331–344). https://doi.org/10.1007/s11157-010-9199-2

Singh, T. S., & Pant, K. K. (2006). Experimental and modelling studies on fixed bed adsorption of As(III) ions from aqueous solution. *Separation and Purification Technology*, *48*(3), 288–296. https://doi.org/10.1016/j.seppur.2005.07.035

Sittipod, S., Schwartz, E., Paravisini, L., Tello, E., & Peterson, D. G. (2020). Identification of compounds that negatively impact coffee flavor quality using untargeted liquid chromatography/mass spectrometry analysis. *ACS Publications*, *68*(38), 10424–10431. https://doi.org/10.1021/ACS.JAFC.0C01479

Soliman, N. K., & Moustafa, A. F. (2020). Industrial solid waste for heavy metals adsorption features and challenges; a review. In *Journal of Materials Research and Technology* (Vol. 9, Number 5, pp. 10235–10253). Elsevier Editora Ltda. https://doi.org/10.1016/j.jmrt.2020.07.045

Solomakou, N., Drosaki, A., Zamvrakidis, G., & Goula, A. M. (2023). Adsorption of phenolic compounds from olive mill wastewaters on spent coffee grounds: isotherms, kinetics, and pure phenol adsorption. *Springer*, *13*(18), 16557–16567. https://doi.org/10.1007/S13399-023-04088-X

Song, Y., Peng, Y., Long, N., Huang, Z., & Science, Y. Y.-A. S. (2021). Multifunctional self-assembly 3D Ag/g-C3N4/RGO aerogel as highly efficient adsorbent and photocatalyst for R6G removal from wastewater. *Elsevier*. https://www.sciencedirect.com/science/article/pii/S0169433220333420

Soto, M., Moure, A., & Domínguez, H. (2011). Recovery, concentration and purification of phenolic compounds by adsorption: A review. *Elsevier*. https://www.sciencedirect.com/science/article/pii/S0260877411000641

Soudagar, S., Akash, S., Venkat, M., … V. P.-M. T., & 2022, undefined. (2022). Adsorption of methylene blue dye on nano graphene oxide-thermodynamics and kinetic studies. *Elsevier*. https://www.sciencedirect.com/science/article/pii/S2214785321079244

Srihari, V., & Das, * -Ashutosh. (2009). *ADSORPTION OF PHENOL FROM AQUEOUS MEDIA BY AN AGRO-WASTE (HEMIDESMUS INDICUS) BASED ACTIVATED CARBON*. http://www.ecology.uni-corvinus.hu•ISSN15891623

Subramaniam, M., Mohamed, A. R., & Lai, S. Y. (2024). One-pot synthesis of regenerative calcium counterions from waste chicken eggshells for SO2-to-sulfur reduction. *Elsevier*, *26*. https://doi.org/10.1016/J.MTSUST.2024.100749

Suliman, S. S., Othman, N., Noah, N. F. M., & Kahar, I. N. S. (2023). Separation of phenolic compounds from fruit processing wastewater using liquid membrane

technology: A short review. *Biochemical Engineering Journal*, *200*. https://doi.org/10.1016/j.bej.2023.109096

Sun, L., Wang, L., Tian, C., Tan, T., Xie, Y., Shi, K., Li, M., & Advances, H. F.-R. (2012). Nitrogen-doped graphene with high nitrogen level via a one-step hydrothermal reaction of graphene oxide with urea for superior capacitive energy storage. *Pubs.Rsc.Org*. https://doi.org/10.1039/c2ra01367c

Sun, L., Wang, L., Tian, C., Tan, T., Xie, Y., Shi, K., Li, M., & Fu, H. (2012). Nitrogen-doped graphene with high nitrogen level via a one-step hydrothermal reaction of graphene oxide with urea for superior capacitive energy storage. *RSC Advances*, *2*(10), 4498–4506. https://doi.org/10.1039/c2ra01367c

Sun, W., & Shahrajabian, M. H. (2023). Therapeutic Potential of Phenolic Compounds in Medicinal Plants—Natural Health Products for Human Health. In *Molecules* (Vol. 28, Number 4). MDPI. https://doi.org/10.3390/molecules28041845

Tan, Y., Chai, M., Wong, L., … M. O.-I. J. of, & 2025, undefined. (2025). Optimizing microwave-assisted extraction of carbohydrate from scenedesmus sp. cultivated in domestic wastewater'. *Ijtech.Eng.Ui.Ac.Id*. https://ijtech.eng.ui.ac.id/article/view/7301

Teoh Cheng, H. (2002). *The Palm Oil Industry In Malaysia From Seed to Frying Pan*.

Thangavel, S. (2014). Understanding the adsorption property of graphene-oxide with different degrees of oxidation levels. *Elsevier*. https://www.sciencedirect.com/science/article/pii/S0032591014001831

The general mechanism of the adsorption process. | Download Scientific Diagram. (n.d.). Retrieved February 4, 2024, from https://www.researchgate.net/figure/The-general-mechanism-of-the-adsorption-process_fig6_346849698

Tsouko, E., Alexandri, M., Fernandes, K. V., Freire, D. M. G., Mallouchos, A., & Koutinas, A. A. (2019). Extraction of phenolic compounds from palm oil processing residues and their application as antioxidants. *Food Technology and Biotechnology*, *57*(1), 29–38. https://doi.org/10.17113/ftb.57.01.19.5784

Tungchaisin, T., Sae-Tan, S., & Rattanaporn, K. (2022). Optimization of Microwave-Assisted Extraction of Palm Kernel Cake Protein. *E3S Web of Conferences*, *355*, 02018. https://doi.org/10.1051/e3sconf/202235502018

Van Chen, T., Tran-Trung, H., Thuy, P. T., Giang An, N. T., Viet, N. T., Ha, N. X., Thao, D. T., Huong, N. T., Khanh Linh, N. N., & Giang, L. D. (2025). Chemical compositions of essential oils from leaves and fruits of Actinodaphne perlucida

CKAllen and their biological activities: Experimental and in silico molecular. *Taylor & Francis*, *28*(3), 487–498. https://doi.org/10.1080/0972060X.2025.2493947

Velusamy, S., Roy, A., Sundaram, S., & Kumar Mallick, T. (2021). Chitosan and graphene oxide-based nanocomposites for water purification and medical applications: a review. *Search.Proquest.Com*, *21*(7), 1570–1610. https://doi.org/10.1002/tcr.202000153

Wang, D., Hu, J., Wei, J., Liu, X., & Hou, H. (2023). Insights into nitrogen-doped carbon for oxygen reduction: the role of graphitic and pyridinic nitrogen species. *Wiley Online Library*, *24*(10). https://doi.org/10.1002/cphc.202200734

Wang, H., Yuan, X., Wu, Y., Huang, H., & Zeng, G. (2013). Adsorption characteristics and behaviors of graphene oxide for Zn (II) removal from aqueous solution. *ElsevierH Wang, X Yuan, Y Wu, H Huang, G Zeng, Y Liu, X Wang, N Lin, Y QiApplied Surface Science, 2013•Elsevier*. https://www.sciencedirect.com/science/article/pii/S0169433213008532

Wang, P., Zhang, D., Tang, H., Li, H., & Pan, B. (2019). New insights on the understanding of the high adsorption of bisphenol compounds on reduced graphene oxide at high pH values via charge assisted hydrogen bond. In *Journal of hazardous materials, 371, 513-520.*

Wei, L., Xia, X., Zhu, F., Li, Q., Xue, M., Li, J., Sun, B., Research, J. J.-W., & 2020, undefined. (2020). Evaluation of carbohydrates and quality parameters in six types of commercial teas by targeted statistical analysis. *Elsevier*. https://www.sciencedirect.com/science/article/pii/S0963996920301472

Wu, B., Meng, H., Morales, D. M., Zeng, F., Zhu, J., Wang, B., Risch, M., Xu, Z. J., & Petit, T. (2022). Nitrogen-rich carbonaceous materials for advanced oxygen electrocatalysis: synthesis, characterization, and activity of nitrogen sites. *Wiley Online Library*, *32*(31). https://doi.org/10.1002/ADFM.202204137

Yang, Z., Liu, Z., Shi, B., Yang, R., Lei, J., … J. W.-C. and S. A., & 2025, undefined. (2025). Adsorption of phenol on a novel porous nanocomposites prepared from coal gangue: studies on preparation conditions, adsorption characteristics and mechanism. *Elsevier*. https://www.sciencedirect.com/science/article/pii/S0927775725014992

Yao, F., Fang, C., Cui, J., Dai, L., Zhang, X., … L. X.-N. S., & 2023, undefined. (2023). Supramolecular assembly-derived carbon-nitrogen-based functional materials for

photo/electrochemical applications: progress and challenges. *Nso-Journal.Org*. https://nso-journal.org/articles/nso/full_html/2023/04/NSO20220039/F2.html

Yeddou, N., & Bensmaili, A. (2007). Equilibrium and kinetic modelling of iron adsorption by eggshells in a batch system: effect of temperature. In *Desalination* (Vol. 206).

Yu, L., Wu, X., Liu, Q., Liu, L., Jiang, X., Yu, J., Feng, C., & Zhong, M. (2016). Removal of phenols from aqueous solutions by graphene oxide nanosheet suspensions. *Journal of Nanoscience and Nanotechnology*, *16*(12), 12426–12432. https://doi.org/10.1166/JNN.2016.12974

Zaini, M. S. M., Arshad, M., & Syed-Hassan, S. S. A. (2023). Adsorption Isotherm and Kinetic Study of Methane on Palm Kernel Shell-Derived Activated Carbon. *Journal of Bioresources and Bioproducts*, *8*(1), 66–77. https://doi.org/10.1016/j.jobab.2022.11.002

Zango, Z. U., Sambudi, N. S., Jumbri, K., Ramli, A., Bakar, N. H. H. A., Saad, B., Rozaini, M. N. H., Isiyaka, H. A., Osman, A. M., & Sulieman, A. (2020). An overview and evaluation of highly porous adsorbent materials for polycyclic aromatic hydrocarbons and phenols removal from wastewater. In *Water (Switzerland)* (Vol. 12, Number 10, pp. 1–40). MDPI AG. https://doi.org/10.3390/w12102921

Zeng, M., & Pan, X. (2022). Insights into solid acid catalysts for efficient cellulose hydrolysis to glucose: progress, challenges, and future opportunities. *Taylor & Francis*, *64*(3), 445–490. https://doi.org/10.1080/01614940.2020.1819936

Zhang, Y., Wan, Q., Yang, N., Zhang, Y., Wan, Q., & Yang, N. (2019). Recent advances of porous graphene: synthesis, functionalization, and electrochemical applications. *Wiley Online Library*, *15*(48). https://doi.org/10.1002/SMLL.201903780

Zhao, H., Wang, W., Lü, Q., Lin, T., & Technology, Q. L.-B. (2015). Preparation and application of porous nitrogen-doped graphene obtained by co-pyrolysis of lignosulfonate and graphene oxide. *Elsevier*. https://www.sciencedirect.com/science/article/pii/S096085241401637X

Zhao, R., Li, Y., Ji, J., Wang, Q., Li, G., Wu, T., & Zhang, B. (2021). Efficient removal of phenol and p-nitrophenol using nitrogen-doped reduced graphene oxide. Colloids and Surfaces A. In *Physicochemical and Engineering Aspects, 611, 125866.*

Zhou, Y., Li, J., Liu, C., & Huo, P. (2018). Construction of 3D porous g-C3N4/AgBr/rGO composite for excellent visible light photocatalytic activity. *Elsevier*. https://www.sciencedirect.com/science/article/pii/S016943321832018X

Zhou, Y., Zhao, X., Liu, F., Chi, W., Yao, J., & Chen, G. (2020). Facile One-Pot Solvothermal Synthesis of the RGO/MWCNT/Fe3O4 Hybrids for Microwave Absorption. *ACS Publications*, *5*(6), 2899–2909. https://doi.org/10.1021/ACSOMEGA.9B03740

Złotek, U., Szymanowska, U., Jakubczyk, A., Sikora, M., & Świeca, M. (2019). Effect of arachidonic and jasmonic acid elicitation on the content of phenolic compounds and antioxidant and anti-inflammatory properties of wheatgrass (Triticum aestivum L.). *Food Chemistry, 288, 256-261.*

APPENDICES

APPENDIX 1

Extraction of Phenolic Compound



Plate A 1 Modified Microwave-Assisted Extraction



Plate A 2 Rotary Evaporator



Plate A 3 Bio-oil Pure Extracted Sample

APPENDIX 2

Synthesis of 3D-Nitrogen Doped Reduced Graphene Oxide (3D-N/rGO)

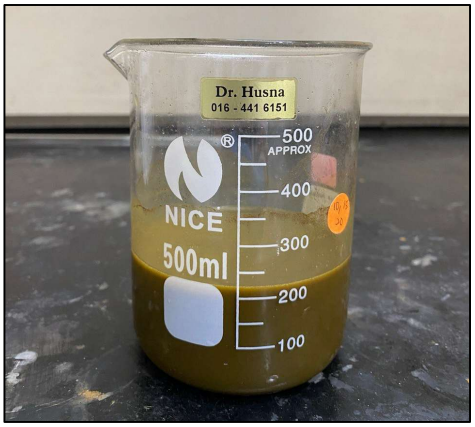


Plate A 4 GO After Peroxide Treatment Uisng Modified Hummer's Method



Plate A 5 GO After Drying Using Oven

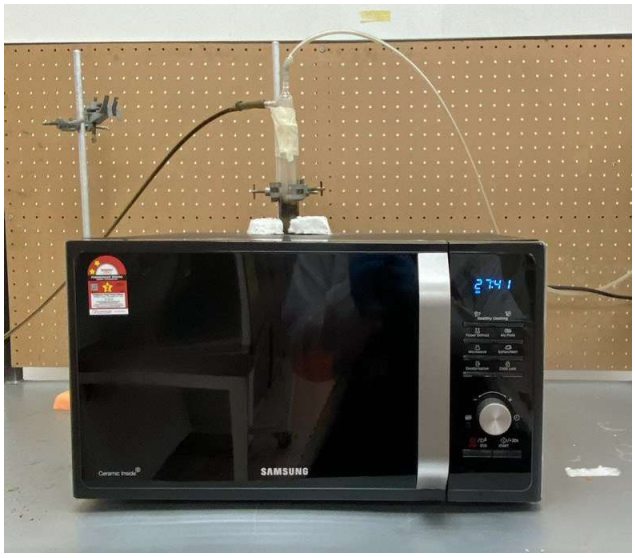


Plate A 6 Microwave Heating of 3D-N/rGO With Continuous of Nitrogen Gas

APPENDIX 3

Purification of Phenolic Extract



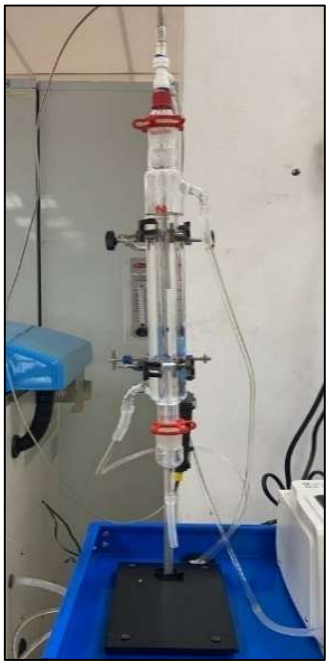


Plate A 7 Adsorption Rig for Phenolic Extract Purification

APPENDIX 4

Calibration Curves

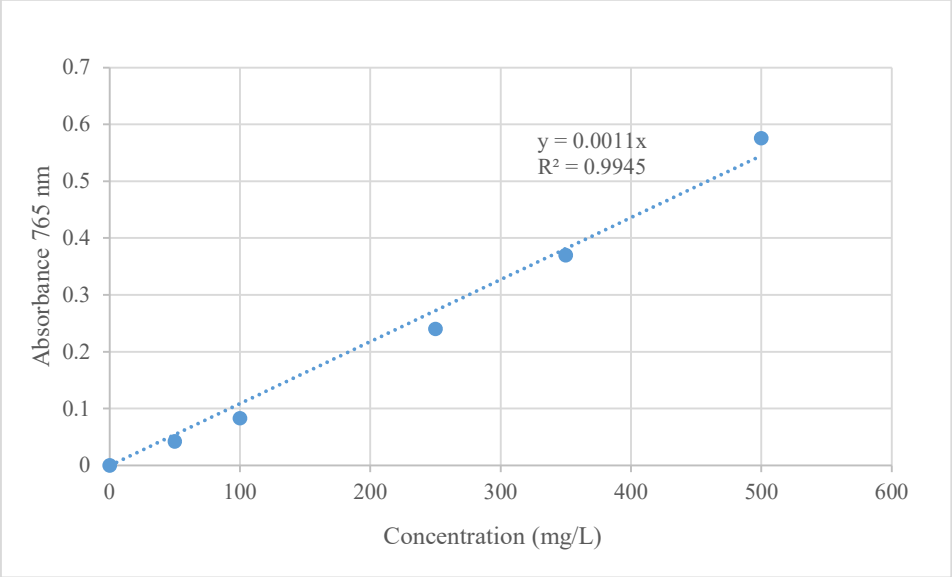


Plate A 8 Calibration Curves of Gallic Acid

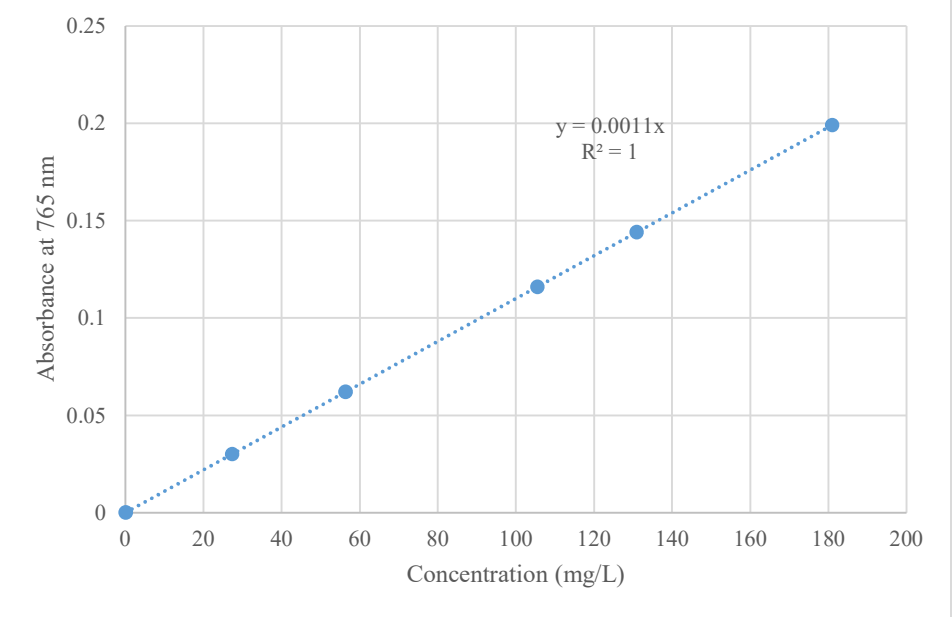


Plate A 9 Calibration Curves for Phenolic Concentration

APPENDIX 5

Sample Calculations

1) Calculation of weight pure extracted sample after rotavap

$$\text{Weight oil extract} = \text{Weight flask after rotavap} - \text{Weight empty flask}$$

Example,

$$\text{Weight flask after rotavap} = 275.11\ \text{g}$$

$$\text{Weight empty flask} = 270.60\ \text{g}$$

Therefore,

$$\begin{aligned}\text{Weight oil extract} &= \text{Weight flask after rotavap} - \text{Weight empty flask} \\ &= 275.11\ \text{g} - 270.60\ \text{g} \\ &= 4.51\ \text{g}\end{aligned}$$

2) Calculation of phenolic concentration by using equation that obtained from calibration curve for phenolic concentration (Plate A7)

Equation from calibration curve,

$$y = 0.0011\,x$$

To get concentration of 50 mg/L, then

$$\begin{aligned}y &= 0.0011\,x \\ &= 0.0011(50) \\ &= 0.055\end{aligned}$$

Thus, the absorbance at 765 nm is 0.055 to get concentration of 50 mg/L

3) Calculation for adsorption capacity

$$\text{Adsorption capacity, } Q_e\ (\text{mg/g}) = \frac{(C_i - C_f)V_s}{m}$$

Where,

C_i is initial concentration of extracted sample (mg/L)

C_f is final concentration (mg/L)

V_s is the sample solution during adsorption process (L)

m is mass adsorbent (g)

Given,

$$C_i = 142.7273\ \text{mg/L}$$

$$C_f = 140.3030\ \text{mg/L}$$

$$V_s = 302.80\ \text{mL} = 0.3028\ \text{L}$$

$$m = 1.0\ \text{g}$$

Therefore,

$$Q_e = \frac{(C_i - C_f)V_s}{m}$$

$$= \frac{(142.7273\ \text{mg/L} - 140.3030\ \text{mg/L}) \times 0.3028\text{L}}{1.0\ \text{g}}$$

$$= 0.7341\ \text{mg/g}$$

4) Calculation for Adsorption Efficiency

$$\text{Adsorption Effieciency, } R_e\ (\%) = \frac{(C_i - C_f)}{C_i} \times 100\%$$

Where,

C_i is initial concentration of extracted sample (mg/L)

C_f is final concentration (mg/L)

Given,

$C_i = 142.7273\ \text{mg/L}$

$C_f = 140.3030\ \text{mg/L}$

Therefore,

$$R_e\ (\%) = \frac{(C_i - C_f)}{C_i} \times 100\%$$

$$= \frac{(142.7273\ \text{mg/L} - 140.3030\ \text{mg/L})}{142.7273\ \text{mg/L}} \times 100\%$$

$$= 1.70\ \%$$

5) Calculation for desorption capacity

$$\text{Desorption capacity, } Q_d\ (\text{mg/g}) = \frac{C_d V_d}{m}$$

Where,

C_d is the sample concentration in the desorption solution (mg/L)

V_d is the sample solution volume during desorption process (L)

m is mass adsorbent (g)

Given,

$C_d = 53.6364\ \text{mg/L}$

$V_d = 50.0342\ \text{mL} = 0.0500\ \text{L}$

$m = 1.0\ \text{g}$

Therefore,

$$Q_d\ (\text{mg/g}) = \frac{C_d V_d}{m}$$

$$= \frac{(53.6364\ \text{mg/L}) \times 0.0500\ \text{L}}{1.0\ \text{g}}$$

$$= 2.6837\ \text{mg/g}$$

6) Calculation for adsorption capacity at breakthrough time

$$\text{Adsorption capacity at breakthrough time, } q_{bt} = \frac{C_o \times V_{bt}}{m}$$

Where,

q_{bt} is adsorption capacity at breakthrough time (mg/g)

C_o is initial concentration of phenolic compound (mg/L)

V_{bt} volume of solution treated at breakthrough (L)

m is mass adsorbent (g)

Given,

$C_o = 50$ mg/L

Breakthrough time, $t_{bt} = 3.06$ minutes

Flowrate $= 3.17$ rpm $= 4.17$ mL/min

$m = 0.5$ g

Calculate V_{bt},

$$V_{bt} = \text{flowrate} \times t_{bt}$$
$$= 4.17 \text{ mL/min} \times 3.06 \text{ min}$$
$$= 12.7602 \text{ mL} = 0.01276 \text{ L}$$

Therefore,

$$q_{bt} \text{ (mg/g)} = \frac{C_o \times V_{bt}}{m}$$
$$= \frac{(50 \text{ mg/L}) \times 0.01276 \text{ L}}{0.5 \text{ g}}$$
$$= 1.276 \text{ mg/g}$$

AUTHOR'S PROFILE



Ellisa Natasya Rosli obtained Bachelor of Chemical Engineering (Environmental) with Honours in 2023 from Universiti Teknologi Mara (UiTM) Cawangan Pulau Pinang. Currently, she is serving as a Graduate Research Assistant while pursuing her Master of Science in Chemical Engineering at the same institution. Her research focuses on the synthesis of three-dimensional nitrogen-doped reduced graphene oxide (3D-N/rGO) for the enhanced recovery and purification of phenolic compounds from palm kernel cake extracts obtained via microwave-assisted extraction (MAE). Her postgraduate work emphasizes adsorption-based purification processes, involving both batch and continuous fixed-bed column systems, with detailed mechanistic studies through isotherm, kinetic, and thermodynamic modelling. She employs advanced analytical techniques such as FTIR, BET, TGA, HRTEM, XPS, LC-MS and Micro-Macronutrients analysis to investigate material structure, doping efficiency, adsorption behaviour and phenolic compounds identification. Her work aligns with sustainable biomass valorisation, supporting the development of high-value bioactive compounds for food, cosmetic, and pharmaceutical applications. She can be contacted at ellisanatasya@gmail.com.

List of Attended Conference:

International Conference on Decarbonization Technology (ICDT2024), World Engineering, Science and Technology Congress (ESTCON 2024), Organizer: Universiti Teknologi PETRONAS (UTP), Venue: Sabah International

Convention Centre (SICC), Kota Kinabalu, Sabah, Malaysia, Date: 10-11 September 2024, Paper Presented: “Kinetics Modeling for The Extraction of Phenolic Compound from Palm Kernel Cake Using Microwave-Assisted Method”.

LIST OF PUBLICATION:

Rosli, E. N., Mohd Ariff, M. A., Mohamad Nor, N., Osman, M. S., Ismail, N. F., & Mat Yaman, S. H. (2025). Kinetics modeling for the extraction of phenolic compound from palm kernel cake using microwave-assisted method. In *Decarbonization Technology: ICDT 2024* (Vol. 53, pp. 173–185). Materials Research Forum LLC. https://doi.org/10.21741/9781644903575-17

Rosli, E. N., Mohamad Nor, N., & Mat Yaman, S. H. (2025). Solvent selection for efficient phenolic extraction from palm kernel cake using microwave-assisted techniques. *Malaysian Journal of Chemical Engineering & Technology, 8*(1), 15–25. https://doi.org/10.24191/mjcet.v8i1.4580

Mat Yaman, S. H., Mohamad Nor, N., **Rosli, E. N**., Mohd Ariff, M. A., Osman, M. S., & Ismail, N. F. (2025). Optimization of supercritical fluid extraction of phenolic-compounds from palm kernel cake and its antioxidant activity. In *Decarbonization Technology: ICDT 2024* (Vol. 53, pp. 241–254). Materials Research Forum LLC. https://doi.org/10.21741/9781644903575-24

List of Submitted Paper:

Rosli, E. N., Nor, N. M., Mat Yaman, S, H., Ariff, M, A., “Synthesis and Characterization of Three-Dimensional Nitrogen-Doped Reduced Graphene Oxide (3D-N/rGO) for Phenolic Compound Recovery from Palm Kernel Cake". Journal of Separation and Purification Technology, submitted.

Rosli, E. N., Nor, N. M., Mat Yaman, S, H., Ariff, M, A., “Adsorption Performance and Mechanistic Insights of 3D-N/rGO for Phenolic Compound Purification: Isotherms, Thermodynamics, and Kinetics”. Journal of the Taiwan Institute of Chemical Engineers, submitted.

UNIVERSITI TEKNOLOGI MARA

PERPUSTAKAAN TUN ABDUL RAZAK
BAHAGIAN SUMBER RUJUKAN UNIVERSITI (BSRU)

BORANG PENYERAHAN BAHAN HARTA INTELEK UiTM

UiTM's Intellectual Property Submission Form

Nama (*Name*) : ELLISA NATASYA BINTI ROSLI

No. Telefon(Pejabat/Hp) : *Telephone No.(Office / handphone)* 0178131400

Fakulti/Pusat Akademik/Bahagian : *Faculty / Academic Centres / Department* KOLEJ PENGAJIAN KEJURUTERAAN

E-mel *(E-mail)* : 2023290186@student.uitm.edu.my

Tarikh *(Date)* : 10-08-2026

Pihak Fakulti / Pusat Akademik / Bahagian / Saya bersetuju bahawa dokumen dan tajuk yang disenaraikan untuk dimasukkan ke dalam Repositori Institusi UiTM.
The Faculty / Academic Centres / Department / I agree that the document and titles listed below to be placed in the UiTM Institutional Repository.

JENIS BAHAN (Sila nyatakan) : *Types of Material (Please specify)* Thesis

Types of Material: Article / Book / Theses / Bulletin / Seminar / Image / Entrepreneurship / Student Project / Research Report / Industrial Training / Annual Report / Manual / Oral History / Exam Paper / Speech / Dataset / Audio / Video / Others

MAKLUMAT BAHAN ***(Information of Materials)*:**

Bil. *No*	JUDUL BAHAN *Title*	HARDCOPY (✓)	SOFTCOPY (✓)
1.	Synthesis of 3D Nitrogen-Doped Reduced Graphene Oxide Adsorbent for Phenolic Purification from Microwave-E		✔

* Sila sediakan lampiran sekiranya ruangan yang disediakan tidak mencukupi *(Please provide attachment if necessary)*

TUJUAN PENYERAHAN BAHAN (Sila tandakan √):

Purpose (Please mark √):

1. **Bahan untuk dimuat naik ke dalam Repositori Institusi UiTM**.
   (Materials for uploading into the UiTM Institutional Repository (UiTM IR)):
   Fakulti / Pusat Akademik / Bahagian / Saya perlu memastikan bahawa setiap dokumen telah dibuat semakan terlebih dahulu dan tidak mengandungi sebarang maklumat sulit sebelum diserahkan kepada pihak PTAR. ✔
   The Faculty / Academic Centres / Department must ensure that each document has been reviewed in advance and does not contain any confidential information before being submitted to PTAR.
2. **Bahan mengandungi maklumat TERHAD yang telah ditentukan oleh organisasi / badan di mana penyelidikan dijalankan:**.
   (Materials consisting of RESTRICTED information which has been determined by the organisation/body where the research was conducted):
   Sila nyatakan tarikh tamat embargo (jika ada):
   (Please indicate the embargo expiry date (if any)):
   Embargo expiry date: Day: Month: Year: ☐
   Nota: Embargo Expiry Date adalah tarikh tamat tempoh yang ditetapkan oleh penulis di mana pada atau selepas tarikh ini, bahan tersebut akan dipaparkan secara langsung di Repositori Institusi UiTM dan ianya boleh diakses.
   Note: Embargo Expiry Date is the date that an author or a publisher imposed embargo expires. On and after this date, this document will be accessible in UiTM Institutional Repository.
3. **Bahan boleh diakses secara teks penuh dan terbuka.** ✔
   (Materials can be accessed in full text via open access).
4. **Bahan dipinjamkan sementara untuk tujuan pendigitalan dan akan dikembalikan semula kepada pemilik.** ☐
   (Materials are on temporary loan for digitization and will be returned to the owner).

Pemberitahuan: Jika Repositori Institusi UiTM menerima bukti pelanggaran hak cipta, bahan yang berkaitan akan dikeluarkan serta-merta.
(Notification: If UiTM Institutional Repository receives proof of copyright violation, the relevant item will be removed immediately).

PERAKUAN :
Declaration:
Saya / kami akan bertanggungjawab ke atas bahan yang diserahkan untuk pendigitalan dan muat naik ke dalam Repositori Institusi UiTM.
I / we will be responsible for the materials submitted for digitization and uploaded into UiTM Institutional Repository.

Tandatangan Pemohon
Applicant Signature
Tarikh (*Date*): 10/08/2026

DR. NORHUSNA MOHAMAD NOR
Pensyarah Kanan
Pusat Pengajian Kejuruteraan Kimia
Kolej Kejuruteraan
UiTM Cawangan Pulau Pinang

Tandatangan dan Cop Ketua Jabatan / Bahagian / Penyelia
Head of Division / Department / Supervisor Signature and stamp
Tarikh (*Date*):

UNTUK KEGUNAAN PEJABAT (*For office use*)

DITERIMA OLEH / *Received By* :
TANDATANGAN / *Signature* :
TARIKH (*Date*):

DISAHKAN OLEH / *Certified By* :
TANDATANGAN / *Signature* :
TARIKH (*Date*):